PLANNING OPTIMAL LOAD DISTRIBUTION AND MAXIMUM RENEWABLE ENERGY FROM WIND POWER ON A RADIAL DISTRIBUTION SYSTEM

by

HANDUWALA DEWAGE DULAN JAYANATHA WEERASINGHE

B.S. Sheffield Hallam University, 2008
M.S. Sheffield Hallam University, 2010

AN ABSTRACT OF A DISSERTATION

submitted in partial fulfillment of the requirements for the degree

DOCTOR OF PHILOSOPHY

Department of Electrical and Computer Engineering
College of Engineering

KANSAS STATE UNIVERSITY
Manhattan, Kansas

2015

Abstract

Optimizing renewable distributed generation in distribution systems has gained popularity with changes in federal energy policies. Various studies have been reported in this regard and most of the studies are based on optimum wind and/or solar generation planning in distribution system using various optimization techniques such as analytical, numerical, and heuristic. However, characteristics such as high energy density, relatively lower footprint of land, availability, and local reactive power compensation ability, have gained increased popularity for optimizing distributed wind generation (DWG) in distribution systems.

This research investigated optimum distributed generation planning (ODGP) using two primary optimization techniques: analytical and heuristic. In first part of the research, an analytical optimization method called "Combined Electrical Topology (CET)" was proposed in order to minimize the impact of intentional structural changes in distribution system topology, in distributed generation/ DWG placement.

Even though it is still rare, DWG could be maximized to supply base power demand of three-phase unbalanced radial distribution system, combined with distributed battery energy storage systems (BESS). In second part of this research the usage of DWG/BESS as base power generation, and to extend the ability to sustain the system in a power grid failure for a maximum of 1.5 hours was studied. IEEE 37-node, three-phase unbalanced radial distribution system was used as the test system to optimize wind turbines and sodium sulfide (NaS) battery units with respect to network real power losses, system voltage profile, DWG/BESS availability and present value of cost savings. In addition, DWG's ability to supply local reactive power in distribution system was also investigated.

Model results suggested that DWG/NaS could supply base power demand of a three-phase unbalanced radial distribution system. In addition, DWG/NaS were able to sustain power demand of a three-phase unbalanced distribution system for 1.5 hours in the event of a power grid failure.

PLANNING OPTIMAL LOAD DISTRIBUTION AND MAXIMUM RENEWABLE ENERGY FROM WIND POWER ON A RADIAL DISTRIBUTION SYSTEM

by

HANDUWALA DEWAGE DULAN JAYANATHA WEERASINGHE

B.S. Sheffield Hallam University, 2008
M.S Sheffield Hallam University, 2010

A DISSERTATION

submitted in partial fulfillment of the requirements for the degree

DOCTOR OF PHYLOSOPHY

Department of Electrical and Computer Engineering
College of Engineering

KANSAS STATE UNIVERSITY
Manhattan, Kansas

2015

Approved by:

Major Professor
Ruth Douglas Miller

Copyright

Abstract

Optimizing renewable distributed generation in distribution systems has gained popularity with changes in federal energy policies. Various studies have been reported in this regard and most of the studies are based on optimum wind and/or solar generation planning in distribution system using various optimization techniques such as analytical, numerical, and heuristic. However, characteristics such as high energy density, relatively lower footprint of land, availability, and local reactive power compensation ability, have gained increased popularity for optimizing distributed wind generation (DWG) in distribution systems.

This research investigated optimum distributed generation planning (ODGP) using two primary optimization techniques: analytical and heuristic. In first part of the research, an analytical optimization method called "Combined Electrical Topology (CET)" was proposed in order to minimize the impact of intentional structural changes in distribution system topology, in distributed generation/ DWG placement.

Even though it is still rare, DWG could be maximized to supply base power demand of three-phase unbalanced radial distribution system, combined with distributed battery energy storage systems (BESS). In second part of this research the usage of DWG/BESS as base power generation, and to extend the ability to sustain the system in a power grid failure for a maximum of 1.5 hours was studied. IEEE 37-node, three-phase unbalanced radial distribution system was used as the test system to optimize wind turbines and sodium sulfide (NaS) battery units with respect to network real power losses, system voltage profile, DWG/BESS availability and present value of cost savings. In addition, DWG's ability to supply local reactive power in distribution system was also investigated.

Model results suggested that DWG/NaS could supply base power demand of a three-phase unbalanced radial distribution system. In addition, DWG/NaS were able to sustain power demand of a three-phase unbalanced distribution system for 1.5 hours in the event of a power grid failure.

Table of Contents

List of Figures

List of Tables

Acknowledgements

First and foremost, I would like to express my utmost gratitude to my graduate advisor, Professor Ruth Douglas Miller, at Kansas State University. It is with immense gratitude that I acknowledge the support, encouragement and the freedom during my graduate studies. I consider it an honor to work with such an experienced scientist.

I owe my deepest gratitude to my outside chairperson Prof. Douglas Goodin, and my Graduate Committee Members: Prof. Anil Pahwa, Prof. Caterina M. Scoglio, and Prof. Mehmet B. Yildirim, for their valuable time, continues support, and suggestions during my graduate studies.

Also I would like to express my gratitude to Prof. Andrew Rys and Prof. Kenneth Klabunde of K-State Chemistry Department for their support at the beginning and during my graduate studies in various ways.

A special thanks goes to Tamara Robinson for her valuable suggestions in improving my dissertation writing.

I am grateful to my peer colleagues for many random conversations during my research studies. A special thanks to Dr.Sakshi Pahwa, Dr. Faryad Darabi, Woldu A. Tuku, Lazaro S. Escalante, Mahdi Sadiqi, Manoaj Vijayarangan, Priyanka Malve, Alireza Afiat and Taylor Edward.

I am grateful to all the Sri Lankan friends in Manhattan, for making me feel K-State a home away home. A special thanks goes to Dr.Thilani Smarakoon, Dhanushka Samarakoon, Dr. Dinusha Udukala, Dr. Dhanushi Welideniya, Gayani Pallewela, Sadish Karunaweera, and Buddhika Karunaweera for all the memorable moments that we spend and cherished during my graduate studies.

My deepest gratitude goes to my parents for the deep love, care and tremendous scarifies that they made to ensure that I had an excellent education. For this and much more, I'm forever in their debt. Special thanks for my brother and sister, for the love and friendship throughout my life. Also, grateful thanks to my parent in-laws for their encouragements love and support during past five years.

Last but not the least, grateful thank for my wife, Dr.Manindu N Weerasinghe, and daughters, Nethyu Ama Weerasinghe and Sithundi Dhara Weerasinghe. They have been my motivation as I hurdle all the obstacles in the completion of this work. I'm truly blessed to have them in my life.

Dedication

To my Parents

Father, Sarath Weerasinghe and Mother, Chithra Kalyani Weerasinghe

To my Wife

Dr. Manindu N Weerasinghe

To my Daughters

Nethyu Ama Weerasinghe and Sithundi Dhara Weerasinghe

For their endless love and care in my life

&

To my County

Sri Lanka

Preface

This dissertation includes extended work of multi-authored work that has been submitted to *Smart Grid*, De Gruyter Online Journal in second part of chapter 2. It's full citation reads: Weerasinghe, D.J., Pahwa, S., Miller, R.D., Scoglio, C.M., "Impact of intentional structural changes in distribution system topology to wind turbine sizing and siting: A complex network approach."

A version of the first part chapter 2 was submitted for publication in the *International journal of Power and Energy Systems,* 2015. It's full citation reads: Weerasinghe, D.J., Pahwa, S., Miller, R.D., Scoglio, C.M., "Use of Combined Electrical Topology Method to Optimize Placement and Size of Distributed Generation Considering Intentional Structural Changes in the Distribution System Topology."

The Matlab code developed to optimize placement and capacity of distributed wind generation and storage with respect to real power losses, voltage profile, DWG/ BESS availability, present value of cost savings, as well as the writing involved in the preparation of the journal article was performed by the author of the current dissertation. The secondary authors advised the primary author edited the journal article prior to its submission.

A version of the chapter 3 was submitted for the publication in the *Elsevier Sustainable Energy, Grids, and Networks,* 2015. It's full citation reads: Weerasinghe D. J., Miller, R.D., "Optimizing placement and capacity of distributed wind generation and energy storage systems, to supply base load of an unbalanced radial distribution system and sustain power in a power grid failure."

This work is to the best of my knowledge original, except where acknowledgements and references are made to previous work. Neither this, nor any significantly similar dissertation has been submitted for any other degree, diploma or other qualification at any other university.

Chapter 1 - Overview: An Executive Summary

Context of the Work

Electricity is a vital component of daily operations around the world. Modern society depends on electric power systems to consistently fulfill the electricity demand. However, power systems are complex, timeworn, and increasingly vulnerable to malicious activities, thereby increasing system fragility and expense.

A majority of electric power systems operate based on the assumption of centralized generation, primarily consisting of generation, transmission, and distribution. In centralized generation, low voltage electricity (2.3kV to 30kV) is generated in bulk in a central location, converted into high-voltage electricity (110kV to 765kV) by step-up transformers, and transmitted to distribution substations through transmission systems. Distribution substations use step-down transformers to lower voltages (less than 66kV) and distribute electricity to consumers (110V and 230V) through distribution systems. Centralized power generation may have many disadvantages, but mainstream power systems are based on this method of power generation [1,2]. Drawbacks of centralized generation include:

1. Costly management of large infrastructures
2. Susceptibility to unreliability and instability-related events
3. Vulnerability to terrorist attacks
4. Efficiency limitations
5. Environmental impacts
6. Stability required to sustain the system
7. Inability to be dispatched, with the exception of biomass.

Advancement in electric power generation related technology, high profit margins, increased power system reliability, and reduced power system losses have promoted increased interest in distributed generation (DG). According to the National Renewable Energy Laboratory (NREL), the average maintenance cost of a natural gas or diesel-powered DG is 20%-25% of the operational cost [1] or fuel cost. DGs are categorized into conventional DG (CDG) and renewable DG (RDG) based on fuel type. Table 1.1 compares CDG and RDG characteristics.

Table 1.1 CDG and RDG comparison in a distribution system

Characteristic	CDG	RDG
Increased system reliability	✓	✓
Improved power quality	✓	✓
Improved infrastructure resilience	✓	✓
Reduced land-use effect	✓	✓
Reduced peak power	✓	✓
Availability of ancillary services (local reactive power supply)	✓	✓
Reduced system vulnerability	✓	✓
Reduced grid dependability	✓	✓
Load following power generation	✓	×
Availability of fuel on-demand	✓	×
Minimum impact on environment	×	✓
Unlimited and free energy sources	×	✓
Promotion of cost-effective energy production	×	✓
Energy price stability	×	✓
Fewer subsidies	×	✓

CDGs use conventional energy sources such as diesel and natural gas to generate electricity. Excessive heat dissipation, noise, high capital costs, and unnecessary operational and maintenance costs are concerns associated with CDGs in distribution systems. CDGs also lack in efficiency and emit greenhouse gases such as carbon dioxide (CO_2). RDG utilizes naturally replenished, theoretically inexhaustible energy sources not derived from fossil or nuclear power in order to produce energy. Examples of energy sources used by RDG include wind power, solar irradiation, ocean waves, and geothermal heat. Environmental impact of RDGs such as wind

turbines, solar panels, tidal wave generators, and geo-thermal units are minimum. Distributed wind generation (DWG) is used as RDGs in this research. Table 1.2 compares advantages and disadvantages of wind turbines to other RGDs.

Table 1.2 Advantages and disadvantages of DWG compared to other RDGs

Characteristic	Wind Turbines	Solar Panels	Biomass	Fuel Cell
Energy capacity	High	Low	High	Medium
Capital cost ($/KW)	High	High	High	Low
Operational and maintenance (O&M) cost	Medium	Low	High	Low
Ancillary services	Yes	No	Yes	No
Stochastic power generation	High	Low	Low	No
Greenhouse gas emission	Low	None	Medium	Low
Efficiency	Medium	Low	Low	High

The primary disadvantage of wind turbine is intermittent power generation. Wind turbines intermittent power generation presents numerous operational and planning challenges when applied to electrical power systems, regardless of technologies used for wind power generation. Negative impact of intermittent power generation can be reduced, by using accurate weather forecasts. However, for a system with high utilization of wind power, distributed energy storage solutions (DESS) [3] are essential to store excess wind energy (spill energy), in order to balance load demand and local renewable power generation. Pumped hydro, flow battery systems, chemical battery storage [4], compressed air energy storage, flywheels, superconducting magnetic energy storage, and supercapacitors are examples of grid energy storage technologies.

Optimum capacity and placement of DWG/DESS in a distribution system is necessary, in order to prevent power system complexities such as overvoltage, increased power loss, unavailability of power, and increased O&M costs [5]. Therefore, optimum distributed generation planning (ODGP) is performed in this study to investigate the impact of CDG and DWG/DESS in a distribution system.

This dissertation structured on progressive ODGP. First, ODGP is performed on CDG with an analytical method, in order to minimize effects of planned power reroutes with respect to O&M costs, voltage profile, and real power losses. Next, DWG and distributed sodium sulfur (NaS) are optimized with reference to power losses, voltage profile, DWG/NaS availability, and present value of savings, in order to supply base power demand of a three-phase unbalanced distribution system and sustain power in a power failure that last for 1.5-hours. A meta-heuristic method, non-dominated sorting genetic algorithm II (NSGA-II), is used in this phase with consideration of technical, economic, and environmental constraints.

Results showed that the NSGA-II method identifies optimum solutions and more efficiently handles multi-objective problems than analytical methods. In-depth analyses of the NSGA-II method compared to other optimization techniques are discussed in chapter 1 under the title "Optimization Methods". The remainder of Chapter 1 is an overview of the scope and content of the progressive ODGP structure, including a detailed guide to the entire dissertation.

Motivation

Power system blackouts are a major concern for centralized generation [6,7]. In 2002, Canadian authorities conducted "Blue Cascades" a simulated terrorist attack on Northwest power grid [8]. The "Blue Cascades" simulation revealed that, if successful, a similar attack could trigger cascading blackouts in Northwest power grid. Recent studies have also suggested the high frequency of blackouts in the United States [9]. Although, human error is the primary cause of power grid blackouts, centralized power generation cause the impact area to cascade. Therefore, increased decentralized generation with multiple power generation points decreases the probability of cascading power grid failures. In addition, providing base power of a power

distribution system with DWG/DESS enhance the system robustness, resource independence, and grid independence.

Objective

This study addressed optimization of DWG/NaS with reference to real power loss, voltage profile, DWG/NaS availability and present value of system savings, using NSAGA-II method in a three-phase unbalanced radial distribution system in order to provide base power demand (40% of peak power demand) of the system and sustain the system for a maximum of 1.5 hours in a event of power grid failure.

Distributed generation as a base power load

Grid independence generates interconnecting micro-grids that use national or regional infrastructure, thereby, providing opportunity to increase revenue by being a small-scale power producer. Additional revenue increases can be achieved by reselling purchased power from the main grid to customers who are connected to the distribution system.

According to the U.S. Energy Information Administration (EIA), in 2013 the United States generated 4,058 billion kilowatt-hours (kWh) of electricity [10]. Approximately 67% of generated electricity was derived from fossil fuels: 39% from coal, 27% from natural gas, and 1% from petroleum. Although electricity can be produced in bulk using fossil fuels, CDGs have the following disadvantages which exclude them from as the base power source in a distribution system: excessive investment cost, high O&M costs, high heat-dissipation, minimum load level limitations, negative environmental impact, and complexities of energy resource logistics. However, natural gas and petroleum-based DGs are currently used as CDG in distribution systems to partially supplement energy demand in peak power conditions and emergency situations such as temporary power grid blackouts. In contrast, RDGs, specifically DWG and

battery energy storage systems (BESS), are prospective candidates for base power sources in distribution systems.

Renewable energy can replace fossil fuels and nuclear energy for electricity generation, hot water/space heating, motor fuels, and rural energy services [11]. In 2013, wind, solar, geothermal, biomass waste, biofuels, wood, and hydropower comprised only 9% of total electricity generated in the U.S. *Annual Energy Outlook* issued by the Department of Energy (DoE) in 2014, ranked renewable power generation second, behind natural gas, in capacity wise projected energy generation by 2040 [12]. In addition, DoE stated that wind, solar, biomass, and fuel cell technologies have established potential as candidates for increased RDG applications [13].

Advantages and disadvantages of wind turbines as RDG are presented in Table 1.3.

Table 1.3 Advantages and disadvantages of wind energy as RDG

Advantages	Disadvantages
Local ownership	Variable generation
Fewer subsidies	Shadow flicker
Price stability	Noise
Short- and long-term job creation	Aesthetic
Cost-effective energy production	Radar interference
Revival of rural economy - Added tax base	Biological resource impact in construction
Conserve and maintenance of clean water	
Land preservation	
Clean air-no harmful particulates	
Negligible greenhouse gases	
Needn’t to mine and transport energy	

As presented in Tables 1.2 and 1.3, wind energy has many advantages compared to other RDG and CDG technologies, making it a leading candidate as a main base power source in a distribution system. Wind turbines produce electricity by converting energy in moving air into mechanical energy and then to AC electrical energy. Two types of wind turbines are available based on mounting axis: vertical and horizontal. Vertical access wind turbines are favorable for

commercial application because of high-energy production and low O&M cost. Wind turbines are categorized based on power ratings, such as small scale (≤ 100 kW), medium scale (100 kW< size ≤ 1 MW), and large scale (>1 MW). Large-scale wind turbines are primarily used for transmission and sub-transmission level applications, and small- and medium-scale wind turbines are used for distribution levels of the power system. In early years, wind turbines operated in pitch controlled, nearly constant-speed, and variable-speed modes. Years of operation and data gathering variable-speed mode to be the preferred mode at present. Primary goals of variable-speed mode include maximizing wind power capture and reducing stress on the blades, tower, and other components of wind turbine. Wind energy generated by an ideal wind turbine is presented in Equation (1.1).

$$P = \frac{1}{2}\rho C_p A V^3 \tag{1.1}$$

Where, P is generated power, ρ is air density, C_p is the Betz constant, A is wind turbine rotor sweep area, and V is wind velocity. For an ideal wind turbine, the Betz constant is 59%. Extractable power in a wind stream for a modern-day wind turbine is in the range of 35% to 45%. The non-ideal performance coefficient is presented in Equation (1.2).

$$C_{p.prac} \approx \frac{2}{5} = 0.4 \tag{1.2}$$

Wind turbines also required a minimum ground clearance in order to extract full potential of available wind. Figure 1.1 illustrates necessary ground clearance for a tower-based wind turbine. However, state-of-the-art technologies, such as Magenn Air Rotor System (MARS), are exempt from the minimum ground clearance code due to high altitude operation.

Figure 1.1 Flat ground clearance necessary for a wind turbine.

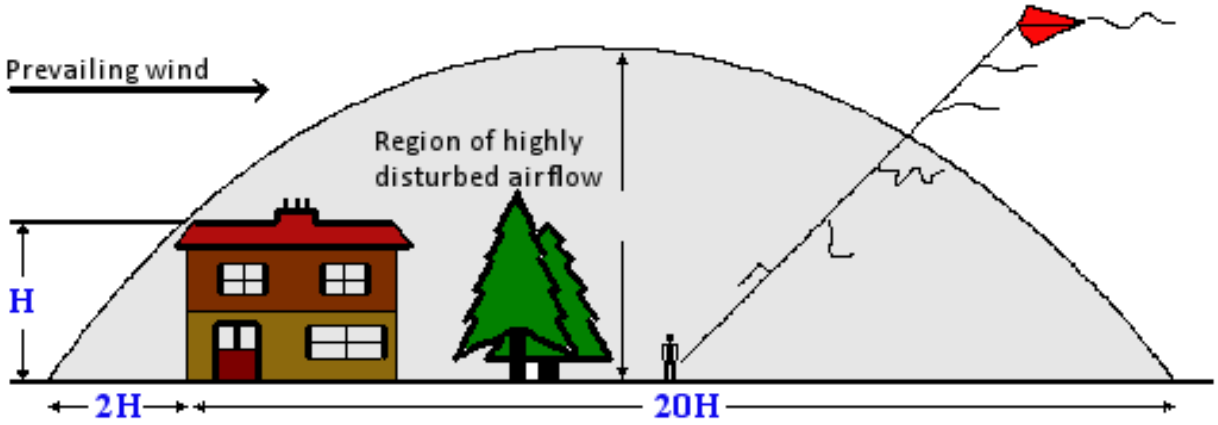

Despite of wind energy's advantages, its primary disadvantage is intermittent power generation. Although, placing wind turbines throughout a large geographical area can reduce variations of wind energy generation, power quality and availability expected in modern power systems is challenging to achieve. In addition, most distribution systems are spread throughout a small geographical area in which the wind speeds remain the same throughout the system.

Wind turbine power generation data used in the research is collected from a Northwind 100 (NW100) wind turbine installed at Riley County Public Works Facility, Manhattan, Kansas. Figure 1.2 illustrates the sample power generation data graph generated using NW100 power production data on November 2, 2011. The NW100 wind turbine has rated power of 100kW at 14.5m/s wind speed. In addition, NW100 is capable of providing ±45kVAR of reactive power regardless of the turbine's operating status (idle, generating, and service).

Figure 1.3 illustrates energy output of 76 wind turbines spread across a large geographical area in Chap-chat wind farm in Quebec, Canada that is connected to the main power grid via the transmission system. A comparison of power generated by a wind turbine (figure 1.2) to total power generated by multiple wind turbines spread throughout a large geographical (figure 1.3) yields that multi turbine power generation is much smoother than single

turbine. Therefore, in order to increase the capacity of DWG allocated in a distribution system a power compensation technique must be applied in order to mitigate the impact of variable wind energy generation in distribution systems. Increased wind energy is therefore, a function of the ability to regulate the power supply, which BESS should solve.

Figure 1.2 Fluctuation of instantaneous power of NW100 wind turbine on November 2, 2011, at Riley County Public Works Facility (Manhattan, KS).

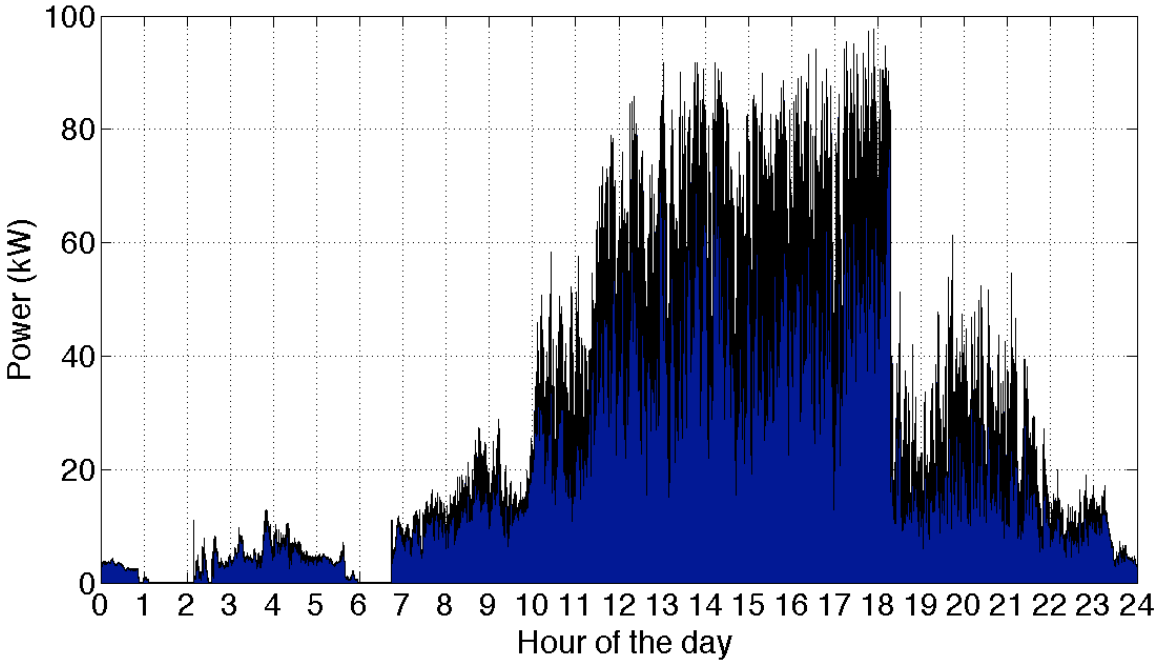

Figure 1.3 Fluctuation of instantaneous power on March 16, 2004, at Champ-chat wind farm (Quebec, Canada) [14]

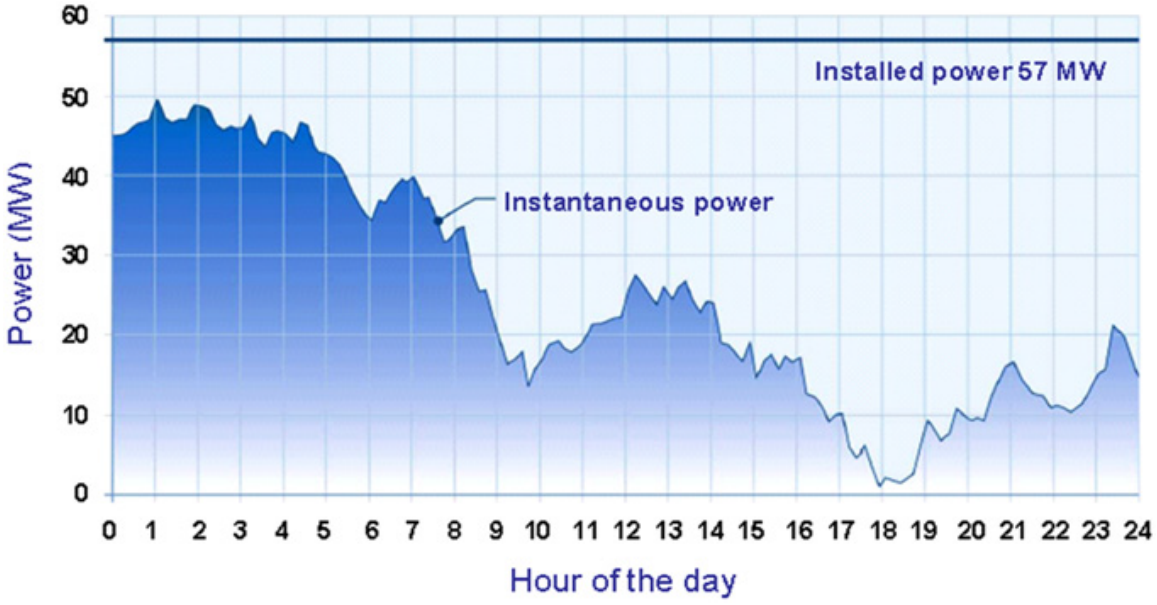

BESS as a compensation power source

Many possible energy storage techniques, found in practically all forms of energy: mechanical, chemical and thermal. These storage techniques can be divided into four categories according to their applications [14]: 1) Low-power application in isolated areas in order to feed transducers and emergency terminals, 2) Medium-power application in individual electrical systems and town supply (isolated areas), 3) Network connection application with peak leveling, and 4) Power quality control application.

Categories 1 and 2 refer to small-scale systems in which energy could be stored as flywheels, chemical battery systems, compressed air systems, or supercapacitors or stored in superconductors. Categories 3 and 4 apply to large-scale systems in which the energy can be stored as thermal energy, chemical energy, or compressed air.

Characteristics of energy storage systems can be categorized based on following criteria [14]: 1) Type of application: permanent or portable, 2) Storage duration: short- or long-term, and 3) Type of production: maximum power needed

Nine types of energy storage systems in the literature are considered as DESS based on the three criteria of energy storage system characteristics [14]: pumped hydro storage (PHS), thermal energy storage (TES), compressed air energy storage (CAES), flow batteries, fuel cells, chemical storage, flywheel energy storage (FES), superconducting magnetic energy storage (SMES), and supercapacitors.

Figure 1.4 illustrates the three primary categories of large-scale permanent energy storage techniques: 1) Required power quality, 2) Buffer and emergency storage, 3) Network management. Increased DWG placement demands large-scale permanent energy storage system that can manage the network. In addition, high-energy efficiency and high life expectancy (figure 1.5), and cost-per charge discharge cycle (figure 1.6) were considered when choosing a

DESS, in order to balance DWG power generation and load demand of the distribution system. A comprehensive analysis of the nine types of grid energy storage systems (PHS, TES, CAES, flow batteries, fuel cells, chemical storage, FES, SMES, and supercapacitors), yield drawbacks associated with each type of energy storage system: PHS requires a water source and water storage system, CAES requires an underground compressed air storage system, TES demonstrates low efficiency, FES require maintained high rotating kinetic power, supercapacitors work most efficiently when coupled with another energy storage system such as a battery, lack of efficiency and cost of SMES do not justify real-world applications, and chemical synthesis of hydrocarbon fuels (methane) has low efficiency if generated hydrocarbon is used to regenerate electricity.

Figure 1.4 Distribution of storage techniques as a function of their field of application [15].

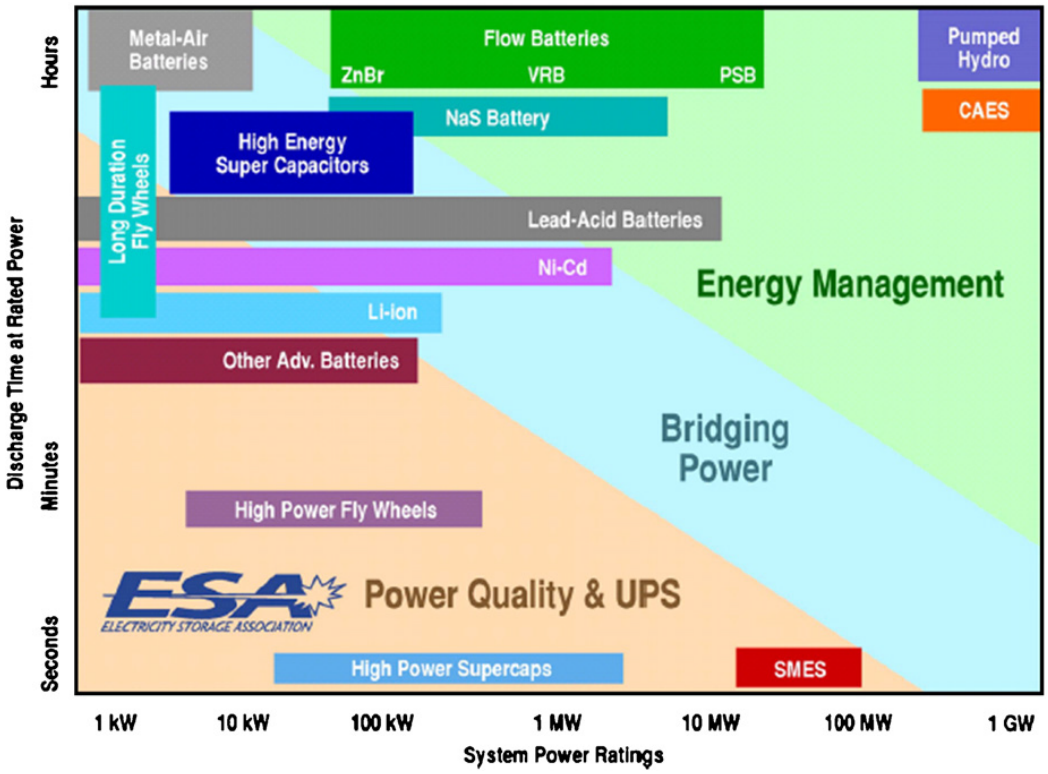

Figure 1.5 Distribution of storage techniques as a function of their energy efficiency and life span [15]

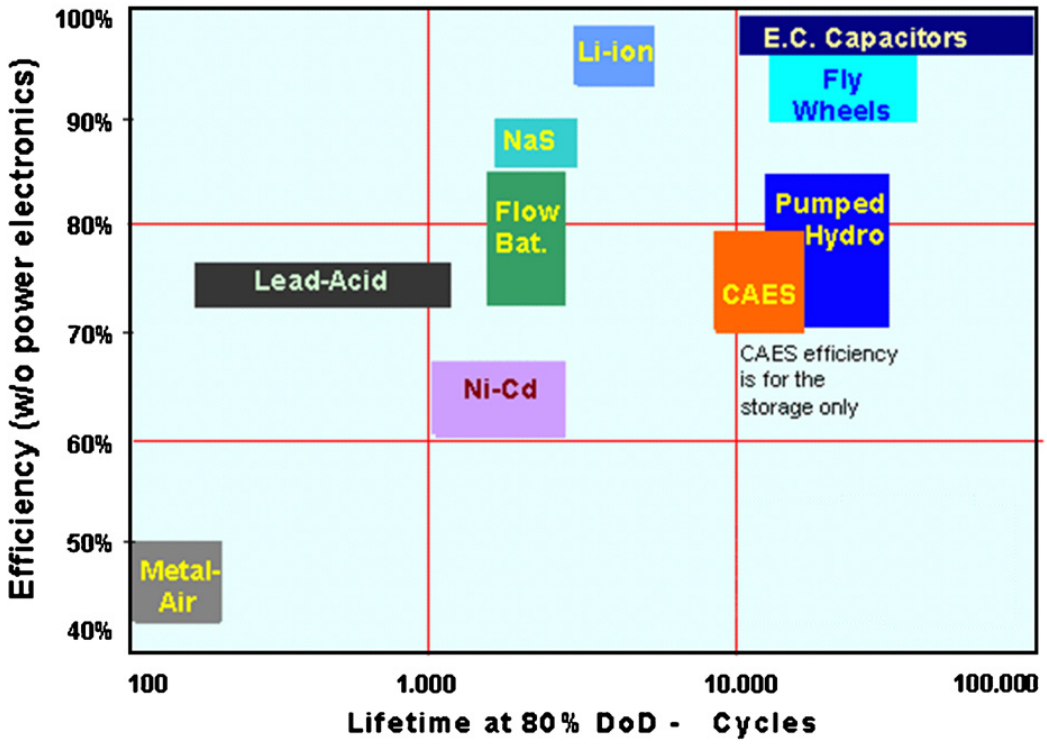

Figure 1.6 Distribution of storage techniques of as a function of investment cost calculated per unit energy [15].

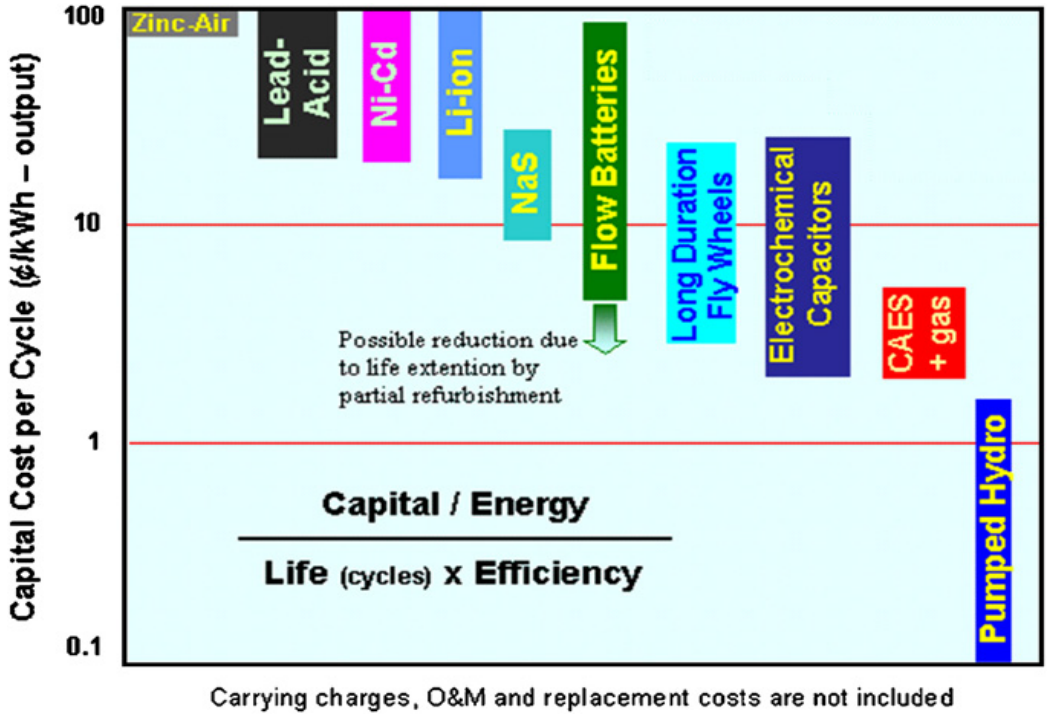

A comprehensive analysis of the nine energy storage techniques discusses in earlier paragraphs yields that FES and chemical battery storage systems have advantageous scalability, portability, high efficiency, low maintenance, and reduced land use [16, 17,18]. Therefore, FES and chemical batteries offer the optimum energy management solution for increased distributed renewable energy applications.

Referenced to the battery storage technology comparisons (Figures 1.4 to 1.6), NaS battery technology performed better than many other technologies. NaS battery systems are suitable for energy management systems and power bridging applications as demonstrated in Figure 1.4. In addition, NaS batteries are highly efficient, with 2000-5000 cycle lifetime at 80% depth of discharge (DoD), low capital cost per cycle ($/kWh) compared to other network management storage technologies such as Lithium-ion (Li-ion) and zinc air (Zn-Air) batteries. Further, NaS pulse power capability makes them a well-suited candidate for our specific grid application. Therefore, NaS batteries were selected as DESS in this study.

Economic viability of increased wind energy applications

Energy payback time is a more useful measurement compared to payback time in order to evaluate economic benefits of renewable generation [19]. Energy payback time is the ratio between total energy produced during a system's expected life span to energy required to build, maintain, and fuel that system. A high ratio indicates enhanced environmental performance. Comparison of convectional and renewable generation has revealed that intense focus of centralized conventional generations on the economic sector limits long-term benefits of renewable generation. As illustrated in Figure 1.7, wind energy demonstrates more than 4 and 6 times the energy payback time compared to coal and natural gas, respectively. In addition, wind energy is second lowest in investment cost ($/kW) compared to other energy resources, as shown

in Table 1.4. According to the DoE and U.S. EIA, wind energy unit costs expects a gradual decrease in the next two decades, allowing wind energy to be a legitimate competitor of coal and natural gas power generation. Therefore, considering portability, deployment, resource availability, and energy payback time, wind energy is a superior candidate for distributed operation compared to other energy generation methods.

Figure 1.7 Energy payback time for various electricity generation methods.

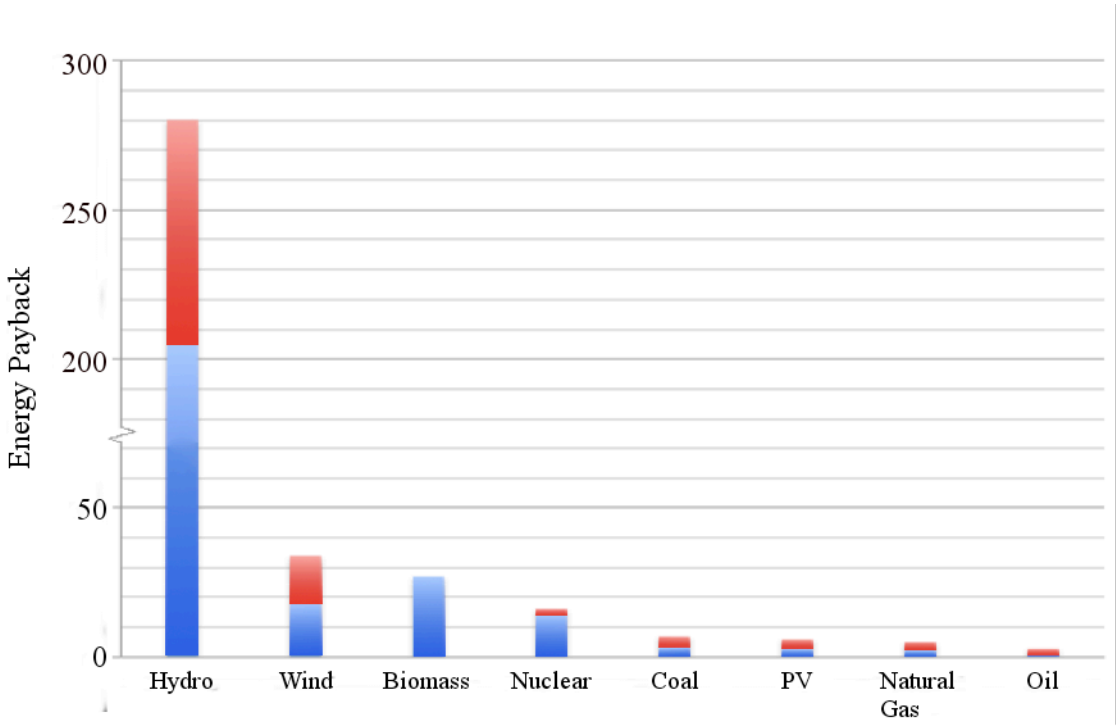

Table 1.4 Capital cost comparison and cost of electricity per kilowatt-hour of various grid energy technologies.

Energy Resource	Investment Cost ($/kW)	Electricity Unit Cost ($/kWh)
Coal	500	0.025
Wind	800	0.060
Natural Gas	1000	0.040
Hydroelectric	1000	0.050
Geothermal	2500	0.080
Nuclear	3000	0.650
Solar (PV)	4000	0.030

Optimization method

Optimization of DWG/NaS placement and size is a complex design challenge. Three primary approaches have been described in literature in order to address this challenge: the analytical approach, the numerical approach, and the heuristic approach [20]. A comparison of analytical, numerical and heuristic methods for ODGP highlights advantages and disadvantages of each method [20]. Analytical methods are easy to implement and can be quickly executed, but their results are suggestive due to simplified assumptions. Therefore, the analytical method may not be appropriate for uncertainties and stochastic optimization [21-23].

Numerical methods can be divided into seven subcategories: gradient [24], linear programming (LP) [25], sequential quadratic programing (SQP) [26], nonlinear programing (NLP) [27], dynamic programming (DP) [28], ordinal optimization (OO) [29], and exhaustive search [30]. Among available numerical methods for ODGP, the most computationally and algorithmically efficient methods are NLP, SQP, and OO. Numerical methods can be used for optimization of small systems but are inappropriate for large systems because of computational complexity. In addition, the DP method is also not suitable for large-scale systems.

The heuristic search method can be divided into eight subcategories: genetic algorithm (GA) [31-37], tabu search (TS) [38,39], particle swam optimization (PSO)[40-42], ant colony optimization (ACO) [43,44], artificial bee colony optimization (ABC) [45,46], differential evaluation (DE) [47,48], harmony search (HS) [49,50], and particle heuristic algorithm [36, 51]. Heuristic methods are typically robust and provide near-optimal solutions for large, complex ODGP problems. Although heuristic methods require high computational effort, that limitation is not necessarily critical to an ODGP problem. Therefore, heuristic methods perform better than analytical and numerical methods when optimizing multi-objective problems.

A meta-heuristic method, NSGA-II [52], was used to optimize the size and placement of DWG/NaS with reference to real power loss, voltage profile, availability, and present valur of savings, in order to provide base power demand using renewable resources and sustain the system in an event of power grid failure. NSGA-II was previously used to optimize DG size and placement in distribution systems [53-58].

The Primary Operational Model

Two scenarios of DWG/NaS optimization based on based load supply and short-term islanded operation are discussed. Energy dispatch scenarios for optimum DWG/NaS system are also discussed. Results indicated the possibility of using DWG/NaS as base power sources and to achieve short-term islanded operation in small-scale three-phase unbalanced radial distribution systems.

Simulations for this study were conducted for IEEE 37-node three-phase unbalanced radial distribution systems. In this study, normalized wind power generation curves, created using 15-minute-by-15-minute power generation data from a NW100 wind turbine, of low- and high-wind profiles, were used to simulate variable generation. Also, 1-hour load demand data gathered for 1-year period for 150 houses were used to generate a normalized load demand curve. Load demand data are interpolated to create 15-minute-by-15-minute load demand data to match the data points of the DWG generation.

The following assumptions were made in this study:

1. The distribution system contains necessary technologies to direct reverse power-flow if necessary.
2. Because distribution systems are spread in a small geographical area, each wind turbine follows normalized generation curves.

3. All connected loads are neighborhood loads, thereby, following the same load demand curve.
4. Every wind turbine continues to function during simulation.
5. NaS has 90% combined efficiency (charging and discharging efficiencies).
6. NaS can charge from DWG, main grid, or a combination of DWG and main grid;
    a. Wind energy and main grid can simultaneously charge the battery only if the battery-charging rate is not met with wind energy. Therefore, wind energy has battery-charging priority over the main grid.
    b. NaS battery banks can be discharged up to 90% of their total capacity.
7. All NaS systems continue to function during simulation.

Results

Use of CET method to optimize capacity and placement of DG in a radial distribution system

In this study, CET method was used to optimize capacity and placement of DGs in a radial distribution system considering intentional structural changes in a distribution system topology. Table1.5 presents capacity and placement of DGs that were required to minimize the effect of intentional structural changes in distribution topology. Table 1.6 presents system savings with respect to results in Table 1.5.

The analytical optimization results showed O&M cost reductions in 12-, 30-, and 69-node systems. Therefore, CET method successfully identified the optimum locations to place DGs, in order to minimize the effect of intentional structural changes in distribution topology due to power reroutes. In addition, CET method based DG placement improved the voltage profile of the system.

Table 1.5 Real power loss reduction percentages of the Network I, II, and III of the 12-, 30-, and 69-node systems according to 25% DG allocation of peak load

System	Peak Load (MVA)	PF(%)	DG Nodes	DG		Network	Loss Reduction
				Size (MW)	PF (%)		
12	31.30	97.3	4	1.2	97.3	I	55.07%
			5	3.1	95.3	II	56.09%
			9	2.7	94.9	III	56.87%
			12	0.8	91.3		
30	71.07	93.2	12	1.5	95.4	I	56.60%
			13	10.8	95.7	II	60.50%
			22	4	92.5	III	57.19%
			27	1.8	93.1		
69	186.40	81.6	32	3.7	93.8	I	64.66%
			41	5.6	93.6	II	69.83%
			57	1.9	95.9	III	64.64%
			65	35.4	92.1		

Table 1.6 NPV of savings from O&M cost reductions for coal and CC power plants

System	Network	NPV of savings from O&M cost reductions ($M)	
		Coal	CC
12	I	0.079	0.029
	II	0.082	0.031
	III	0.088	0.033
30	I	0.260	0.097
	II	0.322	0.120
	III	0.308	0.115
69	I	3.399	1.270
	II	2.731	1.020
	III	3.396	1.260

Optimize capacity and placement of DWG/NaS to supply base power demand of a three-phase unbalanced distribution system

DWG/NaS to supply base load demand

DWG/NaS capacity and placement optimization with respect to real power loss, voltage profile, DWG/NaS availability and present value of savings, in order to supply base load demand of the system contained fifty solutions in first Pareto front. Solution with the lowest amount of

NaS capacity was selected ($f_1 = 428$ kW, $f_2 = 0.01$ p.u., $f_3 = 0.409$, and $f_4 = \$2.33\times10^8$) to explain the optimization results. Table 1.7 presents the total DWG and NaS capacities required to supply the base power demand of the IEEE 37-test feeder.

Table 1.7 Total installed capacity of DWG/NaS

Total number of 75kW/25kW turbines installed	Total number of 50kW/25kW NaS units installed	Total installed wind generation capacity	Total installed NaS capacity	Total installed wind generation as a percentage of peak load demand	Total installed NaS as a percentage of peak load demand
12/12	7/19	1200 kW	825 kW	48.76%	33.52%

Total real power demand at peak load conditions of IEEE 37-node test feeder was 2461.255kW. NSGA-II optimization results yield that with 48.76% of peak load as DWG and 33.52% peak load as NaS can provide base power demand of IEEE 37-node test feeder and sustain power of the system in the event of a power grid failure. Figure 1.8 illustrates the system real power loss with and without DWG/NaS in low-wind profile.

Figure 1.8 Real power loss of the system in low-wind conditions

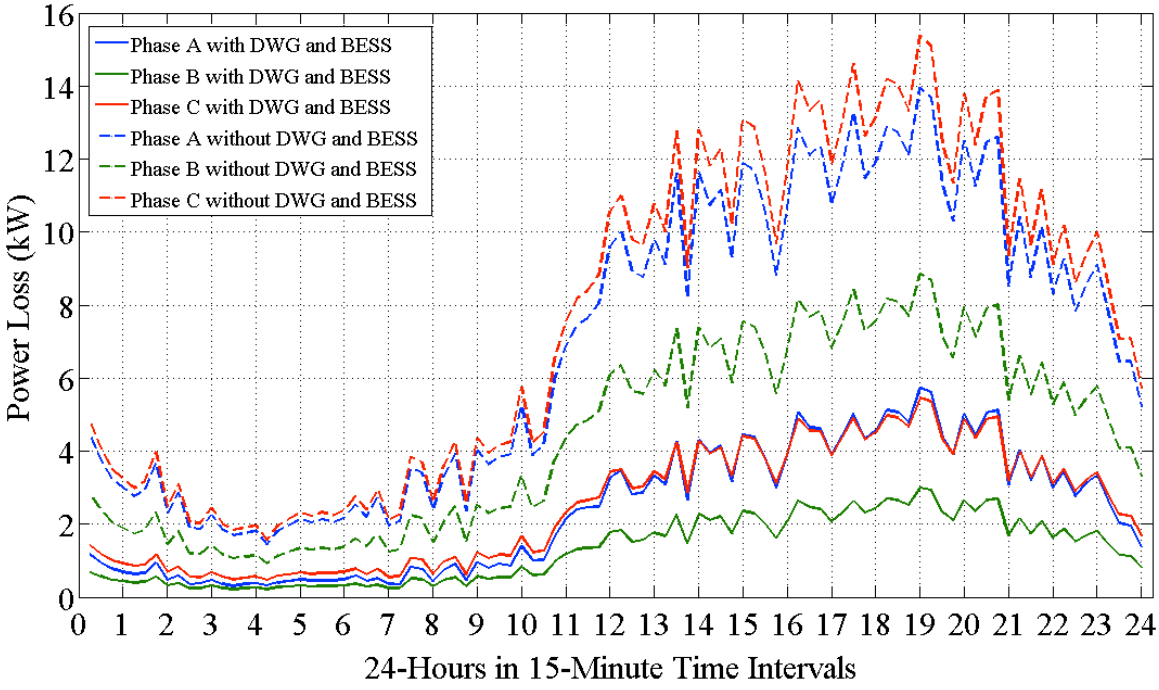

Figure 1.9 illustrates the DWG/NaS availability to provide load demand of the system over a 24-hour period. The DWG/NaS availability during low-wind conditions meets the minimum generation requirements for base load demand (40% of the peak load). Table 1.8 presents the net energy savings (NES) and simple payback period (SPP) calculations for the selected solution.

Figure 1.9 Availability of DWG/ NaS to supply base power demand of the system over a 24-hour period

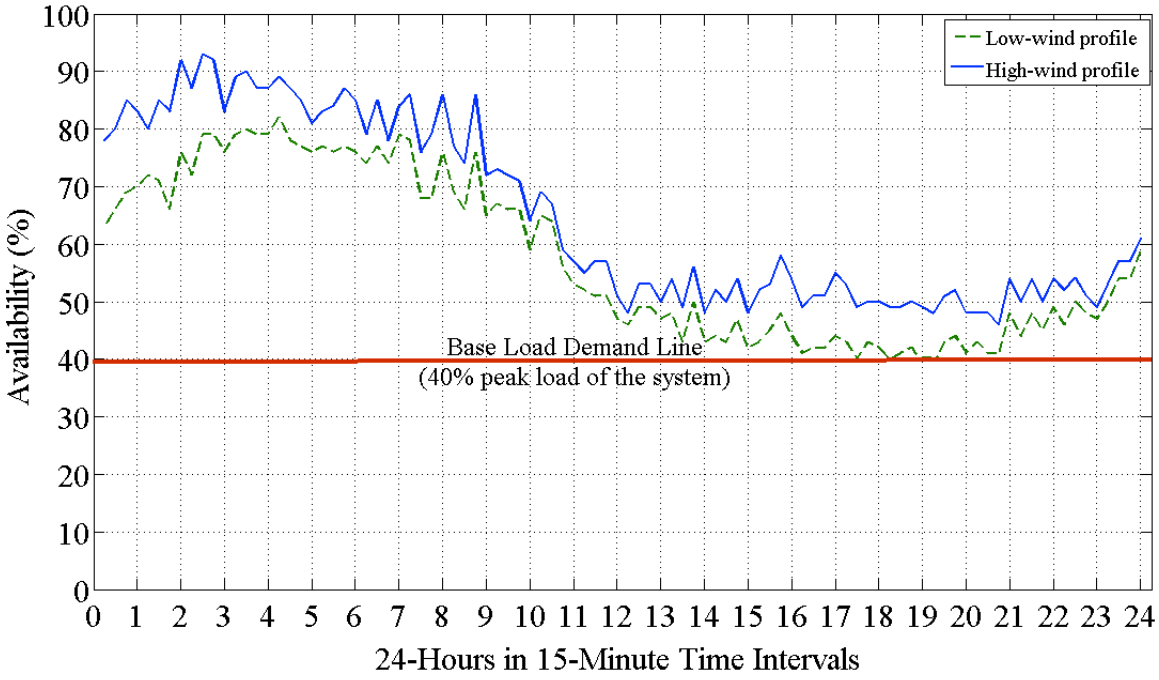

Table 1.8 NES and SPP calculations for the selected solution

SPP (Years)	Revenue of energy savings ($)	SPP (Including NaS salvage benefits) (Years)	Revenue of energy savings ($)
10.85 [a]	1349391.32	9.92 [a]	1486542.57
14.98 [b]	740321.80	14.06 [b]	875998.30

a. Installation cost for a 1-10 MW wind turbine, $2220/kW is used to calculate simple payback period.

b. Installation cost for 10-100 kW wind turbine, $6389/kW is used to calculate simple payback period.

DWG/NaS to sustain power to the system in power grid failure

Optimum capacity and placement of DWG/NaS with respect to real power loss, voltage profile, DWG/NaS availability and present value of system savings, in order to supply base

power demand of a three-phase unbalanced radial distribution system and sustain power for 1.5 hours during a power grid failure were conducted in a single optimization. Power system failure that can last up 1.5 hours was introduced to analyze the system's credibility to sustain power to a distribution system. Power system failure was introduced during the peak demand hours, 6:30 PM to 8:00 PM to maximize effects of power loss.

Figure 1.10 Real power loss of the IEEE 37-node test feeder when islanded operation during the power grid failure between 6:30PM-8PM in low-wind profile.

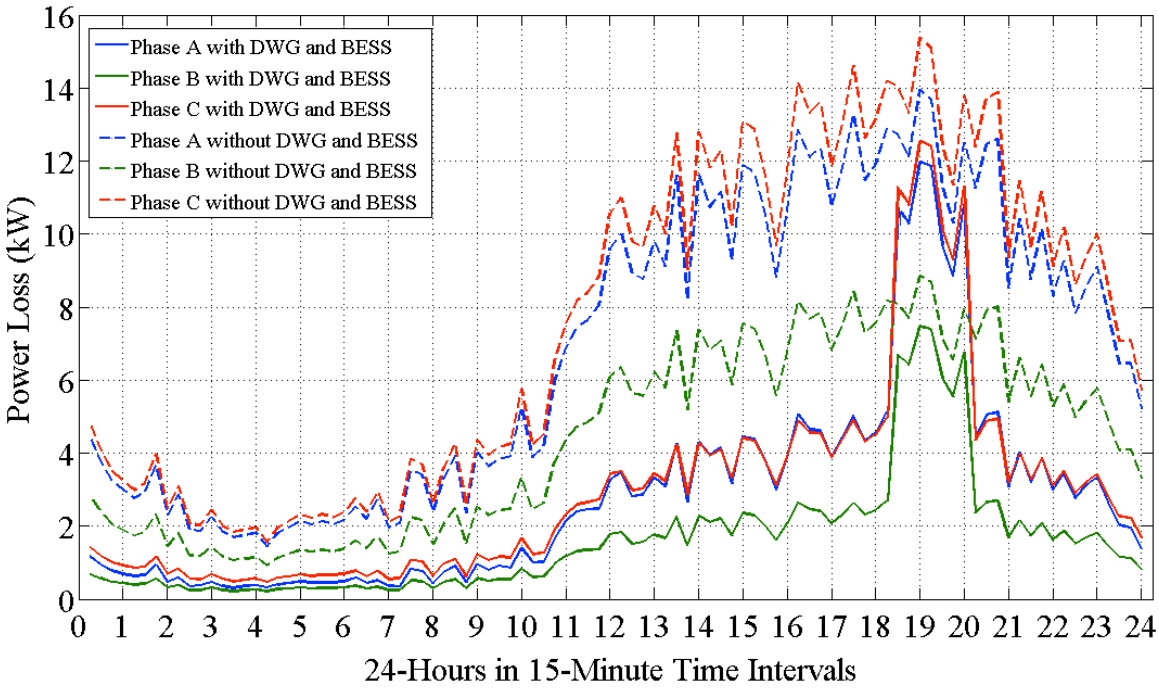

Figure 1.10 illustrates system real power loss during the power failure. Sudden increase in system power loss was a result of low efficiency in NaS pulse power mode and increased power flow in distribution system lines. NaS units were calculated to operate between 100% and 230% of capacity factor during power grid failure. In addition, efficiency of the NaS units was expected to decrease from 90% to 77% in pulse power mode.

Figure 1.11 Availability of DWG/BESS to sustain IEEE 37-node test system in a power grid failure that last for 1.5-hours.

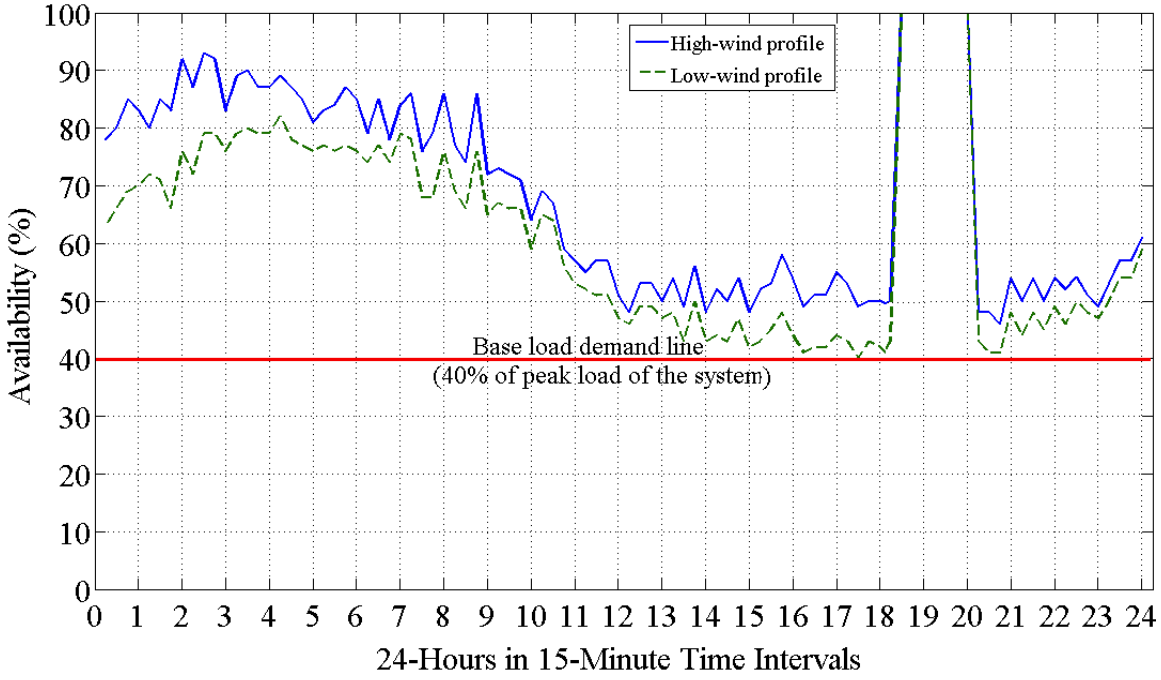

DWG/NAS availability during a power grid failure is illustrated in Figure 1.11. DWG/NaS availability was 100% during the power failure. During the power failure, NaS units' depth of discharge (DOD) was changed from 90% to 100%. At midnight, DOD changed back to 90%. Increased DOD ensured NaS availability during the power grid failure and until end of the day.

Charging/ discharging of NaS units during base power supply states including the power grid failure is illustrated in Figure 1.12. Figure 1.13 illustrates energy variation graph of 50kW and 25kW NaS units with respect to charging/discharging patterns illustrated in Figure 1.12. Managing charge/discharge patterns of NaS units by overseeing total power demand of the system generated two power cures for 50kW and 25kW NaS units.

Figure 1.12 Charging/discharging cycle of 50kW/25kW NaS modules including power usage

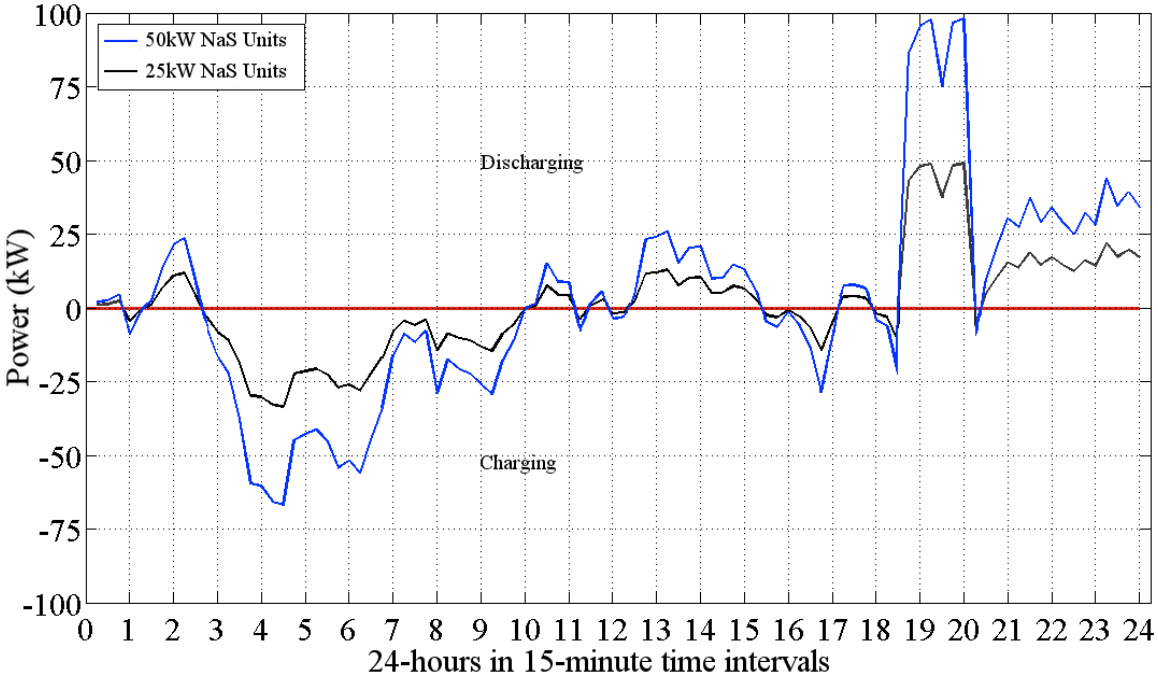

Figure 1.13 50kW and 25kW NaS units' energy variation and pulse power discharge

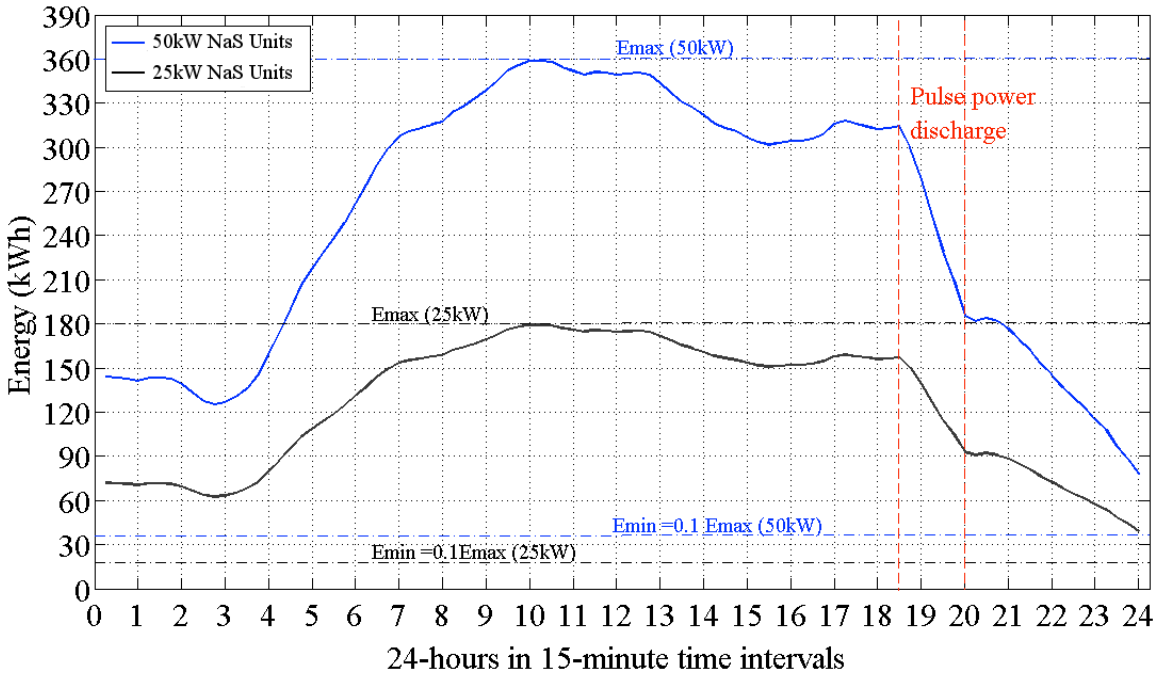

Dissertation Structure

The chapters of this dissertation can generally be read independently since they describe different facets of ODGP problem: statistical, algorithm, modeling, simulations, and review of experimental evaluation. However, the chapters are arranged in a natural sequence and refer to one another.

Chapter 1 presents an executive summary of the research plan, including context of the work, motivation of the research, objectives, an operational research model, and results.

Chapter 2 presents an analytical optimization technique for placement and size of DG with respect to network losses and voltage profile. The primary purpose of this chapter is to resolve the effects of intentional structural changes as they pertain to the topology of a radial distribution system in an ODGP problem. A new method is proposed that is based on electrical centrality in order to neutralize the impact of intentional structural changes and resolve renewable ODGP in radial distribution systems. DG size was calculated using an exhaustive method, and optimum DG penetration was achieved with 1% DG size increments in each step of the iteration.

Chapter 3 discusses placement and size of the optimum amount of DWG/NaS with reference to real power losses, voltage profile, DWG/NaS availability, and present value of savings, in a three-phase unbalanced radial distribution system in order to supply base power demand and sustain power of a distribution system for 1.5 hours in the event of a power grid failure. The NSGA-II method was used to optimize the constrained multi-objective function, and constraints were handled using the penalty factor approach. The solution set or first Pareto font of the NSGA-II method was chosen and specific solutions were selected based on input parameters of the system.

Chapter 4 offers comprehensive discussion of the study, conclusion, recommendation and future direction.

References

[1] J. Martin, "Distributed vs. centralized electricity generation: are we witnessing a change of paradigm," *An Introduction to Distributed Generation.Paris: HEC:< Www.Vernimmen.net/ftp/An_introduction_to_distributed_generation.Pdf,* 2009.

[2] D. Alfonso, C. Perpiñá, A. Pérez-Navarro, E. Peñalvo, C. Vargas and R. Cárdenas, "Methodology for optimization of distributed biomass resources evaluation, management and final energy use," *Biomass Bioenergy,* vol. 33, pp. 1070-1079, 2009.

[3] X. Li, D. Hui and X. Lai, "Battery energy storage station (BESS)-based smoothing control of photovoltaic (PV) and wind power generation fluctuations," *Sustainable Energy, IEEE Transactions on,* vol. 4, pp. 464-473, 2013.

[4] G. Zheng, S. W. Lee, Z. Liang, H. Lee, K. Yan, H. Yao, H. Wang, W. Li, S. Chu and Y. Cui, "Interconnected hollow carbon nanospheres for stable lithium metal anodes," *Nat Nano,* vol. advance online publication, 07/27, 2014.

[5] K. Divya and J. Østergaard, "Battery energy storage technology for power systems—An overview," *Electr. Power Syst. Res.,* vol. 79, pp. 511-520, 2009.

[6] P. Pourbeik, P. S. Kundur and C. W. Taylor. The anatomy of a power grid blackout-root causes and dynamics of recent major blackouts. *Power and Energy Magazine, IEEE 4(5),* pp. 22-29. 2006.

[7] S. Tamronglak, S. Horowitz, A. Phadke and J. Thorp, "Anatomy of power system blackouts: preventive relaying strategies," *Power Delivery, IEEE Transactions on,* vol. 11, pp. 708-715, 1996.

[8] B. J. Hardenbrook, "The need for a policy framework to develop disaster resilient regions," *Journal of Homeland Security and Emergency Management,* vol. 2, 2005.

[9] Dobson, B. A. Carreras, V. E. Lynch and D. E. Newman, "Complex systems analysis of series of blackouts: Cascading failure, critical points, and self-organization," *Chaos: An Interdisciplinary Journal of Nonlinear Science,* vol. 17, pp. 026103, 2007.

[10] U. N. I. Council. Fuels used in electricity generation. 2013.

[11] S. Kaul, "Renewable Power Generation,".

[12] A.E. Outlook. Energy information administration. *Department of Energy* 2014.

[13] A. Khaligh and O. C. Onar, *Energy Harvesting: Solar, Wind, and Ocean Energy Conversion Systems*. CRC Press Inc., 2010.

[14] H. Ibrahim, A. Ilinca and J. Perron, "Energy storage systems-characteristics and comparisons," *Renewable and Sustainable Energy Reviews,* vol. 12, pp. 1221-1250, 2008.

[15] Energy Storage Association, "Technology Comparisons [Online] Available: http://www. electricitystorage. org," *Esa/technologies,* .

[16] B. Dunn, H. Kamath and J. M. Tarascon, "Electrical energy storage for the grid: a battery of choices," *Science,* vol. 334, pp. 928-935, Nov 18, 2011.

[17] J. Eyer and G. Corey, "Energy storage for the electricity grid: Benefits and market potential assessment guide," *Sandia National Laboratories,* 2010.

[18] A. Khaligh and Z. Li, "Battery, ultracapacitor, fuel cell, and hybrid energy storage systems for electric, hybrid electric, fuel cell, and plug-in hybrid electric vehicles: State of the art," *Vehicular Technology, IEEE Transactions on,* vol. 59, pp. 2806-2814, 2010.
[19] L. Schleisner, "Life cycle assessment of a wind farm and related externalities," *Renewable Energy,* vol. 20, pp. 279-288, 2000.
[20] P. S. Georgilakis and N. D. Hatziargyriou, "Optimal distributed generation placement in power distribution networks: Models, methods, and future research," *IEEE Trans. Power Syst.,* vol. 28, pp. 3420-3428, 2013.
[21] H. L. Willis, "Analytical methods and rules of thumb for modeling DG-distribution interaction," in *Power Engineering Society Summer Meeting, 2000. IEEE,* 2000, pp. 1643-1644.
[22] C. Wang and M. H. Nehrir, "Analytical approaches for optimal placement of distributed generation sources in power systems," *Power Systems, IEEE Transactions on,* vol. 19, pp. 2068-2076, 2004.
[23] N. Acharya, P. Mahat and N. Mithulananthan, "An analytical approach for DG allocation in primary distribution network," *International Journal of Electrical Power & Energy Systems,* vol. 28, pp. 669-678, 2006.
[24] N. S. Rau and Y. Wan, "Optimum location of resources in distributed planning," *Power Systems, IEEE Transactions on,* vol. 9, pp. 2014-2020, 1994.
[25] A. Keane and M. O'Malley, "Optimal allocation of embedded generation on distribution networks," *Power Systems, IEEE Transactions on,* vol. 20, pp. 1640-1646, 2005.
[26] P. N. Vovos, G. P. Harrison, A. R. Wallace and J. W. Bialek, "Optimal power flow as a tool for fault level-constrained network capacity analysis," *Power Systems, IEEE Transactions on,* vol. 20, pp. 734-741, 2005.
[27] Y. Atwa, E. El-Saadany, M. Salama and R. Seethapathy, "Optimal renewable resources mix for distribution system energy loss minimization," *Power Systems, IEEE Transactions on,* vol. 25, pp. 360-370, 2010.
[28] N. Khalesi, N. Rezaei and M. Haghifam, "DG allocation with application of dynamic programming for loss reduction and reliability improvement," *International Journal of Electrical Power & Energy Systems,* vol. 33, pp. 288-295, 2011.
[29] R. Jabr and B. Pal, "Ordinal optimisation approach for locating and sizing of distributed generation," *IET Generation, Transmission & Distribution,* vol. 3, pp. 713-723, 2009.
[30] D. Zhu, R. P. Broadwater, K. Tam, R. Seguin and H. Asgeirsson, "Impact of DG placement on reliability and efficiency with time-varying loads," *Power Systems, IEEE Transactions on,* vol. 21, pp. 419-427, 2006.
[31] R. Singh and S. Goswami, "Optimum siting and sizing of distributed generations in radial and networked systems," *Electric Power Components and Systems,* vol. 37, pp. 127-145, 2009.
[32] C. L. Borges and D. M. Falcao, "Optimal distributed generation allocation for reliability, losses, and voltage improvement," *International Journal of Electrical Power & Energy Systems,* vol. 28, pp. 413-420, 2006.
[33] D. Singh and K. Verma, "Multiobjective optimization for DG planning with load models," *Power Systems, IEEE Transactions on,* vol. 24, pp. 427-436, 2009.
[34] H. Hedayati, S. A. Nabaviniaki and A. Akbarimajd, "A method for placement of DG units in distribution networks," *Power Delivery, IEEE Transactions on,* vol. 23, pp. 1620-1628, 2008.

[35] G. Carpinelli, G. Celli, F. Pilo and A. Russo, "Embedded generation planning under uncertainty including power quality issues," *European Transactions on Electrical Power,* vol. 13, pp. 381-389, 2003.
[36] G. P. Harrison, A. Piccolo, P. Siano and A. R. Wallace, "Hybrid GA and OPF evaluation of network capacity for distributed generation connections," *Electr. Power Syst. Res.,* vol. 78, pp. 392-398, 2008.
[37] K. Vinothkumar and M. Selvan, "Fuzzy embedded genetic algorithm method for distributed generation planning," *Electric Power Components and Systems,* vol. 39, pp. 346-366, 2011.
[38] K. Nara, Y. Hayashi, K. Ikeda and T. Ashizawa, "Application of tabu search to optimal placement of distributed generators," in *Power Engineering Society Winter Meeting, 2001. IEEE,* 2001, pp. 918-923.
[39] M. E. H. Golshan and S. Ali Arefifar, "Optimal allocation of distributed generation and reactive sources considering tap positions of voltage regulators as control variables," *European Transactions on Electrical Power,* vol. 17, pp. 219-239, 2007.
[40] W. Prommee and W. Ongsakul, "Optimal multi-distributed generation placement by adaptive weight particle swarm optimization," in *Control, Automation and Systems, 2008. ICCAS 2008. International Conference on,* 2008, pp. 1663-1668.
[41] M. Moradi and M. Abedini, "A combination of genetic algorithm and particle swarm optimization for optimal DG location and sizing in distribution systems," *International Journal of Electrical Power & Energy Systems,* vol. 34, pp. 66-74, 2012.
[42] M. Gomez-Gonzalez, A. López and F. Jurado, "Optimization of distributed generation systems using a new discrete PSO and OPF," *Electr. Power Syst. Res.,* vol. 84, pp. 174-180, 2012.
[43] L. Wang and C. Singh, "Reliability-constrained optimum placement of reclosers and distributed generators in distribution networks using an ant colony system algorithm," *Systems, Man, and Cybernetics, Part C: Applications and Reviews, IEEE Transactions on,* vol. 38, pp. 757-764, 2008.
[44] H. Falaghi and M. Haghifam, "ACO based algorithm for distributed generation sources allocation and sizing in distribution systems," in *Power Tech, 2007 IEEE Lausanne,* 2007, pp. 555-560.
[45] A. A. Seker and M. H. Hocaoglu, "Artificial bee colony algorithm for optimal placement and sizing of distributed generation," in *Electrical and Electronics Engineering (ELECO), 2013 8th International Conference on,* 2013, pp. 127-131.
[46] F. S. Abu-Mouti and M. El-Hawary, "Optimal distributed generation allocation and sizing in distribution systems via artificial bee colony algorithm," *Power Delivery, IEEE Transactions on,* vol. 26, pp. 2090-2101, 2011.
[47] J. Gunda and N. A. Khan, "Optimal location and sizing of DG and shunt capacitors using differential evolution," *International Journal of Soft Computing,* vol. 6, pp. 128-135, 2011.
[48] L. Arya, A. Koshti and S. Choube, "Distributed generation planning using differential evolution accounting voltage stability consideration," *International Journal of Electrical Power & Energy Systems,* vol. 42, pp. 196-207, 2012.
[49] R. Rao, K. Ravindra, K. Satish and S. Narasimham, "Power loss minimization in distribution system using network reconfiguration in the presence of distributed generation," *Power Systems, IEEE Transactions on,* vol. 28, pp. 317-325, 2013.

[50] K. Nekooei, M. M. Farsangi, H. Nezamabadi-Pour and K. Y. Lee, "An improved multi-objective harmony search for optimal placement of DGs in distribution systems," *Smart Grid, IEEE Transactions on,* vol. 4, pp. 557-567, 2013.
[51] S. Ghosh, S. Ghoshal and S. Ghosh, "Optimal sizing and placement of distributed generation in a network system," *International Journal of Electrical Power & Energy Systems,* vol. 32, pp. 849-856, 2010.
[52] K. Deb, A. Pratap, S. Agarwal and T. Meyarivan, "A fast and elitist multiobjective genetic algorithm: NSGA-II," *Evolutionary Computation, IEEE Transactions on,* vol. 6, pp. 182-197, 2002.
[53] A. Dehghani-Arani and R. Maddahi, "Introduction a multi-objective function in unbalanced and unsymmetrical distribution networks for optimal placement and sizing of distributed generation units using NSGA-II," in *Electrical Power Distribution Networks (EPDC), 2013 18th Conference on,* 2013, pp. 1-9.
[54] M. Ahmadi, A. Yousefi, A. Soroudi and M. Ehsan, "Multi objective distributed generation planning using NSGA-II," in *Power Electronics and Motion Control Conference, 2008. EPE-PEMC 2008. 13th,* 2008, pp. 1847-1851.
[55] P. Siano and G. Mokryani, "Evaluating the Benefits of Optimal Allocation of Wind Turbines for Distribution Network Operators," 2013.

Chapter 2 - Use of Combined Electrical Topology Method to Optimize Placement and Capacity of Distribution Generation Considering Intentional Structural Changes in Distribution System Topology

In this chapter, we use an analytical method called “combined electrical topology (CET),” based on electrical centrality to locate the optimum nodes for DG placement, considering power flow reroutes created by intentional structural changes in distribution system. Power flow reroutes provide essential services ensuring service reliability by changing the topology of the original network. The CET method, which utilizes magnitude of impedance matrices of different power systems, created by intentional structural changes, is useful in determining optimum locations for DGs. DG placement based CET method prediction, help minimize real system power loss by improving the voltage profile and reducing O&M costs of the power grid. Sizes of DGs to be allocated were calculated using an exhaustive search algorithm. Results indicated that the CET method can be used to size and site DGs in order to minimize system losses by improving the voltage profile and lowering the O&M costs of the power grid.

Introduction

DG has been defined as “installation and operation of electrical power generation units connected directly to the distribution network or connected to the network on the customer side of the meter” [1]. DG provides system improvements such as resolution of long-distance power transfer complexities, mitigation of cascading failures in power grids, and improvement of power quality [2]. However, unsupervised allocation of DG can cause negative effects in a power system, such as increased system losses and high voltage profile (>1.05 p.u) [3,4].

Recent advances in smart-grid technologies promote high utilization of DG and renewable DG in distribution systems. Related studies suggest that optimum distributed generation planning and design can improve power quality [5], voltage profile [6], and voltage unbalance factors [7] while providing local reactive power support.

In addition, DG allocation into a distribution system impacts planned power reroutes in the system. Rerouting power flow in a distribution system is typically achieved by devices such as network switches, circuit breakers, and fuses. These power flow reroutes ensure uninterrupted service of the network in the event of a line or equipment failure [8]. Rerouted power flow changes the original network structure, resulting in altered power-flow paths while the primary network topology remains intact [9,10]. However, distribution system nodes can bypass the fault via a reroute without interrupting primary network topology of the power flow.

Therefore, siting and sizing of DGs is very critical and need to be optimized with respect to nodal voltage, O&M cost, and real power loss of the system to maximize the efficiency of distribution systems. Electrical centrality [11] is an established analytical method used for the placement of DGs in a distribution system. Electrical centrality distinguishes electrical topology from physical topology of the network. Successful use of the electrical centrality method with the complex network approach to size and site DGs in distribution systems and successfully analyze of transmission system vulnerability can be found in literature [12,13]. Therefore, the electrical centrality method is applicable in DG placement, considering the impact of intentional structural changes of distribution systems.

During this study we used CET method, based on electrical centrality, to determine the placement and size of DGs in a radial distribution system, considering intentional structural changes. The CET method creates an electrical topology common to all sub-networks (networks

created by intentional structural changes) of a given distribution system in order to identify optimum locations for DG allocation. We assumed that all power flow reroutes occurred due to structural changes did not change the radial topology of the system. Results of this research demonstrated the significance and impact of structural changes to optimum DG placement and predicted the optimum nodes for DG placement in descending order.

Method

Electrical Topology and Intentional Structural Changes in a Distribution System

The power distribution system in the United States is aging, consequently causing reliability complexities such as line faults and equipment failures, resulting in power outages that interrupt the typical operation of a power system. Compulsory maintenance for antiquated equipment and lines requires power-flow rerouting in order to ensure uninterrupted service to the end user; therefore, power reroutes are intentionally planned during the power system design phase to safeguard uninterrupted service. DG sizing and siting without consideration of these power reroutes may increase total power loss and outbound the voltage profile of the system.

This study focus on determination of optimum DG placement with respect to nodal voltage, O&M costs and real power loss in a distribution system in order to minimize the impact of planned power reroutes. The study was carried out using 12-, 30-, and 69-node radial distribution systems.

Although DGs can be allocated in multiple locations on a system, a maximum of four locations were selected in this study in order to prevent voltage overload, unnecessary project cost, and high computational complexity. Several assumptions were made to simplify the approach: a) the new branch that reroutes power has equal or higher impedance than the fault line, b) each node of a given system is a candidate node for DG placement, c) DGs are capable of

providing real and reactive power, d) the distribution system is always connected to the main grid, and e) although many power reroutes may be available in a distribution system, only three primary power reroutes were considered for ease of explanation. However, the CET method can be easily modified to accommodate any number of power reroutes. Line segment failures that can affect the highest number of nodes were also considered in order to maximize the impact of power reroutes.

Electrical Centrality

Electrical centrality measures the electrical connectivity of the nodes in a distribution system; therefore, electrical topology differs from the physical topological structure of the network. Figure 2.1 (A), (B) and (C) represent physical topologies, corresponding electrical topologies for the considered power reroutes, and combined electrical topology of 12-node distribution system, respectively. Tangible power flow is illustrated by physical topology of the system (Figure 2.1 (A)), while electrical centrality demonstrates virtual electrical bonds between system nodes (Figure 2.1 (B)).

Electrical centrality is a metric based on the magnitude of impedance matrix (Z_{bus}) of the distribution system. The Z_{bus} matrix is calculated from the admittance matrix (Y_{bus}) of the power system [14], shown in Equations (2.1)-(2.3):

$$Y_{bus} = \begin{cases} G^{kl} + jB^{kl}, k \neq l \\ \sum_{k \neq l}(G^{kl} + jB^{kl}), k = l \end{cases} \tag{2.1}$$

$$\underline{V} = \underline{Y}^{-1}\,\underline{I} \tag{2.2}$$

$$\underline{V} = \underline{Z}\,\underline{I} \tag{2.3}$$

where G^{kl} is conductance of line between node k and l, B^{kl} is susceptance of line between node k and l, V is voltage is voltage (v), I is current (A), and Z is line impedance.

Due to the primary network topology of the power system, Y_{bus} is always a sparse matrix. The non-sparse Z_{bus} matrix is calculated by inverting the Y_{bus} matrix, as shown in Equation (2.2). The magnitude of each element of the Z_{bus} matrix represents electrical connections of each node. Although physical topology of the network consisted of $N-1$ connections, electrical topology of the system has a maximum of $N\ (N-1)/2$ connections, where N is the number of nodes in the distribution system.

Figure 2.1 (A) Physical topologies, (B) related electrical topologies, and (C) combined electrical topology of 12-node radial distribution system. (a), (b), and (c) represents Network I, II, and III. Nodes with distinctive colors represent various degrees of centrality.

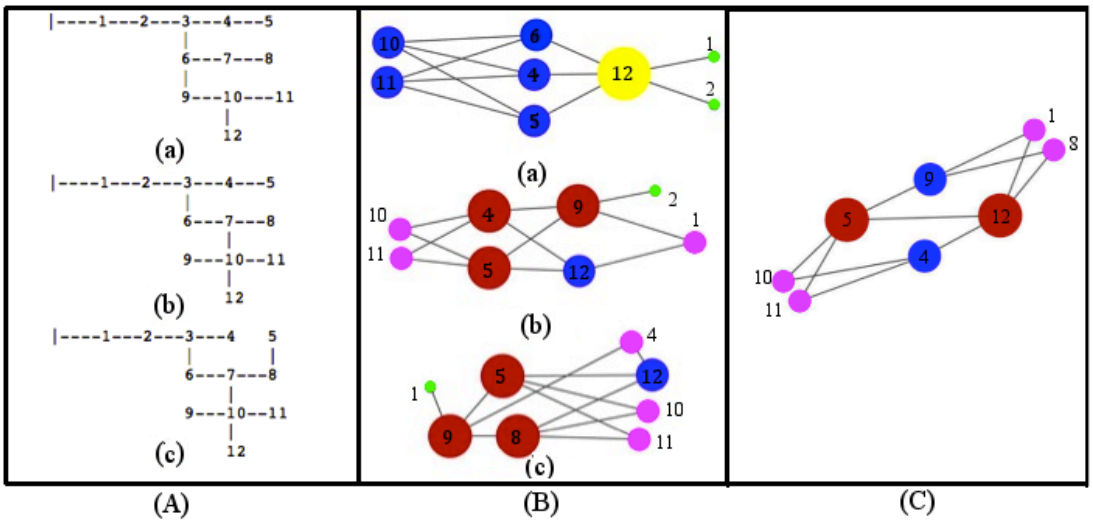

Electrical centrality of a given distribution system is calculated in five steps:

(I) Arrange magnitudes of each element of the Z_{bus} matrix in ascending order.

(II) Select the first $N-1$ number of electrical connections to be compatible with the number of physical connections of the network.

(III) Count the repetition of each node in the selected $N-1$ connections.

(IV) Rearrange nodes in descending order according to the number of repetitions.

(V) Assign electrical centrality ranking to nodes based on the number of repetitions. (The node repeated most often would be assigned Rank #1 and would have the highest electrical centrality of the system.)

A node with a higher centrality indicates a higher number of electrical connections.

Combined Electrical Topology

Assuming only one power flow reroute occurs at a given time and that the system will not have simultaneous multiple power flow reroutes, the first three steps of electrical centrality calculations were repeated for all sub-networks created due to power flow reroutes. The number of repetitions obtained for each node in all three sub-networks was added respectively to obtain overall electrical centrality common to all the sub-networks. This value is represented in Table 2.1 as "Total Node Repetition." Electrical centrality rankings were then assigned to nodes based on the number of repetitions, referred to as "Combined Electrical Node Rank," most often repeated node received Rank #1 and so on, there by helping identify the most electrically central node, Rank #1, common to all three sub-networks and the optimum location to allocate DGs.

Table 2.1 illustrates combined electrical node rankings obtained using the CET method for the 12-node system. According to node ranking calculations, Nodes 5 and 12 had the maximum total node repetition of 11 and ranked #1 in combined electrical node ranking. Similarly, Node 4 had a total node repetition of 9 and ranked #2. This ranking process was applied to the rest of the nodes according to the combined electrical node ranking method, as shown in Table 2.1.

The nodes and electrical connections must be ranked in order to predict the combined electrical topology that represents all sub-networks created by power flow reroutes. Table 2.2

defines electrical connection rankings based on combined electrical node rankings discussed in Table 2.1.

Table 2.1 Pre-Combined Node Ranking of a 12-Node Distribution System

Node	Node Repetitions in Electrical Connections in Each Network			Total Node Repetition	Combined Electrical Node Rank
	I	II	III		
1	1	2	1	4	5
2	1	1	0	2	6
4	3	4	2	9	2
5	3	4	4	11	1
8	3	0	4	7	4
9	0	4	4	8	3
10	3	2	2	7	4
11	3	2	2	7	4
12	5	3	3	11	1

Table 2.2 First (N-1) electrical Connection Selected for a 12-Node Distribution System

Network I		Network II		Network III	
Link	Rank	Link	Rank	Link	Rank
12-5	2	9-5	4	9-5	4
11-5	5	12-5	2	12-5	2
10-5	5	11-5	5	5-11	5
12-4	3	10-5	5	10-5	5
12-8	5	9-4	5	9-8	7
11-4	6	12-4	3	12-8	5
8-11	8	11-4	6	8-11	8
10-4	6	10-4	6	10-8	8
8-10	8	9-1	8	9-4	5
12-1	6	9-2	9	12-4	3
12-2	7	12-1	6	9-1	8

Magnitudes of the elements of Z_{bus} matrix represent electrical connections (links) between system nodes, Table 2.2 represents the optimum $N-1$ electrical connections obtained by following the first three steps of the electrical centrality calculation for each sub-network of a 12-node system. Combined electrical link rankings between two nodes were obtained by adding the corresponding combined electrical node rankings (Table 2.1). For example, Nodes 12 and 5

each had a combined node ranking of 1; therefore, an electrical connection between Nodes 12 and 5 had a combined electrical link ranking of 2. Combined electrical topology formed using the CET method for a 12-node system is illustrated in Figure 2.1 (C).

Combined electrical topologies for 30- and 69-nodes systems were also calculated in this study using the CET method. Figure 2.2 (A) and (B) illustrate physical topologies with planned power reroutes and combined electrical topology of 30-node system. Figure 2.3 (A) and (B) represent physical topologies with planned power reroutes and combined electrical topology of 69-node system.

CET Method

Combined electrical topology represents the electrical network that contain the optimum electrically central nodes common to all three sub-networks. Electrical connection selection for combined electrical topology was achieved in four steps.

(I) Arrange all connections of three sub-networks ($3(N-1)$) in ascending order of combined electrical link rankings.

(II) Remove any repeating electrical connections.

(III) Select the first $(N-1)$ electrical connections to be compatible with the number of physical connections in the system.

(IV) Draw the combined electrical topology using selected $(N-1)$ electrical connections.

As shown in Table 2.2, multiple electrical connections can have identical combined electrical link rankings.

Electrical connection Selection Criteria

Identical combined electrical link rankings can be used to select high-ranked nodes and prevent DG installation in low-ranked nodes. Assume a scenario in which the $(n)^{th}$ electrical connection of a N node radial distribution system is selected, where $1 \leq n \leq N-1$. If the combined electrical link ranking for the $(n)^{th}$ connection is p and X number of electrical connections exists $(X = 1, 2, .., N\ (N-1)/2)$ with an identical link ranking of p, then the electrical connection with highest ranked electrical nodes receives highest priority. Therefore, the electrical link with the highest priority is selected for the $(n)^{th}$ electrical connection. This selection method continues for the remaining $X-1$ electrical connections. Combined electrical topology for a given system was drawn after selecting the optimum $(N-1)$ electrical connections using the described method.

Figure 2.2 (A) Physical topologies and (B) combined electrical topology of 30-node radial distribution system. (a) Network I, (b) network II, and (c) network III. Nodes with different colors represent various degrees of centrality.

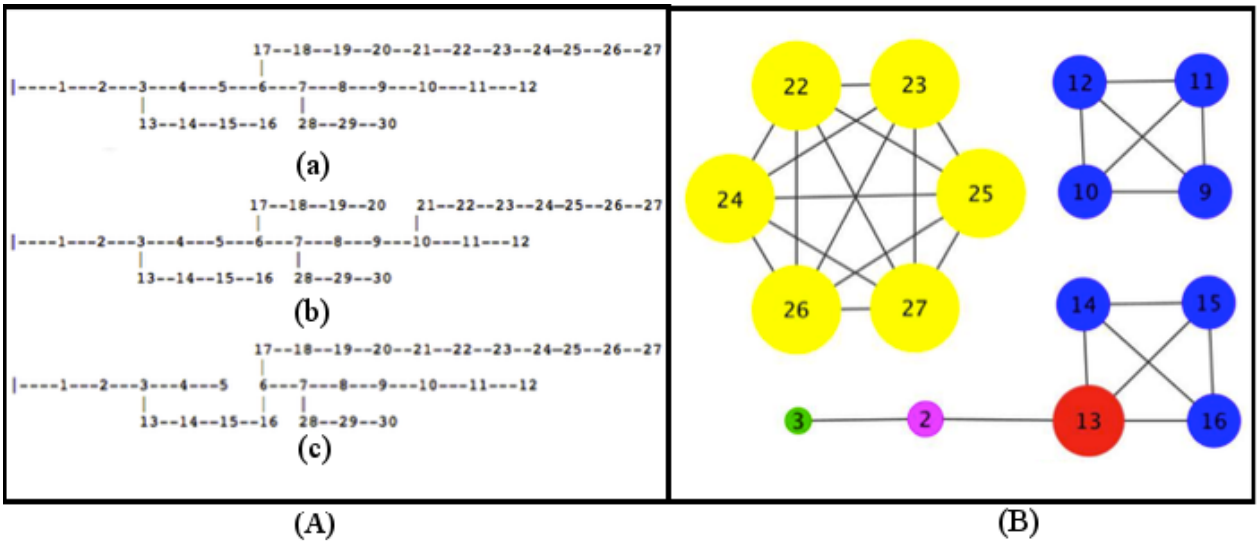

DG Placement

Combined electrical topology was used in this study to identify candidate nodes for DG placement. Although DGs can be placed in all nodes presented in combined electrical topology

of a given radial distribution system, only four candidate nodes were selected in each network, in order to minimize the project cost and over-voltage complications.

Figure 2.3 (A) Physical topologies and (B) combined electrical topology of 69-node radial distribution system. (a) Network I, (b) network II, and (c) network III. Nodes with different colors represent various degrees of centrality.

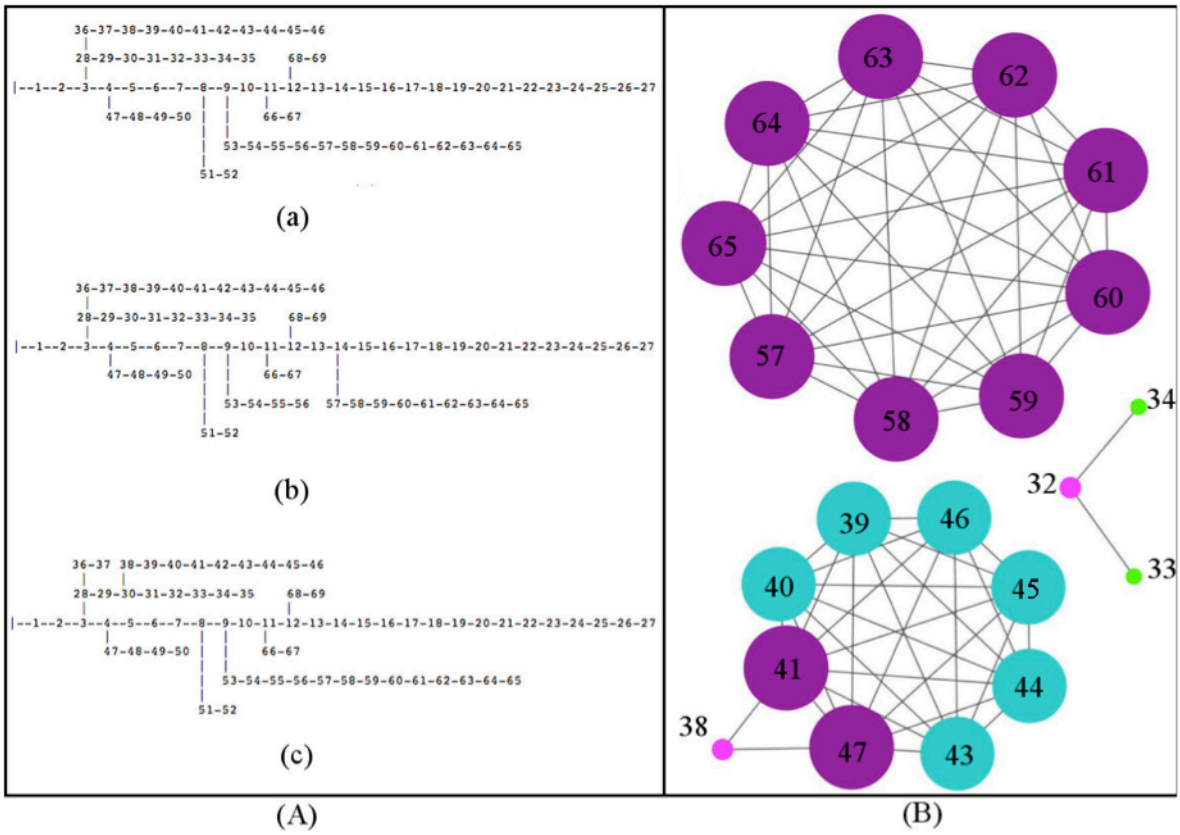

Results unexpectedly revealed that an associated combined electrical topology of radial distribution systems (created due to power flow reroutes) consisted of multiple small electrical systems. This characteristic is proportional to the size of a radial distribution system. Combined electrical topology represented the strength of electrical connections between nodes and existence of multiple small electrical networks signified the coexistence of small independent electrical networks. Coexistence of multiple electrical networks is a distinctive attribute that can be applied in order to micromanage smart-grids. When multiple small electrical networks represented combined electrical topology of a network, at least one candidate node from each

network was selected to allocate DG. Therefore, selection of a minimum of one candidate node from each small combined electrical network presented improved voltage, lower O&M costs and lower loss profile in the system. In this study, four candidate nodes were selected for each of 12-, 30-, and 69-node systems. Among these four candidate locations, a total of 25% peak load capacity of radial distribution system was allocated as DGs, respectively.

DG Sizing

An exhaustive search algorithm determined optimum DG sizes with respect to nodal voltage, O&M costs and real power loss distributed between the four candidate nodes of the system. The exhaustive search algorithm changed DG capacities in candidate nodes in 1% increments in each iteration and then calculates power flow of the system using the Forward-backward load flow algorithm to find bus voltages, O&M costs, and real power losses of the system.

DGs in each candidate node had the following constraints:

$$\sum_{i=1}^{4} DG_{size,i} = 0.25\, P_{peakload} \tag{2.4}$$

$$0 \leq DG_{size} \leq 0.25 P_{peakload} \tag{2.5}$$

$$It_{inc} = 0.01 L_{peak} \tag{2.6}$$

$$0.95 \leq V_i \leq 1.01 \tag{2.7}$$

$$P_{losswDG} < P_{losswoDG} \tag{2.8}$$

where $DG_{size,i}$ is DG size at node i, $P_{peakload}$ is peak load of the system, It_{inc} is DG size increment in each iteration, V_i is voltage at bus i, $P_{losswDG}$ is real power loss of the system with DG and $P_{losswoDG}$ is real power loss of the system without DG.

Real power loss of the system was calculated using Equation (2.9):

$$P_{loss} = \sum_{i}^{N} \sum_{\substack{j=1 \\ j>i}}^{N} V_i V_j Y_{ij} \cos(\theta_i - \theta_j - \delta_{ij}) \quad (2.9)$$

where N is the total number of busses, V_i and θ_i are magnitudes and voltage angle at node i, V_j and θ_j are magnitudes and voltage angle at node j, and Y_{ij} and δ_{ij} are magnitudes and phase angle of admittance between node i and j.

All DGs were assumed to be natural gas-powered combined-cycle (CC) turbines. In this study pulverized coal and CC power plants were considered primary power supplies from the grid side. Table 2.3 presents the variable and fixed O&M cost estimates for year 2020 for coal and CC power plants, predicted by the National Renewable Energy Laboratory [15].

Table 2.3 O&M Cost and Minimum Load Levels for Coal and CC Power Plants

Power Plant	Variable O&M ($/MWh)	Fixed O&M ($/kW-Yr)	Minimum Load (%)
Coal	3.71	23	40
CC	3.67	6.31	50

For calculation purposes, the project life cycle was assumed to be 20 years. Therefore, O&M costs of the main power plant without any DG installed in the system were calculated using Equation (2.10):

$$O\&M_{woDG} = \sum_{i=1}^{3} T_i (P_{LoadwoDG} + P_{losswoDG}) C_{main,O\&M} \quad (2.10)$$

where $P_{LoadwoDG}$ is real power demand of the system without any DGs, T_i is the time of operation in each load level of the system, and $C_{main,O\&M}$ is O&M cost of the main power plant ($/MW).

O&M cost with DGs is calculated using Equation (2.11):

$$O\&M_{wDG} = \sum_{i=1}^{3} T_i [(P_{LoadwDG} + P_{losswDG}) C_{main,O\&M} + (\sum_{i=1}^{4} P_{DG,i}) C_{DG,O\&M}] \quad (2.11)$$

where $P_{LoadwDG}$ is real power demand of the system with DGs, $P_{DG,i}$ is real power production of the DG in node i, and $C_{DG,O\&M}$ is O&M cost of DGs ($/MW).

$$P_{LoadwDG} = 0.75P_{LoadwoDG} \quad (2.12)$$

$$\sum_{i=1}^{4} P_{DG,i} = 0.25P_{LoadwoDG} \quad (2.13)$$

Savings from cost reduction in O&M is presented in (2.14). The total real power loss reduction of the system is presented in Equation (2.15). Using Equations (2.14) and (2.15) savings from cost reductions in O&M can be derived as presented in Equation (2.16). If the difference between O&M costs of the primary power plant and DGs is negligible (Equation (2.17)), savings from O&M costs reduction can be given by Equation (2.18):

$$Savings_{O\&M} = O\&M_{woDG} - O\&M_{wDG} \quad (2.14)$$

$$\Delta P_{loss} = P_{losswoDG} - P_{losswDG} \quad (2.15)$$

$$Savings_{O\&M} = 0.25P_{Load}\left(C_{main,O\&M} - C_{DG,O\&M}\right) + \quad \Delta P_{loss}C_{main,O\&M} \quad (2.16)$$

$$C_{main,O\&M} \approx C_{DG,O\&M} \quad (2.17)$$

$$Savings_{O\&M} = \sum_{i=1}^{3} T_i \, \Delta P_{loss}C_{main,O\&M} \quad (2.18)$$

Net present worth value (NPV) of the savings from O&M cost reduction is shown in Equation (2.19):

$$NPV(Savings_{O\&M}) = Savings_{O\&M}\left(\frac{1+InfR}{1+IntR}\right)^{t} \quad (2.19)$$

where $InfR$ is inflation rate, $IntR$ is interest rate, and *t* is the project life cycle (20 years). Table 2.4 presents technical and business information of various load level for one year (8760 hours). All systems were assumed to follow the load conditions stated in Table 2.4.

Table 2.4 Technical and Business Information of Various Load Levels

Load Level	Peak load Percentage (%)	Time Duration (h/year)
Light load	80	2190
Medium load	90	4818
Peak load	100	1752

Results

Results obtained for optimizing DG with respect to nodal voltage, O&M costs and real power loss of a radial distribution system using CET method are presented in this section.

Table 2.5 presents percentages of real power loss and operational cost reductions of each system with 25% of peak load capacity allocated as DGs in selected candidate nodes. All sub-networks belong to 12-, 30- and 69-node systems achieved a minimum of 55.07% real power loss reduction and High NPV of O&M costs reduction.

Figures 2.4, 2.5, and 2.6 present voltage profile improvements of 12-, 30- and 69- node systems, respectively. DG allocation to represent each small electrical network of an associated combined electrical topology of a radial distribution system improved voltage profile. In-depth analysis revealed that large branches of a distribution system are represented by multiple small electrical topologies. Therefore, consideration of each small electrical topology and corresponding DGs allocation improved voltage profile, and decrease O&M costs and real power loss of the system. High voltage-profile improvements were present when the system was considered a collection of small electrical sub-systems, as shown in Figures 2.5 and 2.6.

Table 2.6 net presents savings (NPV) from O&M cost reduction achieved using the CET method in networks for coal and CC power plants.

Table 2.5 Real Power Loss Reduction Percentages of the Network I, II, and III of the 12-, 30-, and 69-Node Systems According to 25% DG allocation of Peak Load

System	Peak Load (MVA)	PF (%)	DG Nodes	DG		Network	Loss Reduction
				Size (MW)	PF (%)		
12	31.30	97.3	4	1.2	97.3	I	55.07%
			5	3.1	95.3	II	56.09%
			9	2.7	94.9	III	56.87%
			12	0.8	91.3		
30	71.07	93.2	12	1.5	95.4	I	56.60%
			13	10.8	95.7	II	60.50%
			22	4	92.5	III	57.19%
			27	1.8	93.1		
69	186.40	81.6	32	3.7	93.8	I	64.66%
			41	5.6	93.6	II	69.83%
			57	1.9	95.9	III	64.64%
			65	35.4	92.1		

Table 2.6 NPV of Savings from O&M Cost Reductions For Coal and CC Power Plants

System	Network	NPV of savings from O&M cost reductions ($M)	
		Coal	CC
12	I	0.079	0.029
	II	0.082	0.031
	III	0.088	0.033
30	I	0.260	0.097
	II	0.322	0.120
	III	0.308	0.115
69	I	3.399	1.270
	II	2.731	1.020
	III	3.396	1.260

Figure 2.4 Voltage profile of the Network, with the highest real power loss, in a 12-node system with and without DG. Sections separated by the dotted line represent various branches.

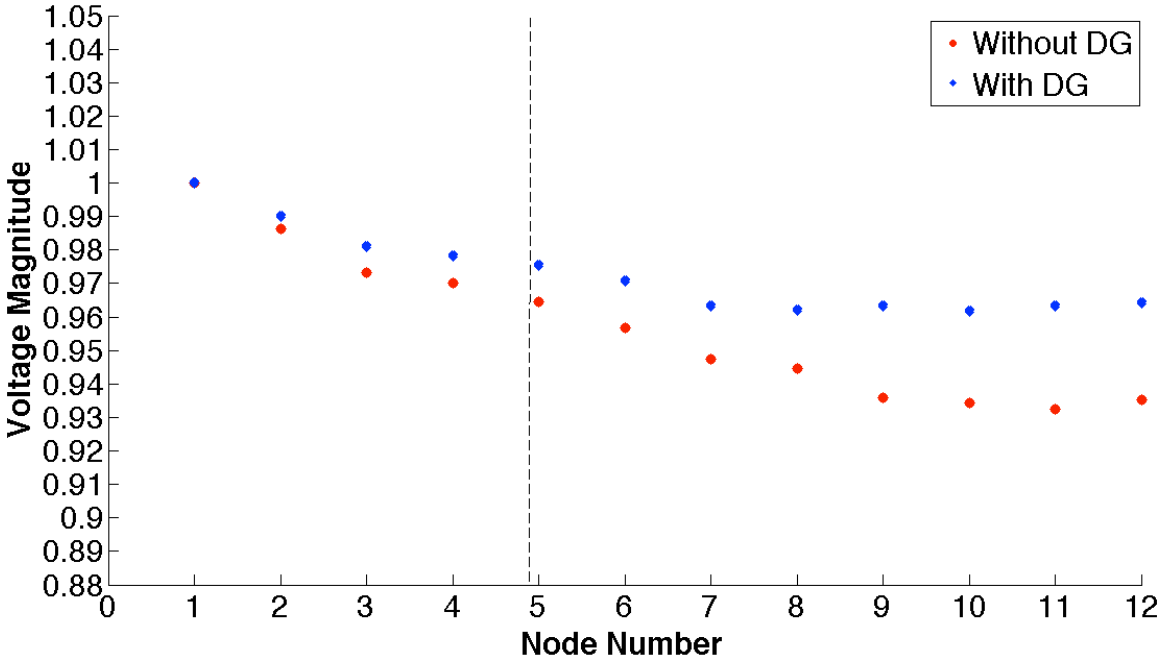

Figure 2.5 Voltage profile of the Network, with the highest real power loss, in a 30-node system with and without DG. Sections separated by the dotted line represent various branches.

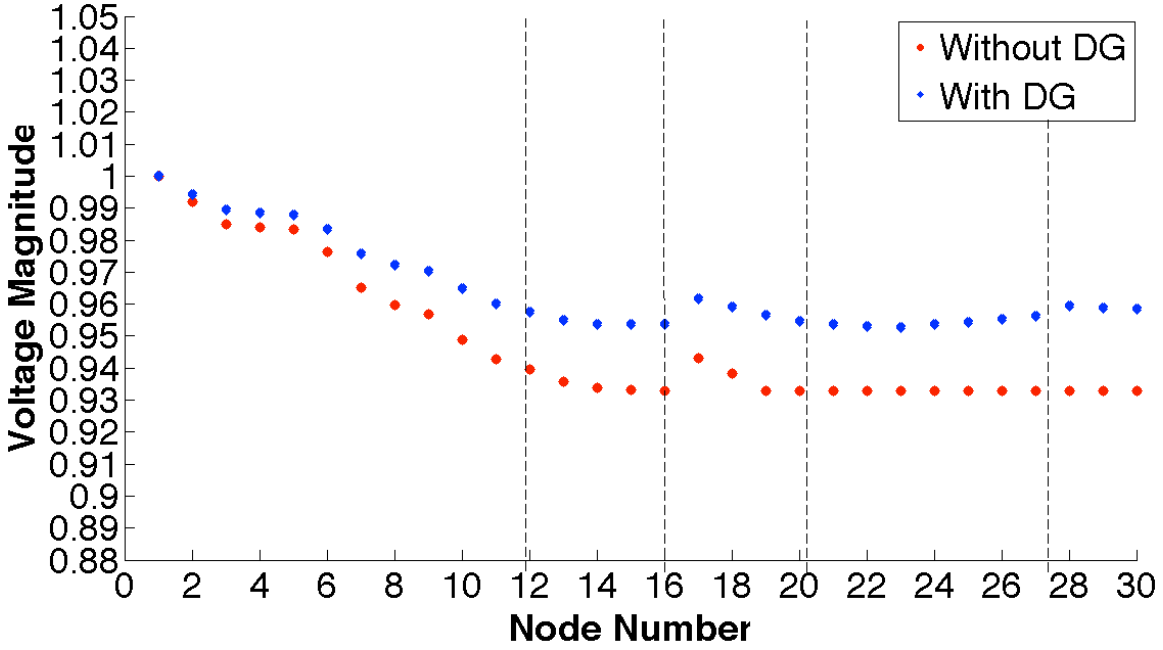

Figure 2.6 Voltage profile of the Network, with the highest real power loss, in a 69-node system with and without DG. Sections separated by the dotted line represent various branches.

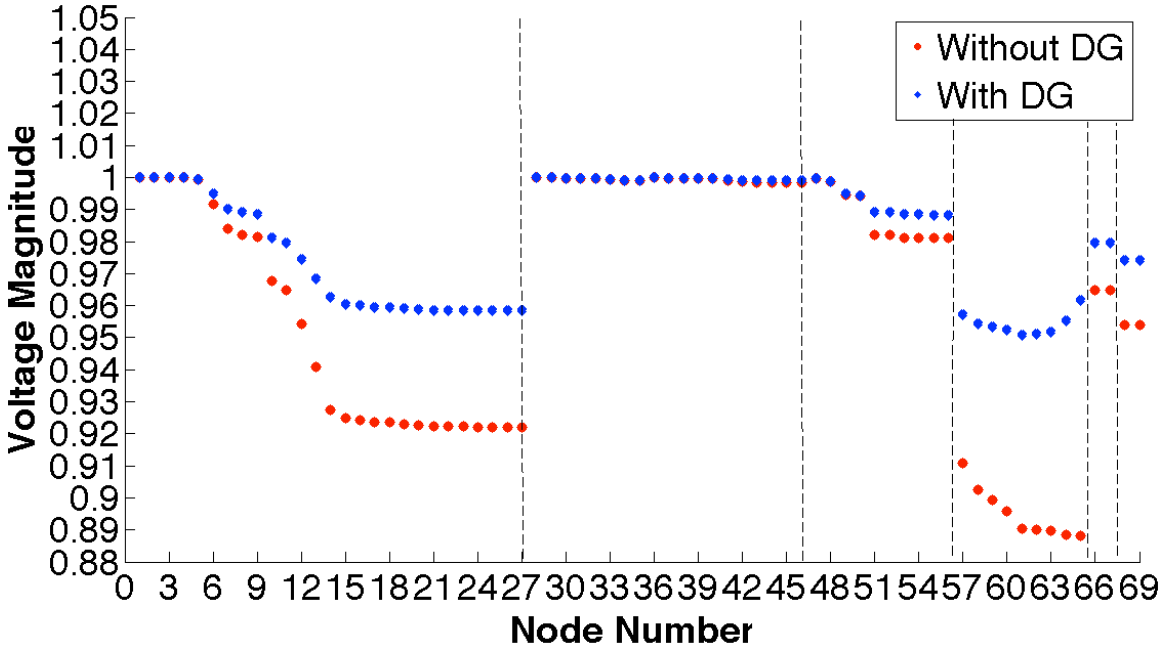

Impact of intentional Structural Changes in Distribution System Topology to Wind Turbine Sizing and Siting: A Complex Network Approach

A version of the research described under above title was submitted and published in De Gruyter Online, Smart Grid. Volume 2, Issue 1, ISSN (Online) 2299-1107, DOI: 10.1515/sgrid-2015-0002, September 2015 [17].

In this study CET method was used to allocate DWG and load distribution planning (LDP) in 12-, 30- and 69-node radial distribution systems described in previous sections of chapter 2. The primary objective underline the study was to identify the impact of intentional structural changes in DWG allocation in radial distribution systems. Wind turbine sizes were identified by an exhaustive search method. Results indicated that the CET method can be used to install wind turbines to minimize the system power loss, and improve voltage profile and power quality of the distribution systems, minimizing the effect of intentional structural changes.

Allocating Wind Turbines in a Radial Distribution System

Allocating wind turbines in the radial distribution system was carried out in two steps. Step 1: Locate the candidate node for the wind turbines. Step 2: Use the exhaustive method to find the number of wind turbines to be installed.

Locating Candidate Nodes for DWG Installation

Candidate node selection for the wind turbines was done considering a hypothetical scenario where nodes to exclude, nodes with poor wind, and nodes with high wind were assigned randomly. In addition, best candidate nodes selected using CET method described in chapter 2 for 12-, 30- and 69-node systems were selected to apply the hypothetical scenario.

Since the radial distribution systems considered were small, they were assumed to spread in small geographical area. There were environmental constraints to follow which limit the locations to place wind turbines. Wind turbine placement followed the hypothetical environmental constraints on nodes illustrated in Figure 2.7. In order to minimize the computational complexity of the exhaustive search, wind turbines were allocated in four locations in each system. Note that when the power distribution system increases in size, electrical centrality suggests several small electrical networks to represent the physical network, rather than a single network.

If multiple nodes were present for one ranking, a maximum of two nodes were selected. When combined electrical topologies of the 12-, 30-, and 69-node systems were considered, highly connected nodes were always toward the end of the branches of the relating physical network.

Figure 2.7 Hypothetical assignment of environmental constraints and wind resource availability, mapped with combined electrical topology (candidate nodes) to illustrate final with turbine placement recommendation. (a), (b), and (c) represent the original 12-, 30-, and 69-node systems.

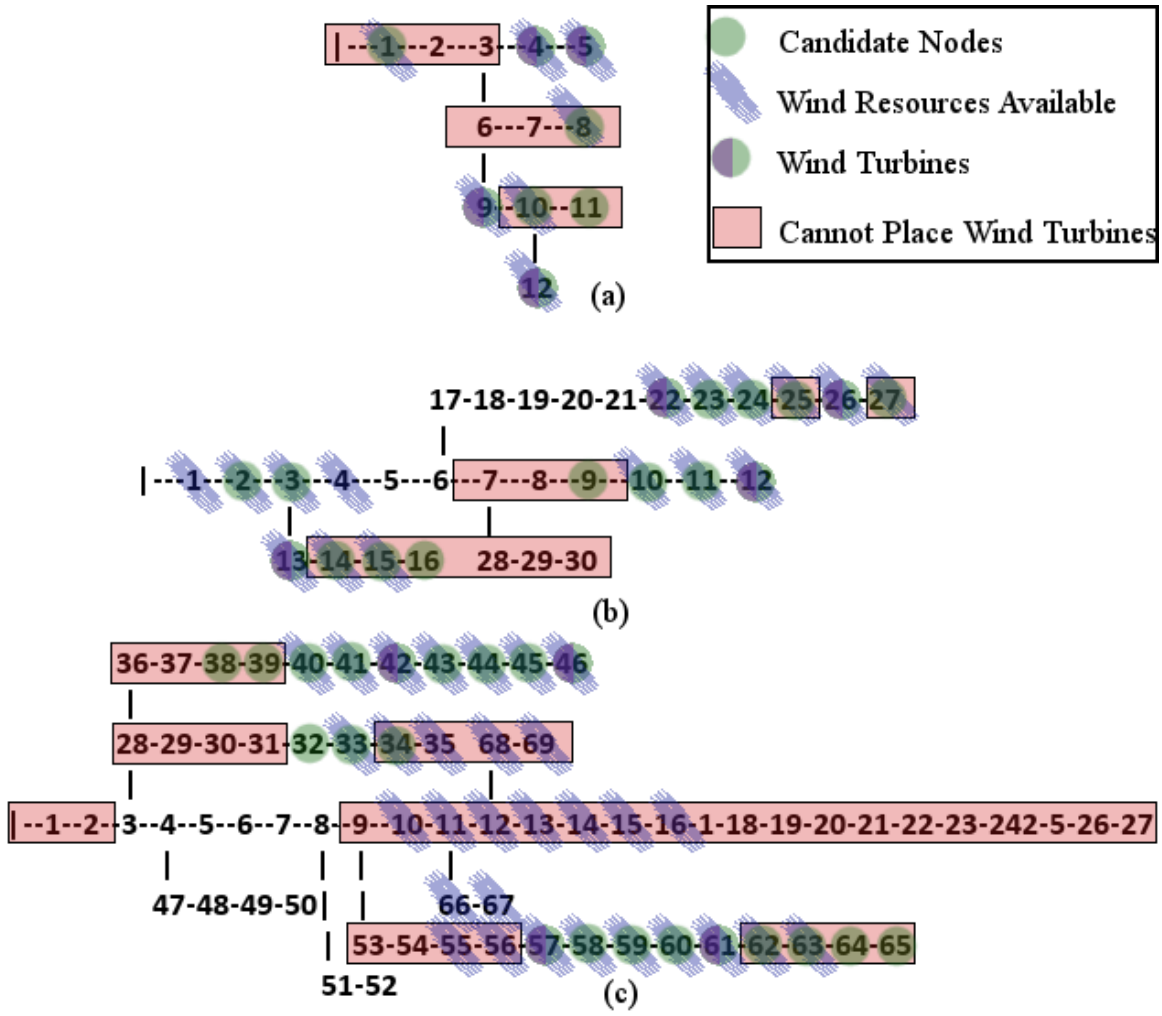

Calculating the Size of the Allocated DWG

Initially 5% wind was allocated as RDG generation from the total peak demand of the system, gradually increasing the wind generation by 5% steps until the minimum network loss was achieved. Gradual increase of wind generation did not affect the wind turbine placement. The final size and site of the wind turbines were selected to have minimum network losses and the best voltage profile.

In this study node 1 was assumed as the slack bus and thereby capable of handling sudden variation of wind generation. Wind generation was generating both active and reactive power with 94% power factor. Power loss of the system was calculated using equation (2.9). Nodal voltage and line current were calculated using the forward-backward load flow method.

Figures 2.8 and 2.9 illustrate the normalized load demand and generation of 12-, 30-, and 69-node systems respectively. The normalized load demand curve was generated using real-world load demand data from 2005. The normalized wind generation curve was generated using real-world wind generation data of a NW100 wind turbine installed on Riley County Public Works premises in Manhattan, Kansas.

Figure 2.8 Normalized load demand for 1 year in 1-hour time intervals.

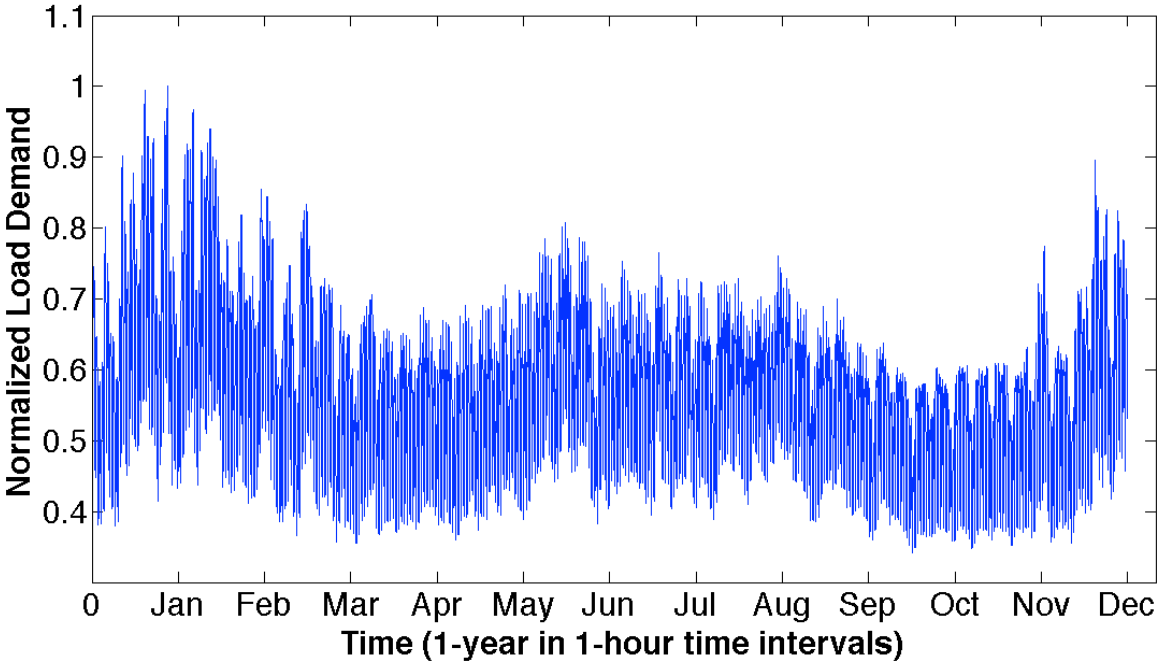

Figure 2.9 Normalized wind generation for 1 year in 1-hour time intervals.

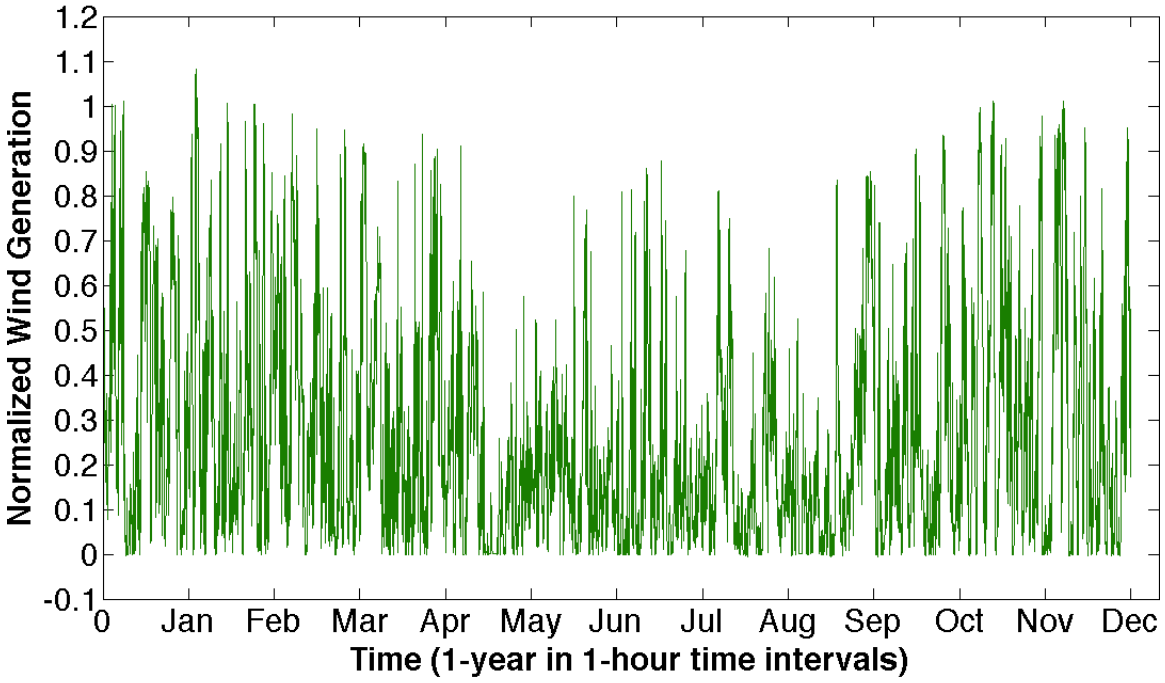

Results

Table 2.7 illustrates candidate nodes for DWG placement and loss minimization percentages compared to system losses without DWG in 12-, 30-, and 69-node systems. Results indicate that electrical centrality can successfully identify candidate nodes for DWG placement in a distribution system.

Table 2.7 Real Power Loss Reduction Percentages of the Network I, II, and III of the 12-, 30-, and 69-node Systems.

Networks in Each System		Placement of RDG	RDG percentage from total load demand	Loss reduction
12	I	4, 5, 9, 12	62.3%	78.39%
	II			85.18%
	III			85.47%
30	I	12, 13, 22, 26	72%	76.88%
	II			78.25%
	III			73.09%
69	I	42, 46, 57, 61	56.50%	79.95%
	II			89.30%
	III			89.91%

The percentage of maximum RDG allocation for loss minimization and voltage profile improvement of a radial distribution system varies based on load distribution and number of nodes in the system. NES and SPP for DWG in 12-, 30- and 69-node systems are presented in Table 2.8. Although it was not envisioned, all three radial distribution systems' had identical SPP.

Table 2.8 NES and SPP for 12-, 30-, and 69-node systems

System	NES ($)	SPP (Years)
12-node	5751.42	15.16
30-node	15092.32	15.16
69-node	31063.58	15.16

Figures 2.10-2.12 illustrate voltage profiles before and after DWG allocation of networks, with highest system losses belonging to 12-, 30-, and 69-node systems. As demonstrated, voltage profiles of each network improved but varied near reference voltage (1, p.u.). Although voltage variance decreased in all nodes, voltage variance remained high due to stochastic wind generation. Technologies such as DESS can minimize the high variance of the voltage.

Figure 2.10 Voltage profile of the 12-node radial distribution network II for 1 year in 1-hour time intervals. (a) and (b) represent voltage profile without and with distributed wind generation, respectively.

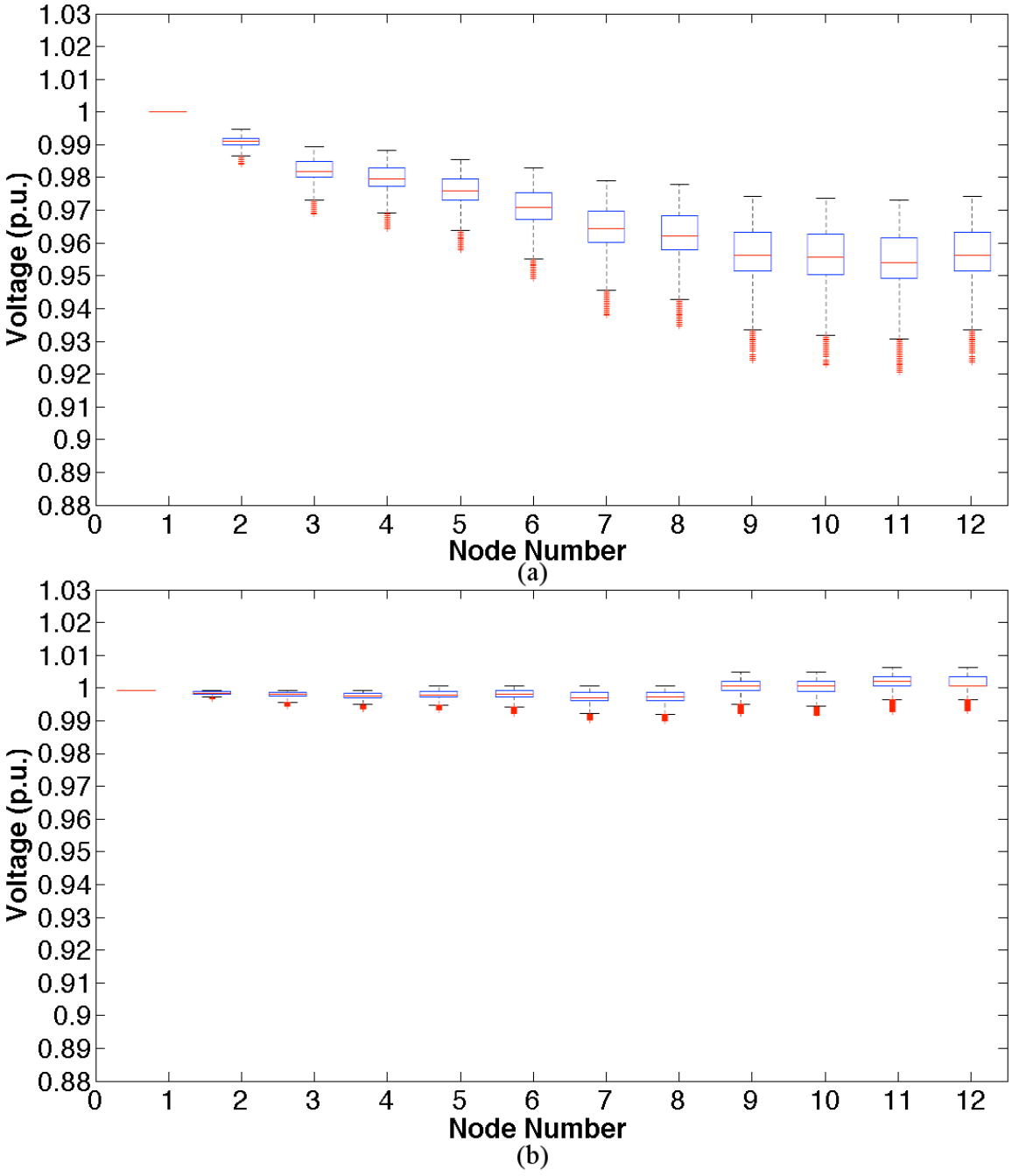

Figure 2.11 Voltage profile of the 30-node radial distribution network II for 1 year in 1-hour time intervals. (a) and (b) represent voltage profile without and with distributed wind generation, respectively.

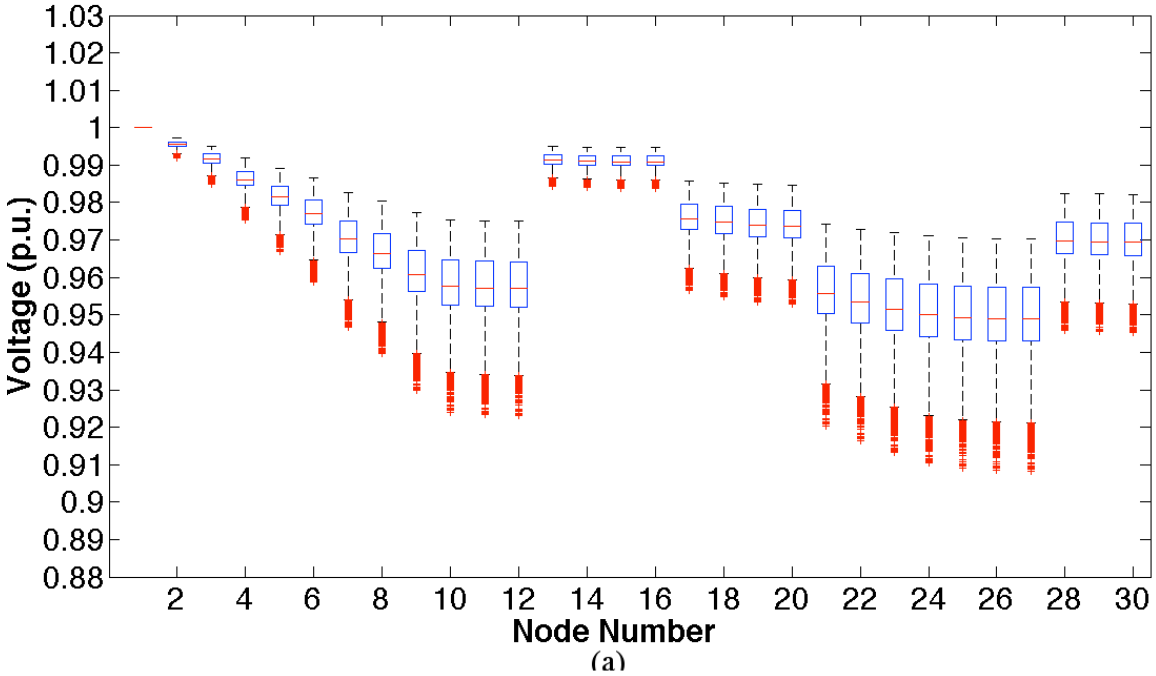

(a)

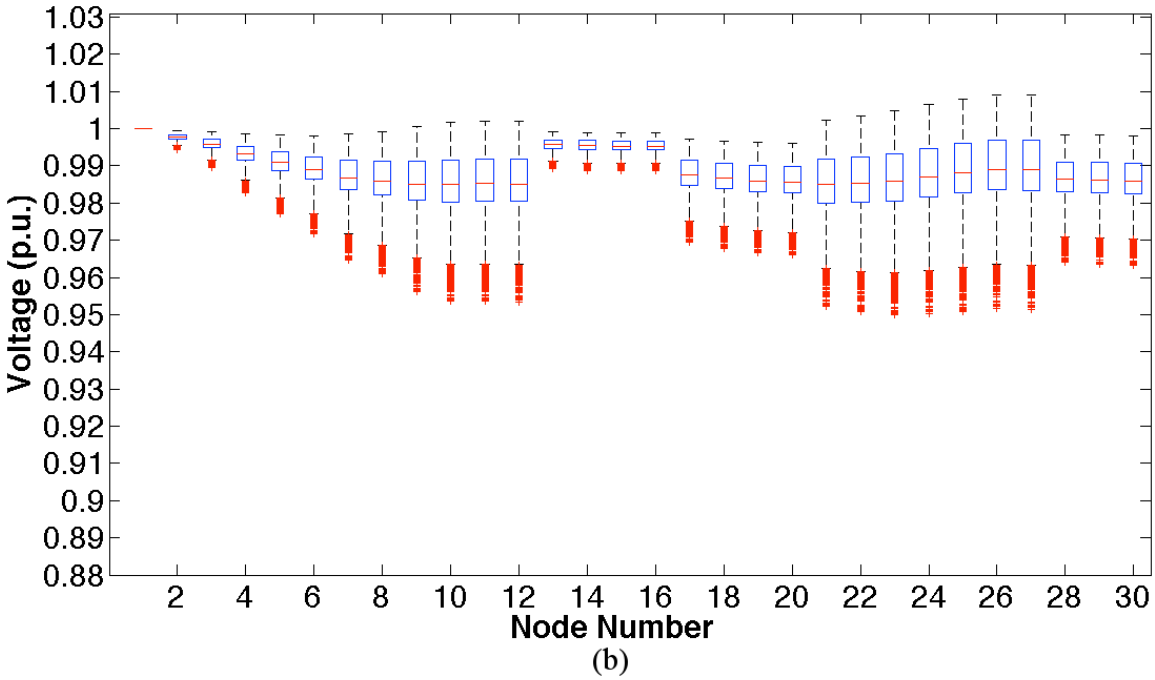

(b)

Figure 2.12 Voltage profile of the 69-node radial distribution network II for 1 year in 1-hour time intervals. (a) and (b) represent voltage profile without and with distributed wind generation, respectively.

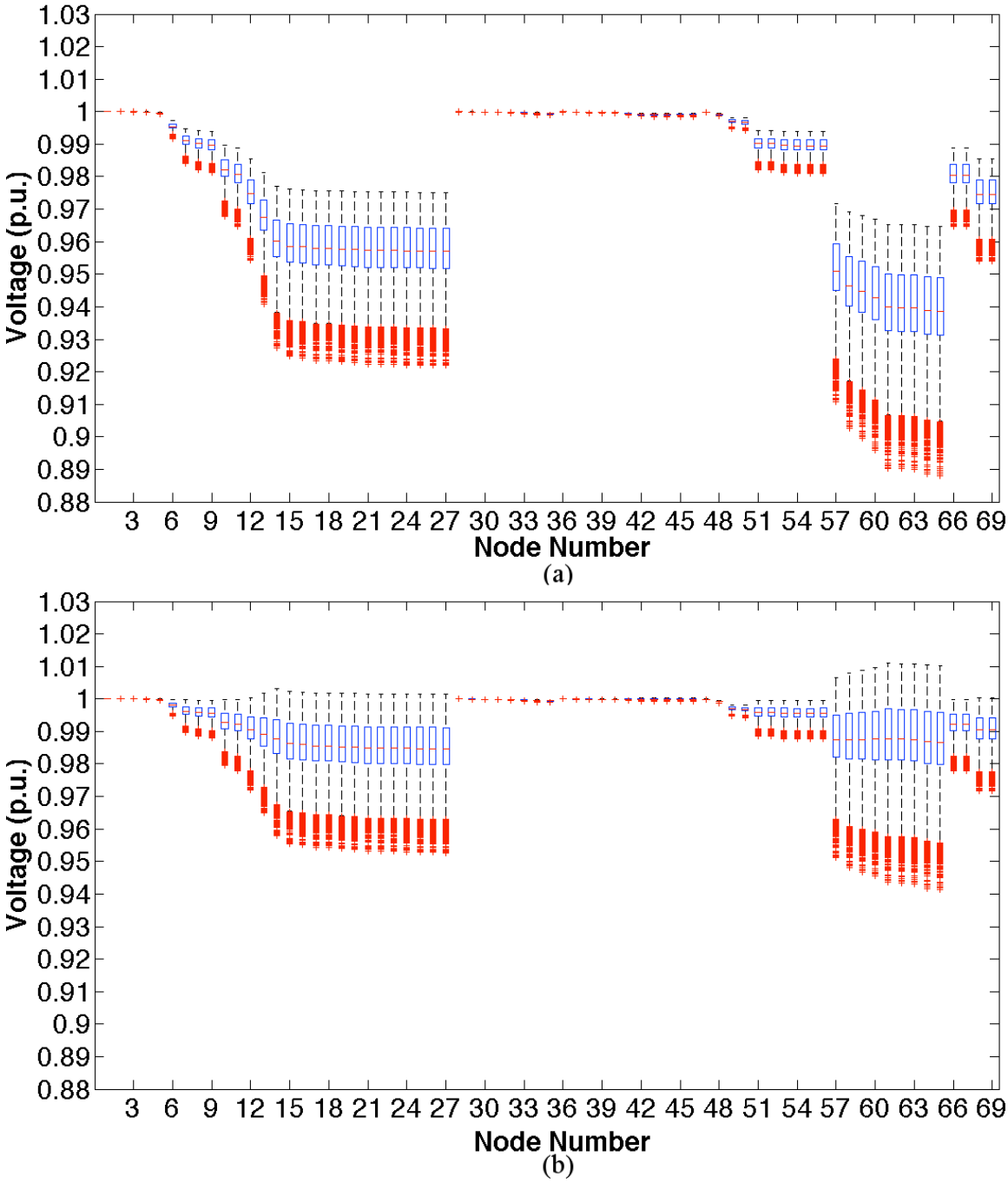

Conclusion

Power flow reroutes provide essential service to ensure uninterrupted power supply to end-users. Therefore, physical topological changes that occur in a power system due to power flow reroutes should be considered when allocating DGs and DWGs in a radial distribution system. In this research we proved the CET method can successfully minimize the impact of intentional structural changes in DG/DWG placement in a distribution system. In addition, the CET method improves voltage profile and decreased real power loss, and O&M costs of a radial distribution system. The use of natural gas-based CC generators as DGs decreases O&M costs compared to DG resources such as diesel and bio-fuel.

References

[1] Ackermann, Thomas, Göran Andersson, and Lennart Söder. "Distributed Generation: A Definition." *Electric Power Systems Research* 57, no. 3 (2001): 195-204.

[2] Alarcon-Rodriguez, Arturo, Graham Ault, and James McDonald. "Planning the Development of Highly Distributed Power Systems."2007.

[3] Prommee, Witoon and Weerakorn Ongsakul. "Optimal Multi-Distributed Generation Placement by Adaptive Weight Particle Swarm Optimization."IEEE, 2008.

[4] Acharya, Naresh, Pukar Mahat, and Nadarajah Mithulananthan. "An Analytical Approach for DG Allocation in Primary Distribution Network." *International Journal of Electrical Power & Energy Systems* 28, no. 10 (2006): 669-678.

[5] Shaaban, Mostafa F., Yasser M. Atwa, and E. El-Saadany. "DG Allocation for Benefit Maximization in Distribution Networks." *Power Systems, IEEE Transactions on* 28, no. 2 (2013): 639-649.

[6] DOE, US. *The Potential Benefits of Distributed Generation and Rate-Related Issues that may Impede their Expansion* (2007).

[7] Juanuwattanakul, P. and MAS Masoum. "Increasing Distributed Generation Penetration in Multiphase Distribution Networks Considering Grid Losses, Maximum Loading Factor and Bus Voltage Limits." *Generation, Transmission & Distribution, IET* 6, no. 12 (2012): 1262-1271.

[8] Guo, Xueli, Jiuju Du, and Changxiao Qi. "Study and Application of Switching Operation of 10kV Lines Ring Network in Urban Power Distribution Network."IEEE, 2012.

[9] Ding, Fei and Kenneth A. Loparo. "A Simple Heuristic Method for Smart Distribution System Reconfiguration."IEEE, 2012.

[10] Tamizkar, R., SAM Javadian, and M-R Haghifam. "Distribution System Reconfiguration for Optimal Operation of Distributed Generation."IEEE, 2009.

[11] Hines, Paul and Seth Blumsack. "A Centrality Measure for Electrical Networks."IEEE, 2008.

[12] Pahwa, S., D. Weerasinghe, C. Scoglio, and R. Miller. "A Complex Networks Approach for Sizing and Siting of Distributed Generators in the Distribution System."IEEE, 2013.
[13] Wang, Zhifang, Anna Scaglione, and Robert J. Thomas. "Electrical Centrality Measures for Electric Power Grid Vulnerability Analysis."IEEE, 2010.
[14] Gungor, BR. "Power Systems-Chapter 6." (1988).
[15] Tidball, Rick, Joel Bluestein, Nick Rodriguez, and Stu Knoke. "Cost and Performance Assumptions for Modeling Electricity Generation Technologies." *Contract* 303, (2010): 275-3000.
[16] Borenstein, Severin, James Bushnell, and Christopher R. Knittel. "Market Power in Electricity Markets: Beyond Concentration Measures." *The Energy Journal* (1999): 65-88.
[17] Weerasinghe, Dulan J., Pahwa, Sakshi, Miller, Ruth Douglas, and Scoglio, Caterina. "Impact of Intentional Structural Changes in Distribution System Topology to Wind Turbine Siting and Sizing: A Complex Network Approach." *Smart Grid*. 2(1): -. Retrieved 25 Jan. 2016, from doi:10.1515/sgrid-2015-0002.

Chapter 3 - Optimizing Placement and Capacity of Distributed Wind Generation and Energy Storage Systems, to Supply Baseload of an Unbalanced and Unsymmetrical Distribution Network and Sustain Power to the system in Power Grid Failure.

This research investigated the possibility of using increased DWG and NaS to supply base power demand of an unbalanced and unsymmetrical distribution network. DWG and NaS placement and size were optimized with reference to network losses, voltage profile, availability, and system savings using NSGA-II. The research also extended and fulfilled empowering islanded operation of a small distribution system, in order to minimize negative effects of cascading power grid blackouts and enable distribution systems to operate independently for a maximum of 1.5 hours, with the assumption that grid power is restored within that time frame. Results indicated that increased DWG and NaS can successfully supply base power to an unbalanced and unsymmetrical network and operate a distribution system in an islanded situation for a maximum of 1.5 hours.

Introduction

Modern power systems are based on centralized power generation associated with complex engineering challenges such as operation and maintenance of large infrastructures, expensive and inefficient long-distance power transmission, and negative impacts of cascading grid failures. Characteristics such as structural layout (topology) of centralized power generation also promote wide-scale power outages [1]. Figure 3.1 illustrates the increased frequency of wide-scale power outages in North America since 1960 [2,3]. All power outages listed in Figure 3.1 adhere to the following criteria:

(I) The service provider did not plan the outage.

(II) The outage affected at least 1,000 consumers and lasted at least 1-hour.

(III) A minimum of 1,000,000 person-hours disrupted.

Figure 3.1 Frequency of wide-scale power outages in North America [2,3]

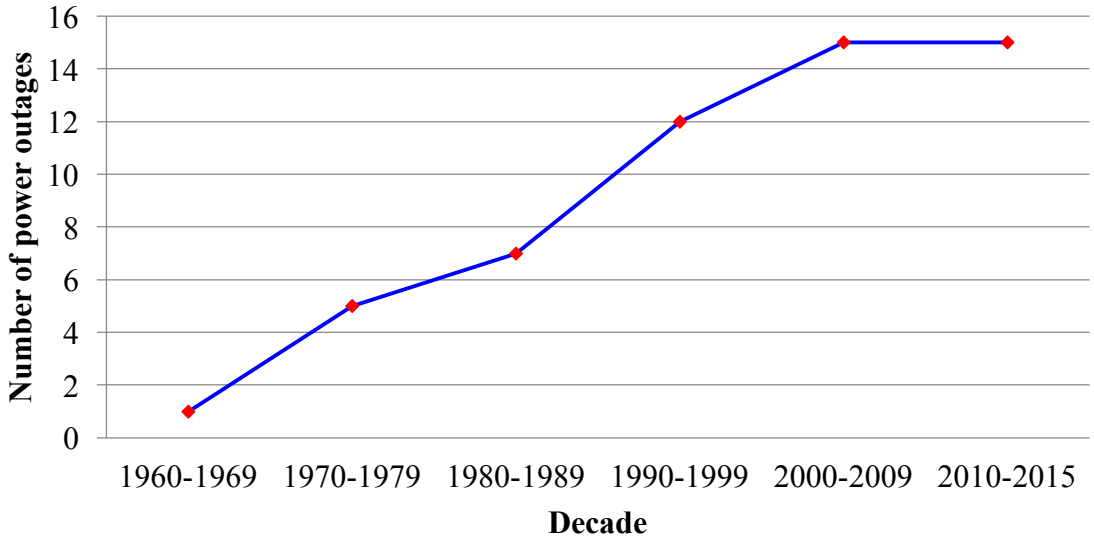

Decentralized or DG, especially DWG combined with BESS presents a successful solutions to cascading power grid failures. Although various articles in literature have considered ODGP [4-11], no article has addressed increased DWG and BESS in a three-phase unbalanced radial distribution system for the purpose of sustaining the system in widespread power outages. Since 1995, ODGP has been investigated as it pertains to various impact indices and optimization techniques. Impact indices investigated in previous researches have included voltage profile, power system losses, cost savings of the system, and reactive power capacity.

The literature emphasizes three primary methods of solving ODGP: analytical, numerical, and heuristic [12]. Analytical methods are easily implemented and quickly executed, but their results are suggestive due to simplified assumptions, such as consideration of only one power system-loading snapshot [4]. Therefore, the analytical method may not be the suitable method for uncertainties and stochastic optimization. Although numerical methods such as exhaustive

search and dynamic programming guarantee the global optimum, they are not suitable for large-scale systems. Heuristic methods are typically robust and provide near-optimal solutions for large, complex ODGP problems.

Since 1998, genetic algorithms (GA) have been extensively used in optimization problems related to power systems [6,10, 13-17]. In this research, ODGP was addressed using a meta-heuristic GA method, NSGA-II [18]. The limited number of articles in the literature that have discussed ODGP using NSGA-II [19-23] have primarily focused on optimizing DG capital cost and running cost [19], optimum load following DG planning during the planning horizon [20], reducing system losses and improving the voltage profile with lower investment [21], and load shedding to achieve grid independency [22]. Although articles in the literature solved the ODGP problem for conventional DG using the NSGA-II method [19-23], none of the articles addressed optimizing DWG and NaS capacity and placement in order to supply base power and operate an unbalanced and unsymmetrical network in an islanded situation for a maximum of 1.5 hours.

Objectives

This research addressed two questions regarding integration of DWG and NaS. In particular, it focused on optimizing DWG and NaS in order to supply system base power. The study also focused on sustains a three-phase unbalanced and asymmetrical distribution system for 1.5 hours in the event of main grid power failure using DWG and NaS.

Research discussed in this chapter established minimum capacity future requirements for the year 2035, postulating a scenario of base power generation using DWG and NaS. The study determined cost-optimal strategies to achieve grid independence in the event of power failure and base power supply requirements for low wind and high wind penetration scenarios. In

addition, capacities and locations of DWG and NaS were optimized with respect to network losses, system voltage profile, DWG/NaS availability, and present value (PV) of system savings.

This research addressed the following questions:

(I) How much DWG/NaS capacity is necessary to meet base power requirements of the IEEE 37-node three-phase unbalanced and unsymmetrical radial distribution system?

(II) How much NaS capacity is necessary to meet total balancing requirements for the IEEE 37-node system with increased DWG?

(III) How cost-effective is DWG/NaS compared to convectional energy generation for supplying base power demand?

(IV) What are the key lessons learned from this research?

Approach and Data Used

Distributed Wind Generation

Complications associated with increased DWG and BESS in a distribution system include increased project costs, availability, and increase system voltages over acceptable limits (system voltage > 1.05 p.u.). According to the American Wind Energy Association (AWEA), in 2013, average installed cost of a 1-10 MW wind turbine was $1630 /kW, $600 less than the apparent peak in 2009 and 2010, indicating possibility of further DWG cost reduction in future renewable projects. This research focused on installed cost of DWG in year 2035, projected by Office of Integrated Analysis & Forecasting U.S. EIA [24]. The U.S. EIA projected that wind turbine productivity measured in kWh generated per year will increase from 28% to 36%, installed costs of DWG will fall by 20% to 24%, economic viability of DWG projects will increase 37% to 44%, O&M costs will fall 10% to 12%, and availability will increase up to 98%. Figure 3.2 presents installed wind power project cost over time [25].

One of the concerns of distributed wind project is wind availability. A site with less wind than wind power Class 3, shown in Table 3.1, is unlikely to be economically successful. This research assumed IEEE 37-node test system is located in a geographical area with a minimum wind power Class 3. A wind penetration scenario able to provide IEEE 37-node systems base power (40% of peak load) is hypothesized.

Figure 3.2 Installed wind power project cost over time [25]

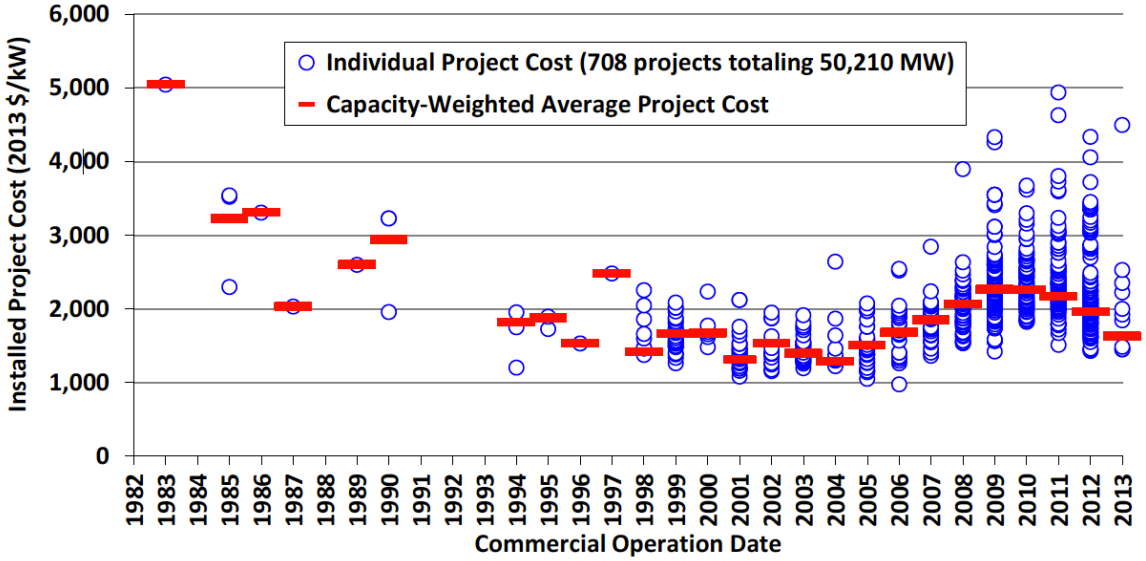

Table 3.1 Specification of wind Power Class 3 [(a)] [26]

Wind Power Class	10 m (33 ft.)		50 m (164 ft.)	
	Wind Power Density (W/m^2)	Speed [(b)] m/s (mph)	Wind Power Density (W/m^2)	Speed [(b)] m/s (mph)
3	150	5.1 (11.5)	300	6.4 (14.3)
	200	5.6 (12.5)	400	7.0 (15.7)

(a) Vertical extrapolation of wind speed based on the 1/7 power law. (b) Mean wind speed is based on Rayleigh speed distribution of equivalent mean wind power density. Wind speed is for standard sea-level conditions. In order to maintain consistent power density, wind speed increases 3%/1000 m (5%/5000 ft.) elevation.

Wind power generation considering wind speed can be calculated using Equation (3.1).

$$P_{wind} = \frac{1}{2}\rho A v^3 C_p \tag{3.1}$$

where P_{wind} is generated wind power (kW), ρ is air density (kg/m^3), A is sweep area of the wind turbine blades (m^3), v is wind speed (m/s), and C_p is the Betz limit (0.59). Although $C_p = 0.59$,

actual wind turbine have a C_p between 0.1 - 0.4. Therefore, all wind turbines in this study were assumed to be $C_p = 0.29$.

In order to obtain balancing requirements of intermittent DWG, 15-minute wind production data was used. Wind hourly forecast was obtained by averaging wind power generation of every hour and superimposing wind forecast error on the hourly average. Wind production of each wind plant in 2035 was assumed to be identical to current wind production. Statistical information of hour-ahead wind forecast error is shown in Table 3.2.

Table 3.2 Statistics of hour-ahead wind forecast error [27]

Parameter	Value (%)
Mean error	0 %
Standard deviation	7 %
Auto correlation	0.6

NW100 wind turbine installed at 37 m hub height at Riley County Public Works facility in Manhattan, Kansas was used to model wind power generation. Technical specifications of the NW100 wind turbine are listed in Table 3.3. All DWG installed assumed to follow the normalized NW100 production curve illustrated in Figures 3.3. In addition, all DWG installed assumed to follow normalized power generation curves in low- and high-wind profiles illustrated in Figures 3.4 and 3.5. NW100 has the ability to provide ±45 kVar of reactive power irrespective of production state of the turbine (active, idle, or service).

Table 3.3 Technical specifications of NW100 turbine

Characteristic	Value
Rated power	100 kW
Design life	20 years
Rated wind speed	14.5 m/s (32.4 mph)
Cut-in wind speed	3.5 m/s (7.8 mph)
Cut-out wind speed	25 m/s (56 mph)
Extreme wind speed	59.5 m/s (133 mph)
Reactive power	+/- 45 kVAR
Power factor (PF)	> 99%

Figure 3.3 NW100 power curve

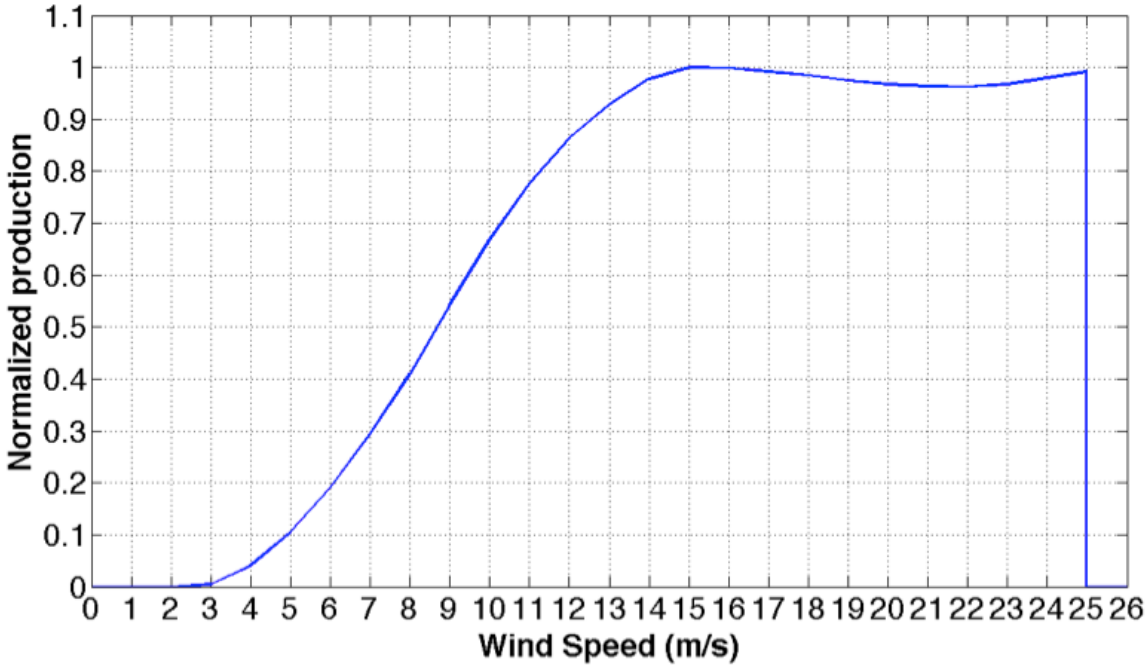

Figure 3.4 NW100 normalized power generation curve in low-wind conditions

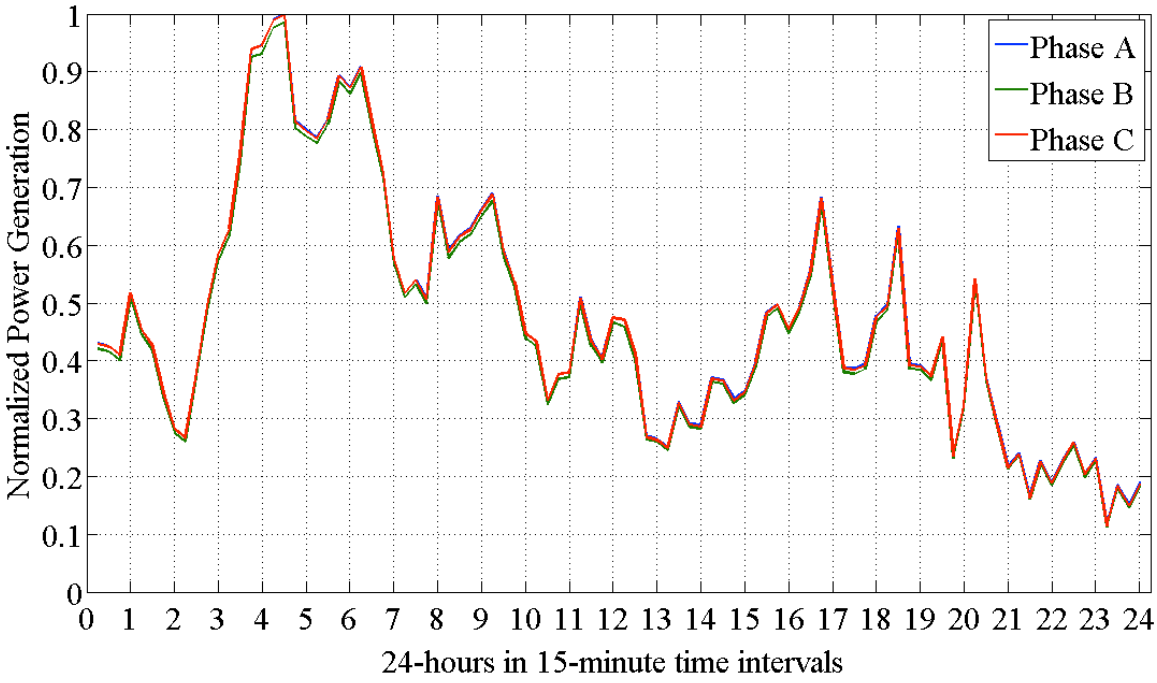

Figure 3.5 NW100 normalized power generation curve in high-wind conditions

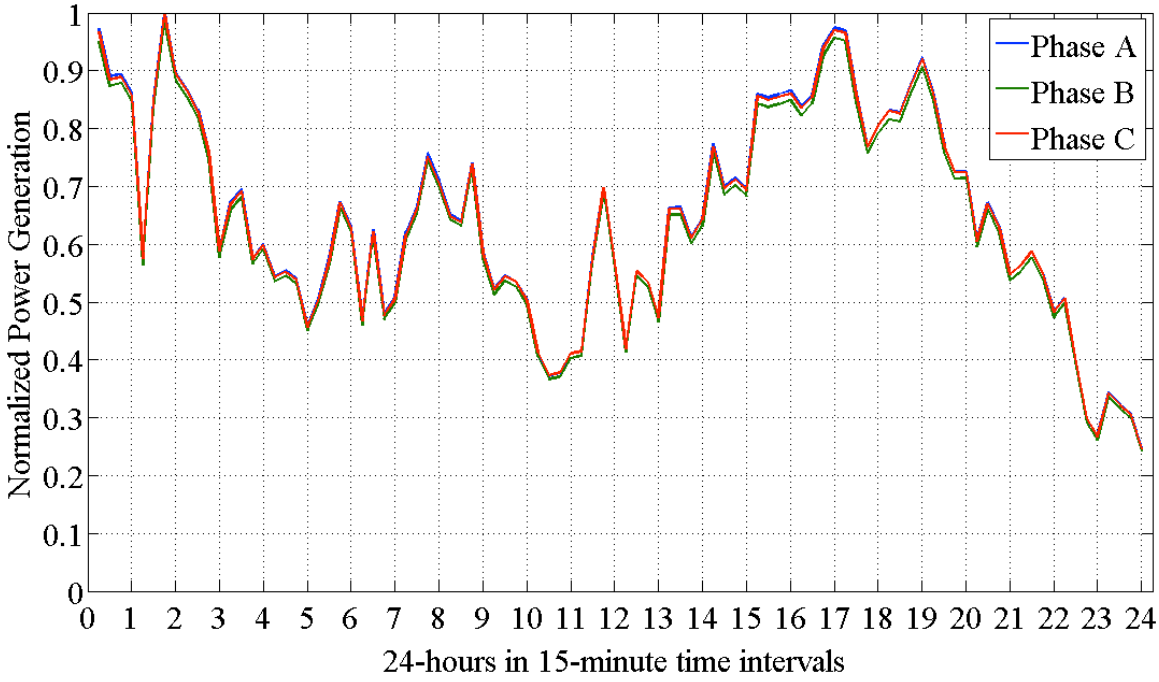

Load Data

Load demand data of 150 houses in California, collected over one-year period, was used to generate the normalized load demand curve illustrated in Figure 3.6. Only 1-hour interval datasets were available for load demand, so 1-hour interval data were interpolated to generate required 15-minute data. The EIA's annual load growth projection to 2040, assuming approximate 0.9% annual growth, was used. No modifications of the current load demand shape were assumed. The addition of load forecast error to the hourly average of load generated the hourly load forecast. Table 3.4 shows statistics for load forecast errors.

Table 3.4 Statistics of hour-ahead load forecast error [27]

Parameter	Value (%)
Mean error	0 %
Standard deviation	2 %
Auto correlation	0.9

Figure 3.6 Normalized load demand curve of 24-hour period

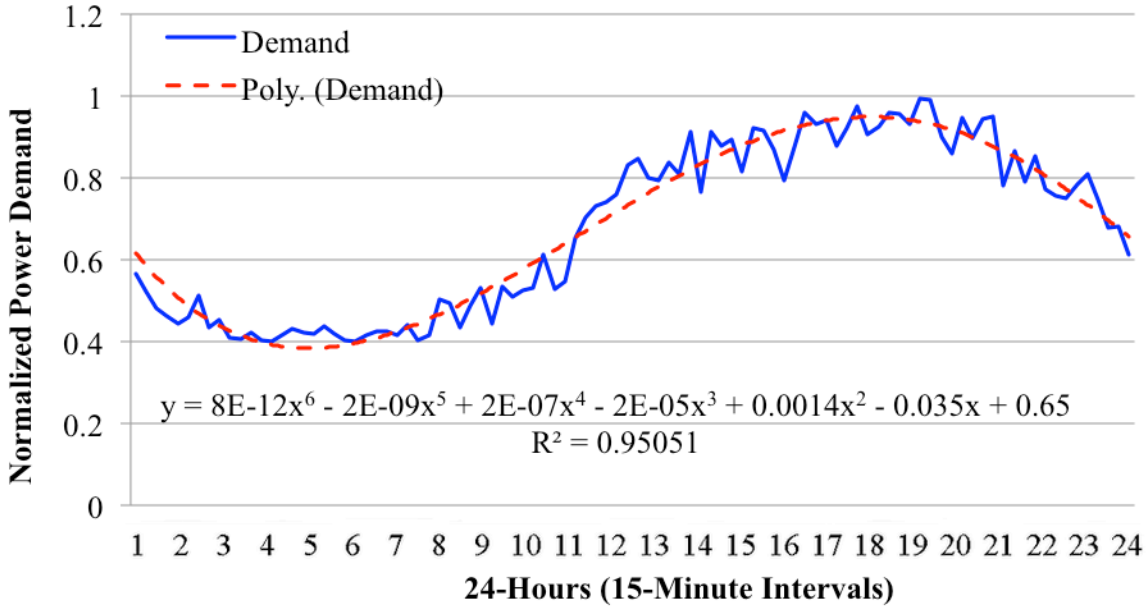

Test Feeder Data

The IEEE 37-node three-phase unbalanced and asymmetrical radial distribution system was used as the test feeder. Load data provided by the IEEE test feeder was treated as peak demand of the system. Node 1 (799) was assumed to be the slack bus, thereby controlling the conventional power injection and reactive power control of the distribution system. Node 1 was also considered in DWG and BESS placement. All nodes in IEEE 37-node test feeder were assumed to have sufficient land area to accommodate DWG and BESS. Figure 3.7 illustrates the IEEE 37-node test feeder.

Figure 3.7 IEEE 37-node three-phase unbalanced and asymmetrical radial distribution test feeder

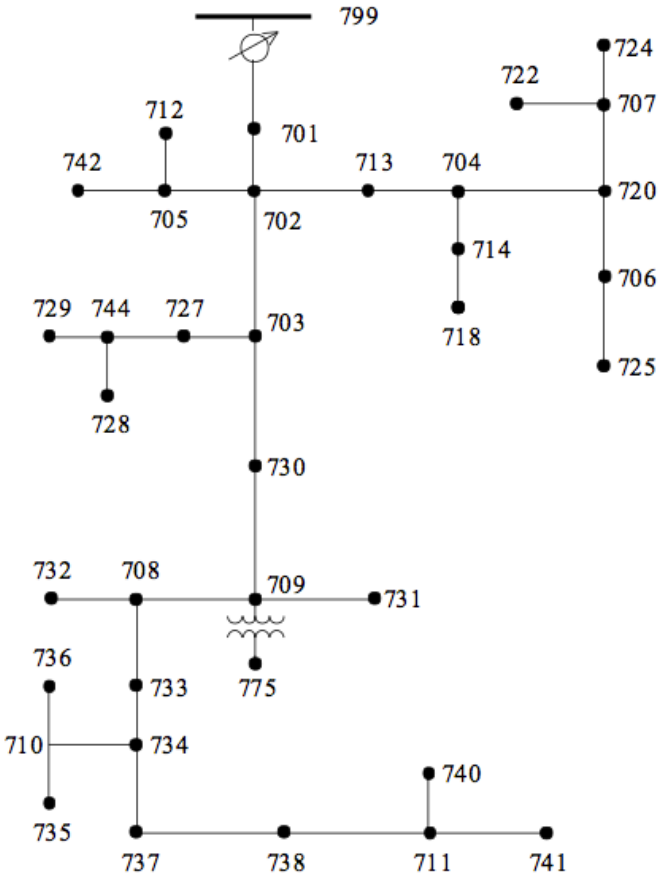

NaS Battery Storage

In this research, NaS batteries were used as BESS units. NaS batteries are suitable for energy, power, or particularly useful energy and power applications [28]. The primary function of NaS batteries is long duration of energy storage, used for load leveling, arbitrage, "islanding," and renewable output smoothing [29-31]. In addition, rapid response time (1 millisecond) and the ability to provide pulse power make NaS suitable for many power quality applications [28,32].

Energy output of NaS ranges from 360kWh to tens of MWh, and nominal discharge capacity ranges from 50kW to 100 MW [33]. An energy density between 100 and 250Wh/kg and

power density of 260W/kg allows NaS to ne install in a small land [33]. The estimated lifespan of a NaS battery is between 10 and 15 years depending on frequency of use and DOD. NaS used in this study were estimated on 300 charge-discharge cycles per year. Currently NaS batteries are commercially available in an energy/rated power (E/P) ratio of 6-7. For this study, the assumption was made that future batteries will be available with E/P as low as 1 in order to avoid oversizing the batteries.

NaS batteries consist of many cells that are series-parallel connected and fused, and operate at high temperatures (300 °C to 350 °C). Figure 3.8 illustrates a NaS cell, and technical specifications are listed in Table 3.5.

Figure 3.8 NaS Cell

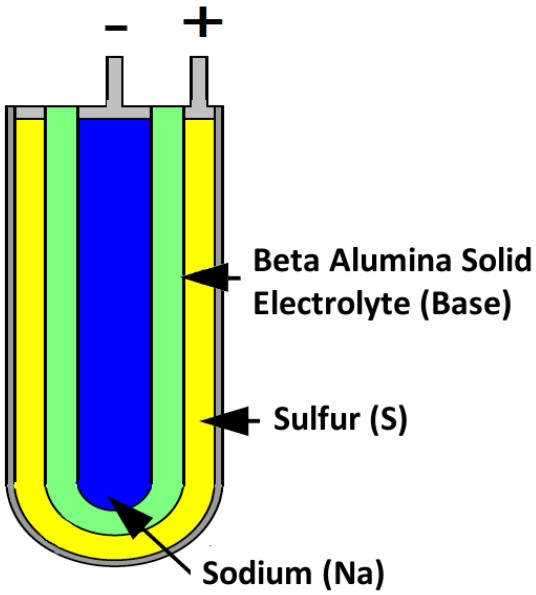

NaS were assumed to charge either from the grid or using power generated by DWG. In an islanded situation, NaS and DWG operate instantaneously to fulfill load demand of the power system. In a grid-connected operation, NaS charge using spill wind energy or power from grid no matter the time of day (free-running mode). The NREL describes four challenges related to widespread deployment of BESS: development of cost-competitive energy storage technologies,

validation of reliability and safety, equitable regulatory environment, and industry acceptance [34]. Therefore, minimizing total BESS/NaS capacities in the system will decrease project costs and increase system profitability.

Table 3.5 Technical specification of NaS battery module

Characteristic	Value
Rated power	50kW to 1 MW
Design life	15 years (4500 cycles)
Charge- discharge efficiency	90%
Pulse power	2ms (Full)
Continuous discharge time	7.2 hours
DOD	90%

Overview of the Methodology and Multi-Objective Optimization

In this research, four objective functions were used to optimize the capacity and location of DWG and NaS: network losses, voltage profile, availability of DWG/NaS to provide base power demand, and PV of savings. Multi-objective optimization with respect to objective function was a minimization. Constraints were implemented individually for each objective function using the penalty factor approach [35].

Network Losses

Only real power loss of the distribution system was considered in this study. Real power loss of the system was obtained using Equation (3.3) [36,37].

$$g_1 = P_{loss} = \sum_{\phi=A,B,C} P_{loss}^{\phi} \tag{3.2}$$

$$g_1 = \sum_{\phi=A,B,C} \left[\sum_{i=1}^{n} \sum_{\substack{m=1 \\ m>i}}^{n} V_i^{\phi} V_m^{\phi} Y_{im}^{\phi} \cos\left(\theta_i^{\phi} - \theta_m^{\phi} - \delta_{im}^{\phi}\right) \right] \tag{3.3}$$

where n is number of nodes in the system, ϕ is phase of the line (A, B, C), V_i^{ϕ} and V_m^{ϕ} are magnitude of voltage in phase ϕ at bus *i* and bus *m* respectively, θ_i^{ϕ} and θ_m^{ϕ} are phase angle of voltage in phase ϕ at bus *i* and bus *m* respectively, Y_{im}^{ϕ} is magnitude of admittance phase ϕ between bus *i* and bus *m,* and δ_{im}^{ϕ} is phase angle of admittance phase ϕ between bus *i* and bus *m.*

The following constraint was set for system loss reduction limits:

$$P_{\text{losswR\&S}} \leq P_{losswoR\&S} \tag{3.4}$$

where $P_{\text{losswR\&S}}$ is total active power loss of the system with DWG and NaS and $P_{losswoR\&S}$ is total active power loss of the system without DWG and NaS. Using the constraint for loss reduction, penalty factors for network losses can be calculated:

$$f_{\Delta P_{loss}} = \left\{\frac{1}{|P_{losswoR\&S} - P_{losswR\&S}|}\right\} \tag{3.5}$$

Therefore, loss minimization of the system after implementing constraints can be calculated by:

$$f_1 = g_1 f_{\Delta P_{loss}} \tag{3.6}$$

Voltage Profile

Voltage improvements were achieved by minimizing maximum voltage deviation of each phase in each bus using Equation (3.7). The objective of minimization was to achieve voltage profile close to 1 p.u.

$$VD^{\phi} = \left|V_{ref} - V_i^{\phi}\right| \tag{3.7}$$

$$g_2 = \max\left(VD_{\phi=A,B,C}\right) \tag{3.8}$$

where V_{ref} is reference voltage (1 p.u.). The following constraint was set for voltage limits:

$$V^{min} \leq V_i^{\phi=A,B,C} \leq V^{max} \tag{3.9}$$

where V^{min} is allowed minimum voltage limit (0.95 p.u.) of the system and $V^{max}$is allowed maximum voltage limit of the system (1.05 p.u.). Constraints were introduced to the system using the following equation:

$$f_v = \begin{cases} 1 & ,0.95 \le V_i^{\phi} \le 1.05 \\ \max\left(V_i^{\phi}\right) & ,\max\left(V_i^{\phi}\right) > 1.05 \; and \; \min\left(V_i^{\phi}\right) \ge 0.95 \\ 1 \Big/ \min\left(V_i^{\phi}\right) & ,\max\left(V_i^{\phi}\right) \le 1.05 \; and \; \min\left(V_i^{\phi}\right) < 0.95 \\ max\left\{\max\left(V_i^{\phi}\right), 1 \Big/ \min\left(V_i^{\phi}\right)\right\} & ,else \end{cases} \quad (3.10)$$

Objective function of the voltage profile of the system with constraints: can be calculated by

$$f_2 = g_2 f_v \quad (3.11)$$

The objective of f_2 was to achieve nodal voltage close to 1 p.u. for all system.

Availability

Availability is the ability to supply power to the loads. Availability is a primary factor affecting the total installed capacity of a DWG project. For example, a highly reliable wind turbine can have low availability if insufficient energy storage supports the load's power requirement during high demand period or on a day with low wind. Availability for the system is presented in Equation (3.12):

$$g_3 = \sum_{i=1}^{m} \sum_{t=1}^{T} \left(S_D(t) + S_L(t) - \left(S_i^R(t) + P_i^S(t) \right) \right) \quad (3.12)$$

where S_D is total load demand of the system at time *t*, S_L is total loss of the system at time *t*, S_i^R is total power generated by DWG at time *t,* and P_i^S is total power transactions of NaS. DWG and NaS power supply is not limited to the node they are connected. Availability of the DWG and NaS power supply is constraints as follows:

$$\sum_{i=1}^{n}\left(S_i^R(t)+P_i^S(t)\right)\geq S_D(t)+S_L(t) \tag{3.13}$$

Constraints were implemented using the penalty factor for availability:

$$f_a=\begin{cases}1\,,(S_D(t)+S_L(t))>\sum_{i=1}^{n}\left(S_i^R(t)+P_i^S(t)\right)\\0\,,(S_D(t)+S_L(t))\leq\sum_{i=1}^{n}\left(S_i^R(t)+P_i^S(t)\right)\end{cases} \tag{3.14}$$

Objective function of availability with constraints can be calculated by

$$f_3=g_3f_a \tag{3.15}$$

Economic Analysis

Economic optimization regarding DWG and NaS is explained in this section. Economic optimization of the system was achieved by minimizing the present value of DWG and NaS implementation. Present values of each system component include capital cost(s), O&M costs, revenues associated with DWG, and net benefits associated with salvage. Equation (3.16) calculates the present value of system savings.

$$PV=\sum_{i=1}^{m}\left[PV_i^{cap}+PV_i^{O\&M}+PV_i^{sal}-PV_i^{rev}\right] \tag{3.16}$$

$$f_4=\min\left(PV\right) \tag{3.17}$$

where i is the node number and m is total number of nodes in the system, PV_i^{cap} is capital cost of DWG and NaS at node *i,* $PV_i^{O\&M}$ is O&M cost of DWG and NaS at node *i,* PV_i^{sal} is salvation value of DWG and NaS at node *i,* and PV_i^{rev} is revenue of DWG and NaS at node *i.* Engineering economics were applied to the model to calculate the present value using two equations that accounted for the time value of money. Net benefits incurred uniformly over time were accounted for using the Uniform Series Present Worth factor (USPW) (Equation (3.18)), and

present value of a future benefit or cost was determined using the Single Payment Present Worth factor (SPPW) (Equation (3.19)) [38]:

$$PV = R\left[\frac{(1+i)^n-1}{i(1+i)^n}\right] = R[USPW(i,n)] \quad (3.18)$$

where PV is present value, R is net benefit, i is appropriate interest or discount rate (3%), and n (L=20 years) is the number of time periods within the lifetime of the project. All costs or benefits were assumed to occur at the end of each time period.

$$PV = \frac{S}{(1+i)^n} = S[SPPW(i,n)] \quad (3.19)$$

where S is the assumed future value. The present value of an initial cost is equal to the initial cost itself. Functions were not applied to initial costs because the time value of money does not affect their present value. Discount rates were adjusted to account for the varying cost of electricity:

$$i_{esc} = \frac{i-e}{1+e} \quad (3.20)$$

where e is escalation rate (1.01%). One benefit of the system is the present value of active power reduction, which is the reduction of power transmitted from grid to distribution system. Power transmitted to a distribution system without DWG is equal to system power demand and line and equipment loss.

DWG Cost Evaluation

When sizing DWG in a distribution system, the primary objective is to minimize present value of the implementation. The decision variable of the DWG objective function is power rating of wind turbines at each node *i.* Therefore, a constraint was set to the minimum power rating of the total DWG present in the system at time *t*:

$$\sum_{i=1}^{m}(S_i^R + P_i^{ST}) \geq \max\,(S_D(t) + S_L(t)) \quad (3.21)$$

where S_i^R is power generation of DWG at node *i*, P_i^{ST} is power from/to BESS at node *i*, $S_D(t)$ is total power demand of the system at time *t*, and $S_L(t)$ is total power loss of the system at time *t*. Present value of costs associate with DWG are capital cost(s), O&M costs, and benefits associated with salvage.

$$PV_R = PV_{Rcap} + PV_{RO\&M} + PV_{Rsal} \tag{3.22}$$

where PV_{Rcap} is capital cost(s) of DWG, $PV_{RO\&M}$ is O&M costs of DWG, and PV_{Rsal} is salvage costs of DWG. Capital costs associated with DWG implementation include turbine units, installation, balance of plant (BOP), and substation and/or interconnection expenses [25]. Present value of total DWG installed in the system was calculated using Equation (3.23):

$$PV_{Rcap} = \sum_{i=1}^{m} P_i^R \, C_1 \tag{3.23}$$

where P_i^R is total power rating of DWG at node *i* and C_1 is DWG capital cost coefficient ($2220/kW). Values related to DWG O&M costs are highly uncertain because O&M costs vary with changes in renewable energy technology, O&M costs generally increase with the age of an energy system, and lack of O&M cost data. DWG O&M costs divided in to fixed and variable O&M costs. Fixed and variable O&M cost associated with DWG were calculated using Equation (3.24).

$$PV_{RO\&M} = PV_{Fixed\ O\&M} + PV_{Variable\ O\&M} \tag{3.24}$$

$$PV_{Fixed\ O\&M} = \sum_{i=1}^{m}(P_i^R \; C_2[USPW(i = i_{eff}, n = L)]) \tag{3.25}$$

$$PV_{Variable\ O\&M} = \sum_{t=1}^{T}\sum_{i=1}^{m}(E_i^R C_3 \; [USPW(i = i_{eff}, n = L)]) \tag{3.26}$$

where C_2 is fixed O&M cost coefficient ($28/kW-yr), E_i^R is energy generated by DWG at node *i* over the time period *t*, and C_3 is variable O&M cost coefficient ($0.01/kWhr).

A fair amount of uncertainty is associated with DWG salvage net benefit estimation. Decommissioning costs and salvage values vary significantly between projects and do not

indicate strong relationship between net decommissioning cost and total installed power rating. Studies have shown negative and positive net benefits associated with DWG decommissioning, ranging from -$27.79/kW to $0.64/kW of installed power rating. A cost of $10/kW of installed power was used to assess net benefit associated with salvage of DWG. Therefore, DWG salvage cost coefficient was calculated as an average decommissioning cost observed in the literature using Equation (3.27) [39-41].

$$PV_{DWG,Salvage} = \sum_{i=1}^{m} P_i^R V_1 \left[SPPW\left(i = i_{eff}, n = L\right)\right] \quad (3.27)$$

where V_1 ($10/kW) is DWG salvage value cost coefficient.

NaS cost evaluation

The objective of sizing NaS systems for economic optimality is to minimize the present value of implementation. Decision variables of storage system optimization include NaS capacity and DoD at each node. The present value NaS implementation in a distribution system is a function of capital cost, O&M cost, and salvage cost, calculated by

$$PV_S = PV_{Scap} + PV_{SO\&M} + PV_{SSal} \quad (3.28)$$

where $PV_{Scap}$is capital cost(s) of NaS, $PV_{SO\&M}$ is O&M costs of NaS, and PV_{SSal} is salvage cost of NaS. Energy capacity and power rating categorize NaS unit size. Energy capacity is the amount of energy that can be stored in a NaS unit and power rating is the rate at which NaS charges or discharges energy. NaS capacity and power rating cannot be sized independently; therefore, power rating is determined as a function of capacity in which capacity is a decision variable. The functional relationship between power rating and capacity was determined using the U.S. DOE International Storage Database [31] and information regarding two NaS modules available by NGK Insulators LTD. The database provides specification information of nine NaS

storage systems located around the world. Figure 3.9 illustrates the relationship between the BESS capacity and power rating.

Figure 3.9 Relationship between BESS capacity and power rating

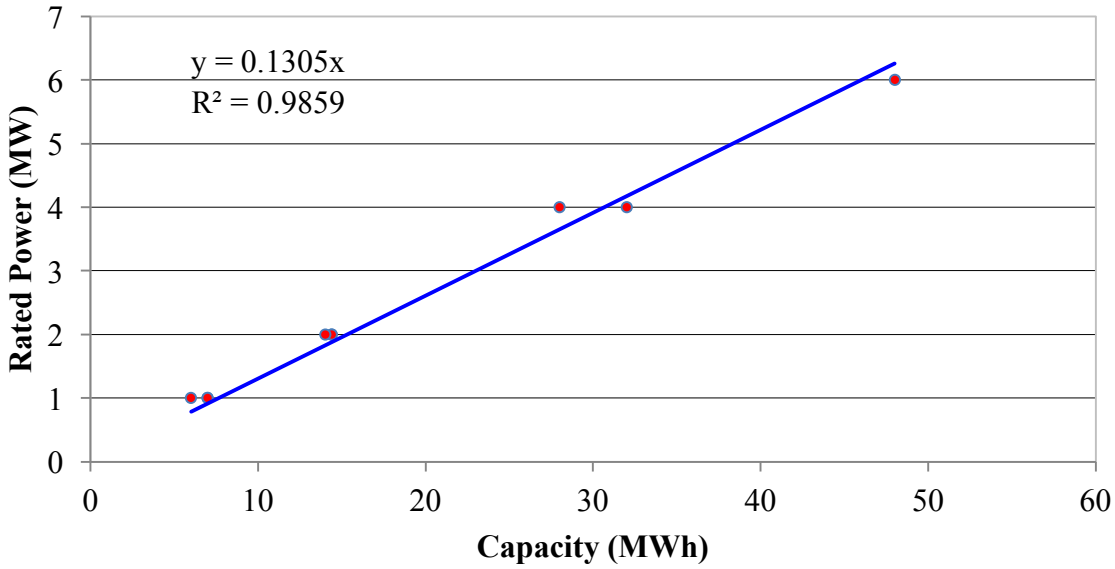

Capital costs of a NaS system include initial cost of the energy storage system, initial cost of the power conditioning system (PCS), and reoccurring capital costs. NaS modules and PCSs may be replaced during the lifetime of the project, resulting in reoccurring costs. Any node in the IEEE 37-node test feeder was a candidate node for NaS system. NaS capital costs were calculated by

$$PV_{Scap} = PV_{initial} + PV_{reoccuring} \tag{3.29}$$

$$PV_{initial} = \sum_{i=1}^{m}\left(E_i^S C_4 + P_i^S (C_i^{PCS} + C_5)\right) \tag{3.30}$$

where E_i^S is storage device capacity at node i (kWh), C_4 ($285/kWh) is the NaS capital cost coefficient, P_i^S is the storage device power rating at node i, C_i^{PCS} ($220/kW) is the PCS cost coefficient at node i, and C_5 ($40/kW) is the BOP cost coefficient. Present value of NaS reoccurring capital costs was calculated by

$$PV_{Reoccuring} = \sum_{i=1}^{m} \left\{ \begin{matrix} \sum_{p=1}^{n} \left(E_i^S C_4\right) \left[SPPW\left(i = i_{eff}, n = L_i^S\ p\right)\right] \\ + \sum_{q=1}^{k} \left(P_i^S C_i^{PCS}\right) \left[SPPW\left(i = i_{eff}, n = L_i^{PCS}\ q\right)\right] \end{matrix} \right\} \quad (3.31)$$

where m is the number of storage device capital purchases required at node i, k is the number of required capital PCS purchases at node i, L_i^S (15 years) is storage device lifetime at node i (years), L_i^{PCS} (7-years) is PCS lifetime at node i, p is the number of batteries at node i, and q is the number of PCS at node i.

Lifetime of the NaS unit is related to its specified DOD. The relationship between lifetime cycling capacity (EL_i^c) and DOD was developed for lead-acid batteries, as demonstrated in Equation (3.32).

$$EL_i^c = \frac{6L_i^c}{(5(DoD_i)+1)} \quad (3.32)$$

where L_i^c is the cycling lifetime of the storage device at 100% DOD, and DOD_i is the average depth of discharge of the storage system at node i (90%).

The cycling lifetime of NaS storage devices at 100% DOD was approximately 3,000 [42], and recommended maximum DOD for NaS storage devices was 85% - 95% of capacity [28]. The required number of capital purchases of a NaS is related to the NaS's expected average cycles per year, project lifetime, and effective lifetime cycling capacity of the NaS system. In this study, NaS units were assumed to function immaculately for 15 years with 300 cycles expected per year. Therefore, all NaS units were expected to reinstall every 15 years. PCSs were assumed to have a life cycle of 7.5 years.

O&M costs of the NaS were divided as fixed and variable costs. Fixed O&M costs are associated with maintenance of NaS units and PCSs. Variable O&M costs are based on the electrical throughput of the NaS units. Fixed and variable O&M costs can be calculated as

$$PV_{SO\&M} = \sum_{i=1}^{m}\left(E_i^S C_6 + P_i^S C_7 + \sum_{t=1}^{8,760} ET_i^S(t)\, C_8\right)\left[USPW\left(i = i_{eff}, n = L\right)\right] \quad (3.33)$$

where ET_i^S is energy transfer from NaS to user at time *t* at node *i,* C_6 ($3/kW-yr) is storage system cost coefficient, C_7 ($2/kW-yr) is PCS cost coefficient, and C_8($0.007/kWh) is variable O&M cost coefficient of NaS. Value of ET_i^S is treated as a repeating series over the project's lifetime.

Salvage values of NaS battery modules are relatively high compare to Li-Ion battery modules. NaS energy storage modules 99% recyclable [29]. The salvage value of each NaS storage system was treated as a benefit and assumed to be 15% of the battery system's capital cost [44]. Present value of the NaS salvage is calculated by

$$PV_{BESS\ Salvage} = \sum_{i=1}^{m}\sum_{p=1}^{N}\left(E_i^S C_6\right)\left[SPPW\left(i = i_{eff}, n = L_{BESS,i}p\right)\right] 0.15 \quad (3.34)$$

where E_i^S is energy capacity of NaS units at node *i,* and C_6 ($3/kW-yr) is storage system cost coefficient .

Revenue of DWG and NaS

Renewable energy generated by DWGs was distributed in the system in four ways:

(I) Sell energy to "the grid".

(II) Store energy in NaS (charging).

(III) Use stored energy in NaS (discharging).

(IV) Consume of energy directly from DWG.

Energy is not transferred from NaS to the grid. Revenue experienced from distribution of DWG energy is calculated by Equation (3.35):

$$R = \sum_{i=1}^{m}\sum_{t=1}^{T}\left[E_i^{SU}(t) + E_i^{RU}(t) + E_i^{RG}(t)\right] p(t) \quad (3.35)$$

where E_i^{SU} is energy transferred from NaS unit at node *i* to user at time *t*, E_i^{RU} is energy transferred from DWG unit to user at node *i* at time *t*, E_i^{RG} is energy transferred from DWG unit

to grid at node *i* at time *t*, and $p(t)$ is the energy price matrix. Present value of revenue was calculated by treating the calculated value of *R* as a uniform series:

$$PV_{revenue} = R[USPW(i = i_{esc}, n = L)] \quad (3.36)$$

Two types of energy price information are contained within the energy price matrix p. The first type of price information is electrical company's electricity price and time schedule. A customer is charged for energy consumption based on the time-of-use (TOU) rate schedule. TOU rate schedules often vary depending on type of customer and amount of energy the customer demands. The TOU rate schedule used for this analysis was the Tier 1, E-7 residential TOU rate schedule shown in Table 3.7. Minimum energy charge ($0.14784) and a meter charge per day ($0.11532) were applied to all TOU periods.

Table 3.6 TOU rate schedule [45]

TOU Period	Cost of Energy ($/kWh)	
	Summer	Winter
Peak [(a)]	0.32251	0.11426
Off-Peak [(b)]	0.08159	0.08510

(a) Summer (May-October) and winter (November- April) peak our period is T2:00 noon to 6:00 pm Monday to Friday

(b) Summer and winter off-peak hours are all the other hours except peak hours

The second type of energy price information in energy price matrix p is the power purchase agreement (PPA). A PPA is an agreement between the power company and another party that defines the terms to which the energy company will purchase energy from the party. PPA information is readily available for DWG. Pacific Gas and Electrics' (PG&E) small-scale DWG PPA information was used in this analysis. PG&Es' PPA agrees to purchase power from customers renewable generation capacity up to 1.5 MW. Adopted 2011 market price referents (MPR) of PG&E long-term contracts are shown in Table 4.8. MPR value in Table 3.8 was multiplied by a Time-of-Day (ToD) factor to illustrate that electricity produced during peak

times is more valuable than electricity produced during other times. ToD factors for PG&E are shown in Table 3.9.

Table 3.7 Adopted 2011 market price referents – long-term contracts [47]

Resource Type (Base load MPR)	10-Years ($/kWh)	15-Years ($/kWh)	20-Years ($/kWh)
2012	0.07689	0.08353	0.08956
2013	0.08104	0.08776	0.09376
2014	0.08454	0.09150	0.09755
2015	0.08804	0.09519	0.10132
2016	0.09156	0.09883	0.10509
2017	0.09488	0.10222	0.10859
2018	0.09831	0.10570	0.11218
2019	0.10185	0.10927	0.11586
2020	0.10550	0.11296	0.11965
2021	0.10916	0.11675	0.12353
2022	0.11299	0.12066	0.12752
2023	0.11691	0.12468	0.13160

Table 3.8 ToD periods and factors [47]

Monthly-period	Super peak[1]	Shoulder[2]	Night[3]
June - Sep	2.38	1.12	0.59
Oct-Dec, Jan & Feb	1.10	0.94	0.66
Mar - May	1.22	0.90	0.61

1 – Hours ending 13-20 PPT, Monday – Friday except holidays,

2 – Hours ending 7-12, 21, and 22 PPT except holidays

3 – Hours ending 1-6, 23, and 24 PPT

Energy generated by DWG over time step *t*, distributed directly to the user, the grid, and BESS units is constrained by

$$E_i^R(t) \geq E_i^{RS}(t) + E_i^{RU}(t) + E_i^{RG}(t) + E_{ij}^L(t), \forall\, i, \forall j, i \neq j \tag{3.37}$$

where $E_i^R(t)$ is total energy generated by DWG at node *i* in time step *t,* E_{ij}^L is energy loss of the system from node *i* to *j*, and E_i^{RU} is energy transferred to the NaS unit at node *i* in time step *t.* A greater-than-or-equal-to sign is used in the energy balance to allow for the disposal of excess energy. Excess energy may be generated when load demand is met by NaS systems and O&M

costs of generating electricity are greater than revenues that produced by selling energy to the electrical company.

The amount of energy discharged by the NaS unit is constrained by

$$SoC_i(t) = SoC_i(t-1)(1-d_i) + \eta(E_i^{RS}(t)) - E_i^{SU}(t) \quad (3.38)$$

where SoC_i is state of charge of the NaS unit at node *i*, d_i is self-discharge rate (%) of the NaS unit at node *i* and η is round-trip efficiency of the NaS unit. A review of the literature showed that studies included a self-discharge rate for NaS systems in order to account for required temperature control [46]. However, this research did not consider temperature control, so self-discharge was ignored. A round-trip efficiency of 90% was considered for NaS battery systems [28]. The following constraints were applied to define maximum and minimum limits of SoC of each NaS unit:

$$SoC_i(t) \leq SoC_{max,i} \ , SoC_{max,i} = 0.9E_i^S \ \forall \ i \quad (3.39)$$

$$SoC_i(t) \geq SoC_{min,i} \ , SoC_{min,i} = E_i^S(1 - DoD_i) \ \forall \ i \quad (3.40)$$

where $SoC_{max,i}$ is maximum allowed state of charge of NaS unit at node *i*, $SoC_{min,i}$ is minimum allowed state of charge of NaS unit at node *i*, and DoD_i DOD of NaS at node *i*.

The amount of energy that can be charged or discharged from storage systems is constrained by storage system SoC and rated power:

$$E_i^{SU} \leq SoC_i(t) \ \forall \ i \quad (3.41)$$

$$E_i^{RS} \leq SoC_{max,i} \ , (-SoC_i(t)) \ \forall \ i \quad (3.42)$$

$$E_i^{SU} \leq tP_i^S \ \forall \ i \quad (3.43)$$

$$E_i^{RS} \leq tP_i^S \forall \ i \quad (3.44)$$

Where, *t* is time duration in hours. Energy consumption by each load is constrained:

$$\sum_{i=1}^{m} E_i^{RU}(t) + E_i^{SU}(t) \leq E_D(t) + E_L(t) \quad (3.45)$$

where E_D is total energy demand of the system over the time period *t*. Energy consumption constraints show that DWG supplies the total demand of the system, not just demand at wind turbines' respective nodes.

Objective function of present value of the renewable system was calculated using Equation (3.16). Equation (3.16) is rewritten in detail in Equation (3.46) [48]:

$$f_4 = \Bigg\{ \left[\sum_{i=1}^{m} P_i^R \, C_1\right] + \left[\sum_{i=1}^{m} (P_i^R \; C_2[USPW(i = i_{eff}, n = L)])\right] + \left[\sum_{t=1}^{T}\sum_{i=1}^{m} (E_i^R C_3 \, [USPW(i = i_{eff}, n = L)]) \;\right] + \sum_{i=1}^{m} P_i^R V_1 \left[SPPW\big(i = i_{eff}, n = L\big)\right] + \left[\sum_{i=1}^{m} \big(E_i^S C_4 + P_i^S (C_i^{PCS} + C_5)\;\big)\right] + \left[\sum_{i=1}^{m} \begin{Bmatrix} \sum_{p=1}^{n} \big(E_i^S C_4\big)\big[SPPW\big(i = i_{eff}, n = L_i^S \, p\big)\big] \\ + \sum_{q=1}^{k} \big(P_i^S C_i^{PCS}\big)\left[SPPW\big(i = i_{eff}, n = L_i^{PCS} \, q\big)\right] \end{Bmatrix}\right] + \left[\sum_{i=1}^{m} \big(E_i^S C_6 + P_i^S C_7 + \sum_{t=1}^{8,760} ET_i^S(t) \, C_8\;\big)\big[USPW\big(i = i_{eff}, n = L\big)\big]\right] \Bigg\} - \Big\{ \Big[\sum_{i=1}^{m}\sum_{p=1}^{N} \big(E_i^S C_6\big)\big[SPPW\big(i = i_{eff}, n = L_{BESS,i} p\big)\big] 0.15\Big] + \Big[\Big(\sum_{t=1}^{T}\sum_{i=1}^{m} \Big(E_i^{SU}(t) + E_i^{RU}(t) + E_i^{RG}(t)\Big) p(t)\Big) \; \big(USPW(i = i_{esc}, n = L)\big)\Big] \Big\} \quad (3.46)$$

where P_i^R is total power rating of DWG at node *i*, C_1 is DWG capital cost coefficient ($2220/kW), C_2 is fixed O&M cost coefficient ($28/kW-yr), E_i^R is energy generated by DWG at node *i* over the time period *t*, C_3 is variable O&M cost coefficient ($0.01/kWhr), V_1 ($10/kW) is DWG salvage value cost coefficient, E_i^S is storage device capacity at node i (kWh), C_4 ($285/kWh) is the NaS capital cost coefficient, P_i^S is the storage device power rating at node i, C_i^{PCS} ($220/kW) is the PCS cost coefficient at node *i*, C_5 ($40/kW) is the BOP cost coefficient, m is the number of storage device capital purchases required at node i, k is the number of

required capital PCS purchases at node i, L_i^S (15 years) is storage device lifetime at node i (years), L_i^{PCS} (7-years) is PCS lifetime at node i, p is the number of batteries at node i, q is the number of PCS at node i, ET_i^S is energy transfer from NaS to user at time t at node i, C_6 (\$3/kW-yr) is storage system cost coefficient, C_7 (\$2/kW-yr) is PCS cost coefficient, C_8(\$0.007/kWh) is variable O&M cost coefficient of NaS, E_i^{SU} is energy transferred from NaS unit at node i to user at time t, E_i^{RU} is energy transferred from DWG unit to user at node i at time t, E_i^{RG} is energy transferred from DWG unit to grid at node i at time t, and $p(t)$ is the energy price matrix.

Power Flow Calculation and NSGA-II Optimization

Backward/forward sweep power flow algorithm

System power flow was calculated using a backward/forward sweep load flow algorithm (B/FA). In backward sweep, Kirchhoff's voltage law (KVL) and Kirchhoff's current law (KCL) were used to calculate bus voltage from the furthest nodes (leaf-nodes). In forward sweep, downstream bus voltage was updated beginning at source node. Backward sweep stopped after mismatch of calculated and specified voltage at the substation was less than a convergence tolerance. The B/FA method can be used to solve load flow of a distribution network without solving any set of simultaneous equations. Major steps of the B/FA method are summarized below.

Backward Sweep

1. Assume the rated voltage at end node is equal to 1 p.u. Starting with end node, compute the node current.

   PQ loads:

   $$I_{ij} = \frac{S_i}{V_i} \tag{3.47}$$

Constant current loads:

$$Z_i = \frac{V_i^2}{S_i} \tag{3.48}$$

$$I_{ij} = \frac{V_i}{Z_i} \tag{3.49}$$

Constant impedance loads:

$$I_{ij} = \frac{S_i}{V_{nom}} \tag{3.50}$$

2. Use KCL to calculate line current coming from node *i* to node *j*:

$$I_{ij} = I_j + \sum_{j=i+1}^{n} \sum_{\substack{k=j+1 \\ k \neq j}}^{n} I_{j,k} \tag{3.51}$$

3. Compute voltage at node *i* :

$$V_i = V_{i+1} + Z_{ij} I_{ij} \tag{3.52}$$

4. Continue Step 3 until a junction node is reached. Repeat Steps 2 and 3, starting with another end node.
5. Calculate the most recent voltage at the junction node and perform Steps 1 - 4 until reaching reference node (node 1).
6. Compare calculated voltage with rated voltage at reference node. Stop, if the voltage difference is less than specified criteria, otherwise continue to forward sweep.

Forward Sweep

1. Starting with rated voltage at reference node, compute node voltage in the forward direction from reference node to the end node(s).

$$V_{i+1} = V_i - Z_{ij} I_{ij} \tag{3.53}$$

2. Repeat backward sweep using updated nodal voltages.

where I_{ij} is line current from node *i* to *j*, S_i is apparent power demand at node *i,* V_i is nodal voltage at node *i*, Z_i is impedance at node *i,* Z_{ij} is line impedance from node *i* to *j*, and V_{nom} is nominal voltage (1 p.u).

NSGA-II Optimization

NSGA-II one of the fastest meta-heuristic methods to address the complex ODGP problem, has a $O(MN)^2$ computational complexity, where M is the number of objectives and N is the population size. Stepwise procedure of NSGA-II method is illustrated in Figure 3.10.

First, a combined population of $R_t = P_t \cup Q_t$ was formed for NSGA-II optimization. Population size of R_t was $2N$. Population in $R_t$is then sorted according to nondomination. Because all members of $2N$ were included in R_t, elitism was ensured. Solutions belonging to the best non-dominated front F_1 were emphasized. The new population P_{t+1} including F_1 was selected. If solutions in F_1 were less than population size N, the next non-dominated solution set F_2 was chosen. Nondominated fronts were chosen until the original population size N or the last nondominated front $F_1$was achieved. In general, solution count from F_1 to F_l was larger than population size. Therefore, crowding-distance operator ($\prec_n$) was used to sort the solution in F_l in descending order and choose optimal solutions to fill all population slots. The new population P_{t+1} was used for selection, crossover, and mutation to create new population Q_{t+1} of size N. The process was repeated until the condition was met (number of generations or solutions) [18].

Figure 3.10 NSGA-II Procedure

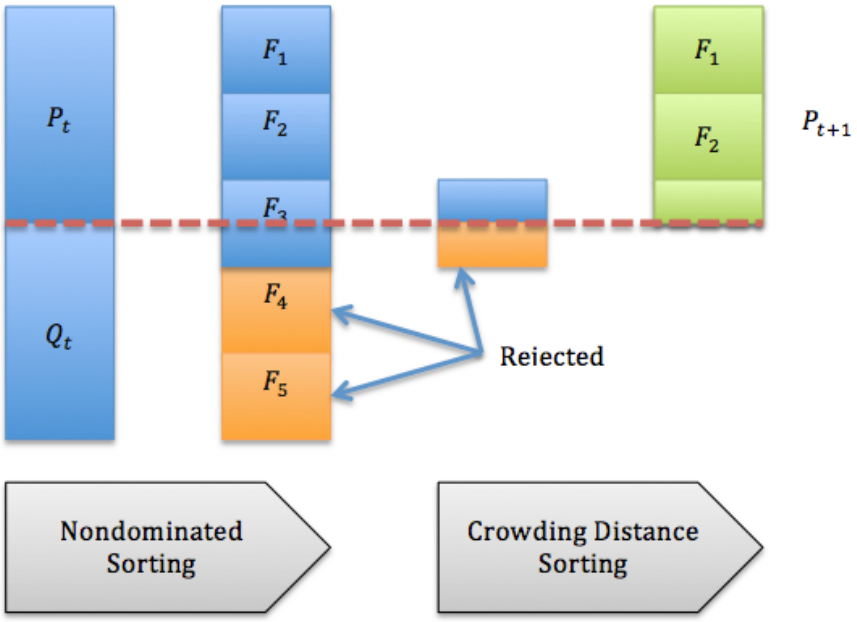

NSGA-II method generates a set of solutions known as a "Pareto optimal set" that consists of all optimal solutions for the given multi-objective function. Solution sets are categorized into Pareto fronts in which no solution dominates any other solution in same Pareto front.

Optimization of DWG and NaS capacity and placement, with respect to network losses, voltage profile, DWG/NaS availability to supply base system power demand, and present value of system savings, is illustrated in Figure 3.11.

Figure 3.11 Multi-objective optimization procedure of DWG and BESS

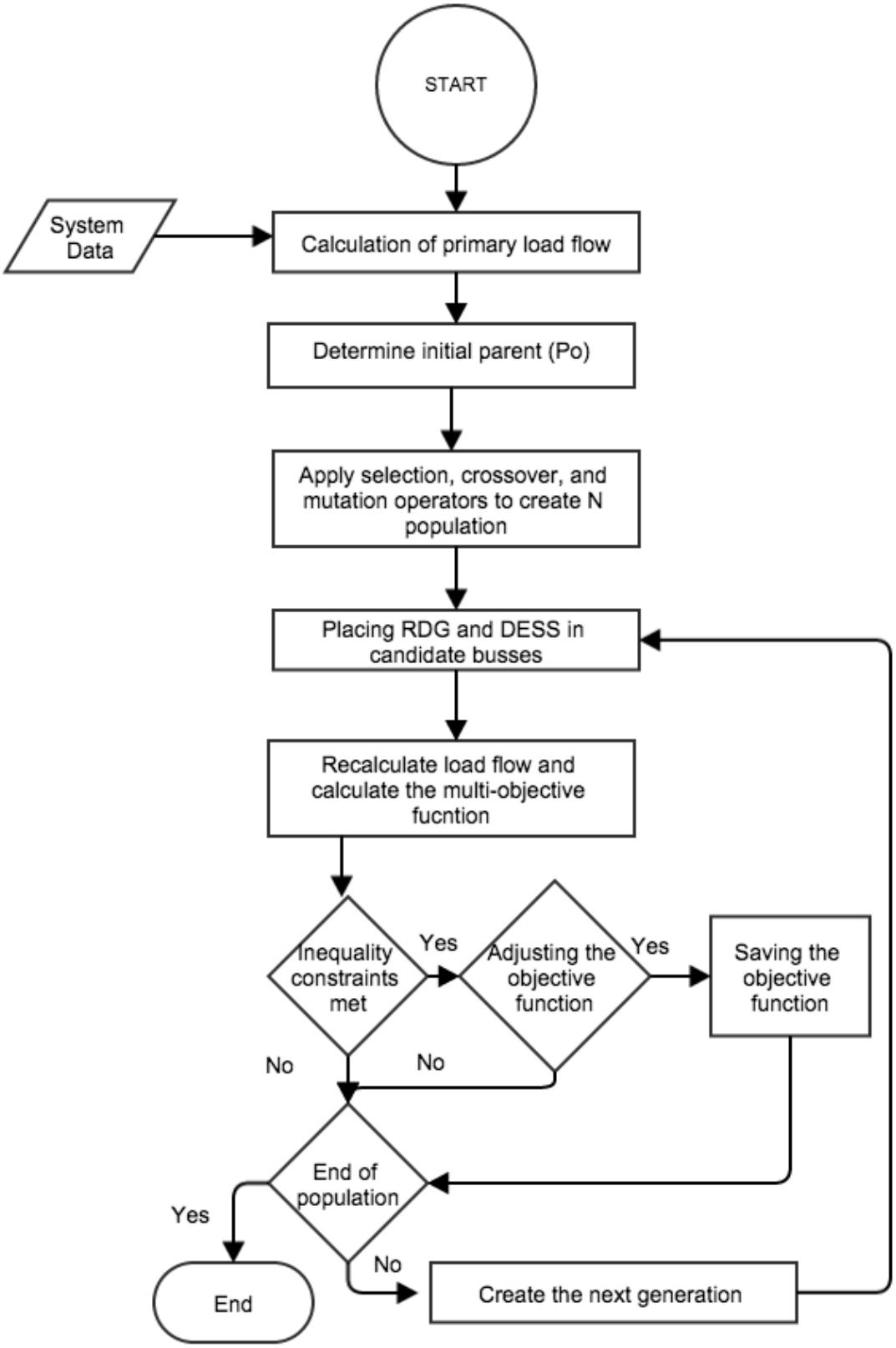

Results

Results of NSGA-II optimization were divided into two sections based on the amount of power demand fulfilled by DWG and NaS. In the first section, DWG and NaS supply a minimal base power. Equation (3.45) was modified in order to constrain power supplied by DWG and NaS, calculated by

$$0.4\left(S_{Dpeak}\right) \leq \sum_{i=1}^{m}(S_i^{RU}(t) + P_i^{SU}(t)) \tag{3.54}$$

where S_{Dpeak} is peak power demand of the system, S_i^{RU} is DWG power at time *t*, and P_i^{SU} is NaS power to user at time *t*.

Next, the system was optimized to sustain a power grid failure for 1.5 hours using only DWG and NaS. Objectives considered in this optimization were real power loss, voltage availability of DWG and NaS, and present value of system savings.

The following assumptions were made the second section of the optimization:

1. All hardware necessary to handle bidirectional power flow, without compromising power system security were presented in the system
2. Distribution system can inject power into the grid
3. Power cannot flow from grid to distribution system.

Parameters for NSGA-II optimization are presented in Table 3.9.

Table 3.9 NSGA-II parameters used for the multi-objective optimization

Population Size	Number of Generations	Selection	Crossover (Intermediate)	Mutation (Gaussian)
50	100	Binary	0.027	0.027

Providing base power of the system with DWG and BESS

Base power demand of the system was assumed to be 40% of total power demand in peak load conditions of the IEEE 37-node test feeder significant distribution system loss reductions,

power quality improvements, and present value if system savings. In order to prevent undersizing installed BESS capacity and model the impact of a power outage last for a maximum of 1.5 hours, power outage was assumed to occur between 6:30-8 PM in peak power demand conditions.

Pareto front of the multi-objective optimization is illustrated in Figure 3.12. Table 3.10 presents the total number of 75kW/ 25kW wind turbines and 50kW/25kW NaS units installed in IEEE 37-node test feeder based on the selected result. All wind turbines were assumed to follow NW100's power generation curve. The solution with lowest NaS capacity with objective values $f_1 = 428$ kW, $f_2 = 0.01$ p.u., $f_3 = 0.409$, and $f_4 = \$2.33\times10^8$ was selected to explain optimization results.

Figure 3.12 4D Scatter plot of optimization results. Objective 1, 2, 3, and 4 represent real power loss (kW), voltage deviation from reference voltage (1 p.u.), availability of DWG/BESS, and PV of cost savings ($), respectively.

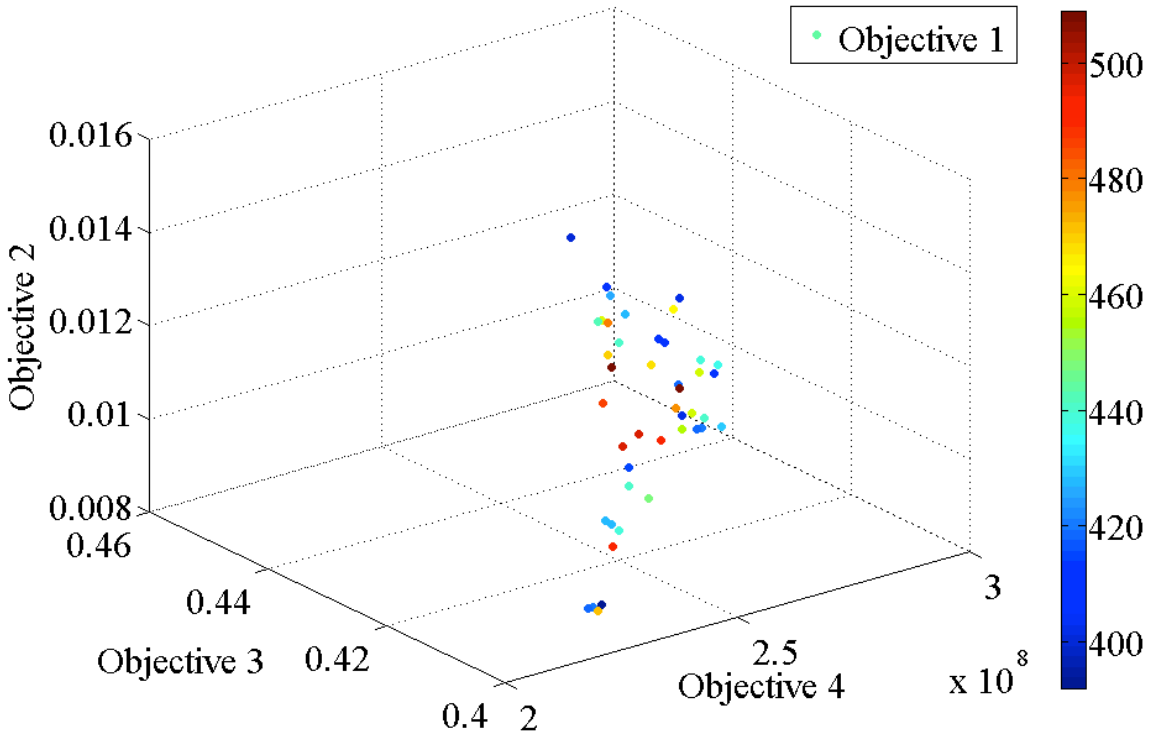

3D scatter plot and respective surface plot of selected objective function combinations are illustrated in figures 3.13 and 3.14.

Figure 3.13 3D Surface plot of objectives 1, 2, and 4. F1, F2, and F4 represent total real power loss (kW), maximum voltage deviation from reference voltage (1 p.u), and PV of network cost savings ($), respectively.

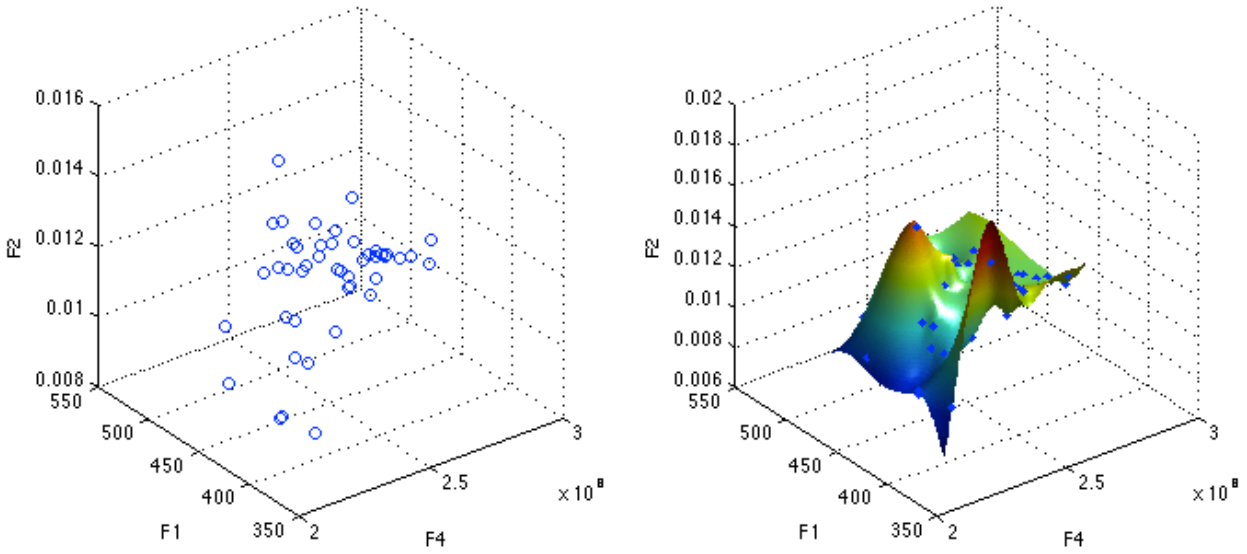

Figure 3.14 3D Surface plot of objectives 1, 3, and 4. F1, F3, and F4 represent total real power loss (kW), DWG/NaS availability, and PV of network cost savings ($), respectively.

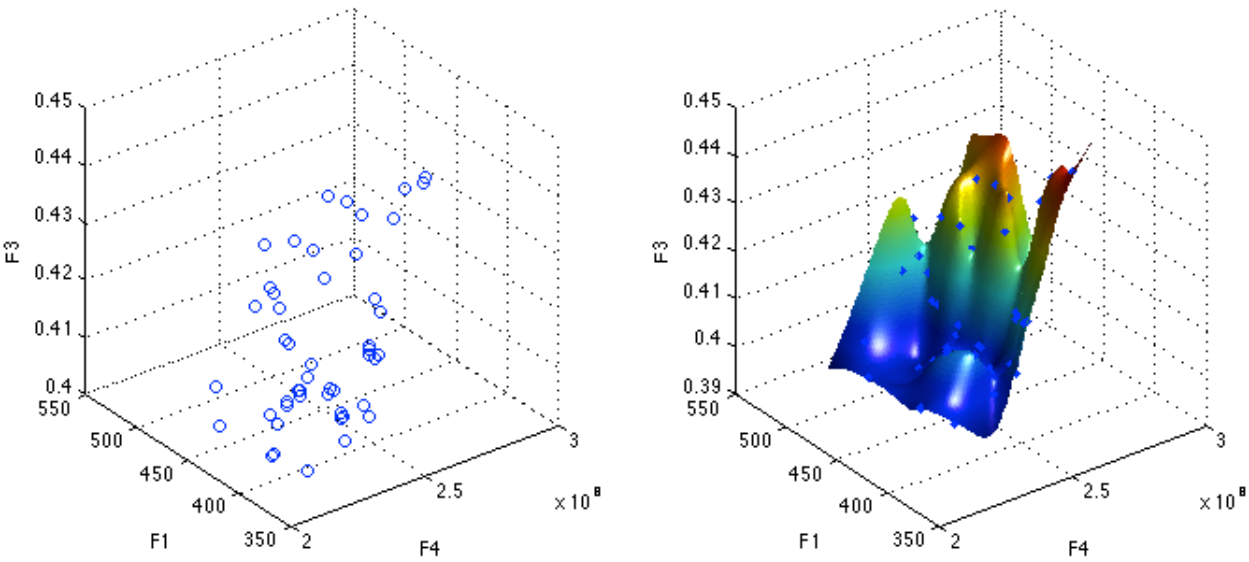

Table 3.10 Total installed capacities of DWG and NaS for the selected solution

Total number of 75kW/25kW turbines installed	Total number of 50kW/25kW NaS units installed	Total installed wind generation capacity	Total installed NaS capacity	Total installed wind generation as a percentage of peak load demand	Total installed NaS as a percentage of peak load demand
12/12	7/19	1200 kW	825 kW	48.76%	33.52%

Figure 3.15 shows optimum capacity and placement of DWG and NaS to supply base power demand of the IEEE 37-node test feeder based on the selected solution. DWG and NaS optimization with reference to real power loss, voltage profile, DWG/NaS availability, and present value of system savings, proved that candidate nodes of NaS placement were not necessarily nodes with DWG. This is characteristic of the constraint on system power demand as described in Equation (3.54), in which DWG supplied a minimum of 40% total system demand instead of demand at wind turbines' respective nodes. NaS systems charged using wind generation or power from grid, have the ability to charge or discharge simultaneously. All NaS units were assumed to be a minimum 20% filled at the beginning of optimization.

Figure 3.15 IEEE 37-node test feeder with optimized locations to place WDG and NaS

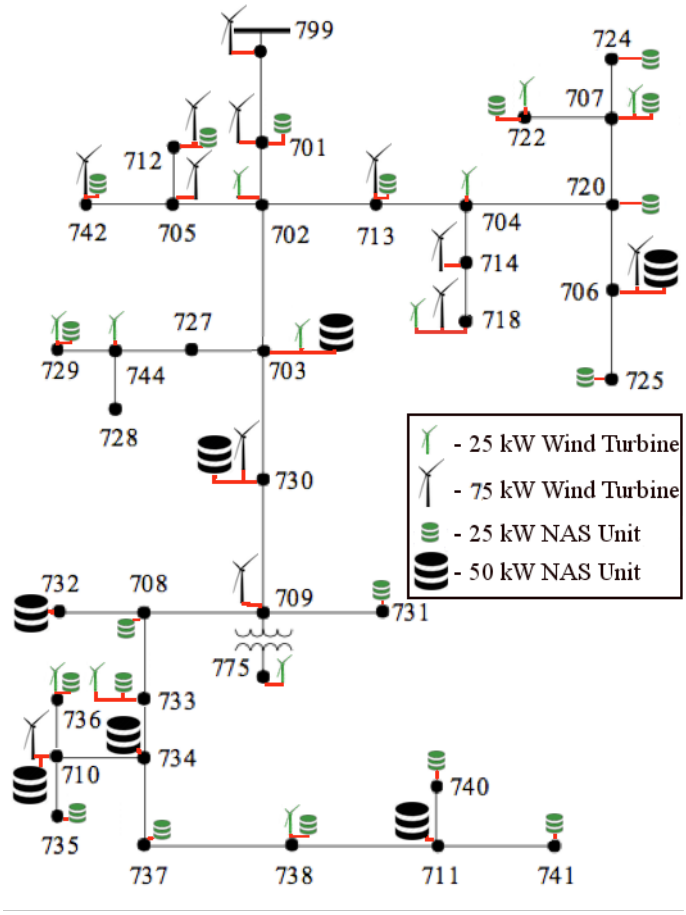

Figures 3.16 and 3.17 illustrate total real power loss of the system in each phase: original system and DWG and NaS in high-wind profile and original system and DWG and NaS in low-wind, respectively. Maximum power loss reduction was achieved with DWG, NaS, and reactive power compensation method.

Figure 3.16 Power loss of IEEE 37-node test feeder with and without DWG, NaS, and reactive power compensation in high-wind profile

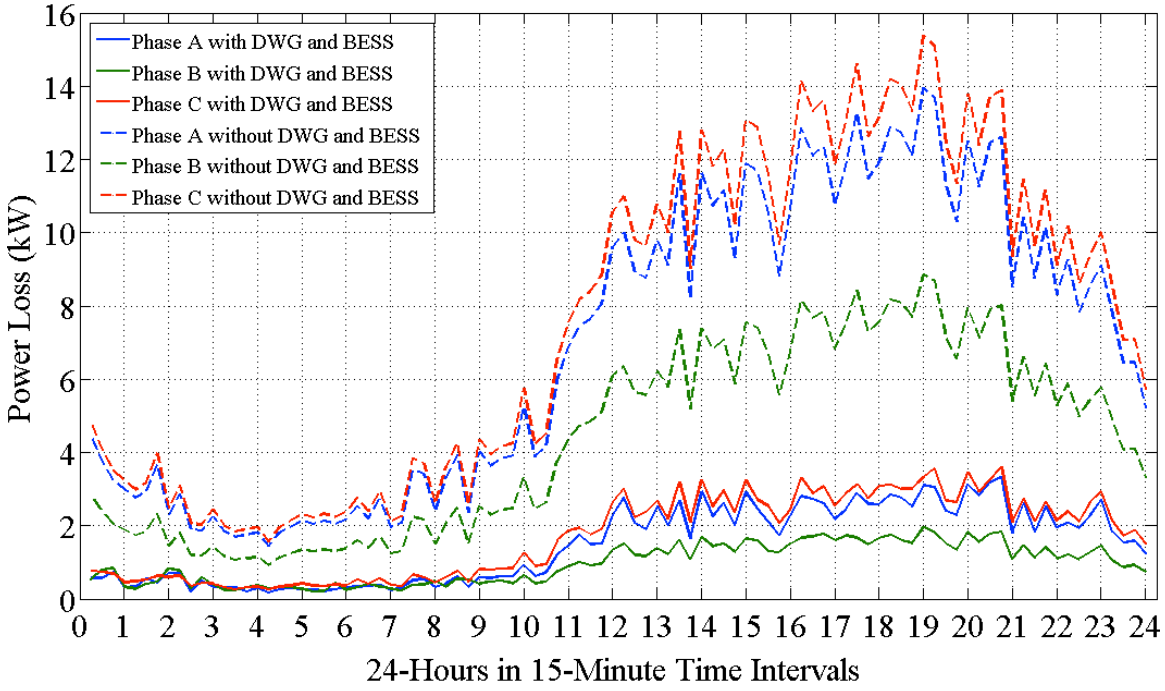

Figure 3.17 Power loss of IEEE 37-node test feeder with and without DWG, NaS, and reactive power compensation in low-wind profile

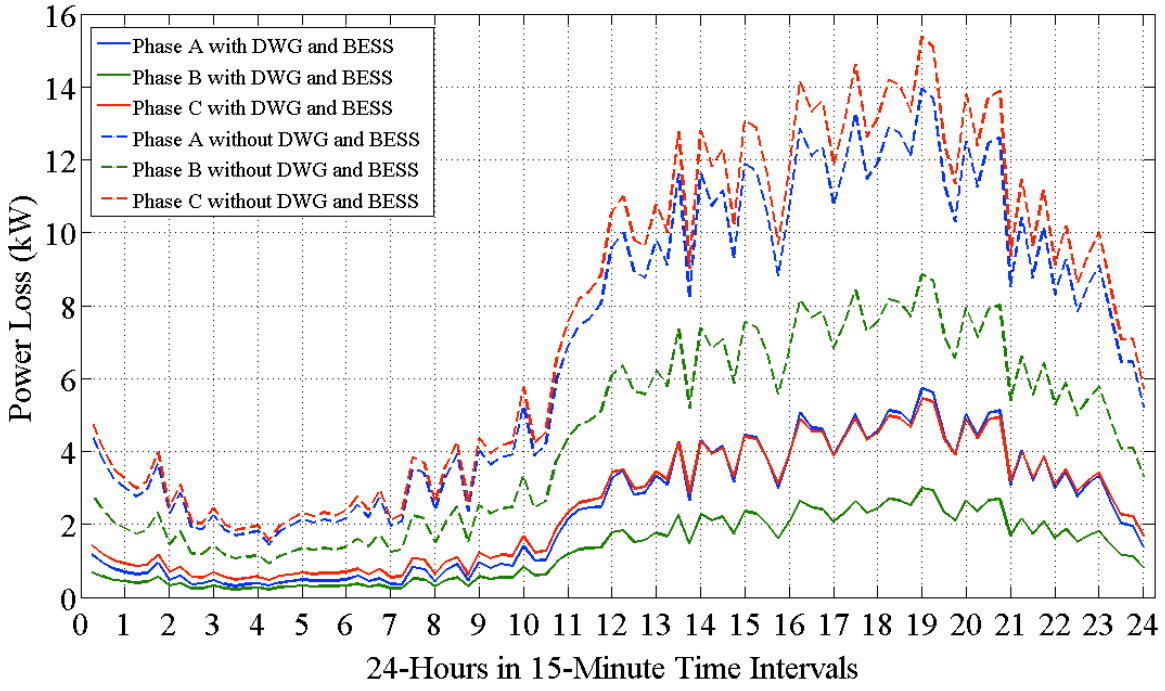

Figure 3.18 presents voltage profile improvements of the system with DWG and NaS in high-wind profile: (a) voltage profile without DWG and NaS, and (b) voltage profile with DWG,

NaS, and reactive power compensation in high-wind profile. Figure 3.19 presents voltage profile improvements of the system with DWG and NaS in low-wind: (a) voltage profile without DWG and NaS, and (b) voltage profile with DWG, NaS, and reactive power compensation in low-wind profile. System voltage was between 0.9847 (p.u.) and 1.0437 (p.u.) without DWG and NaS installation. Acceptable range of voltage in a distribution system is in between 0.95 and 1.05 p.u. DWG and NaS optimization improved the voltage profile of the system to between 0.9896 p.u. and 1.0091 p.u.

Figure 3.18 Voltage variation of IEEE 37-node three-phase system over 24-hour period in high-wind profile. Sub figures (a) and (b) represent voltage without DWG/NaS and voltage with DWG/NaS/Reactive power compensation, respectively.

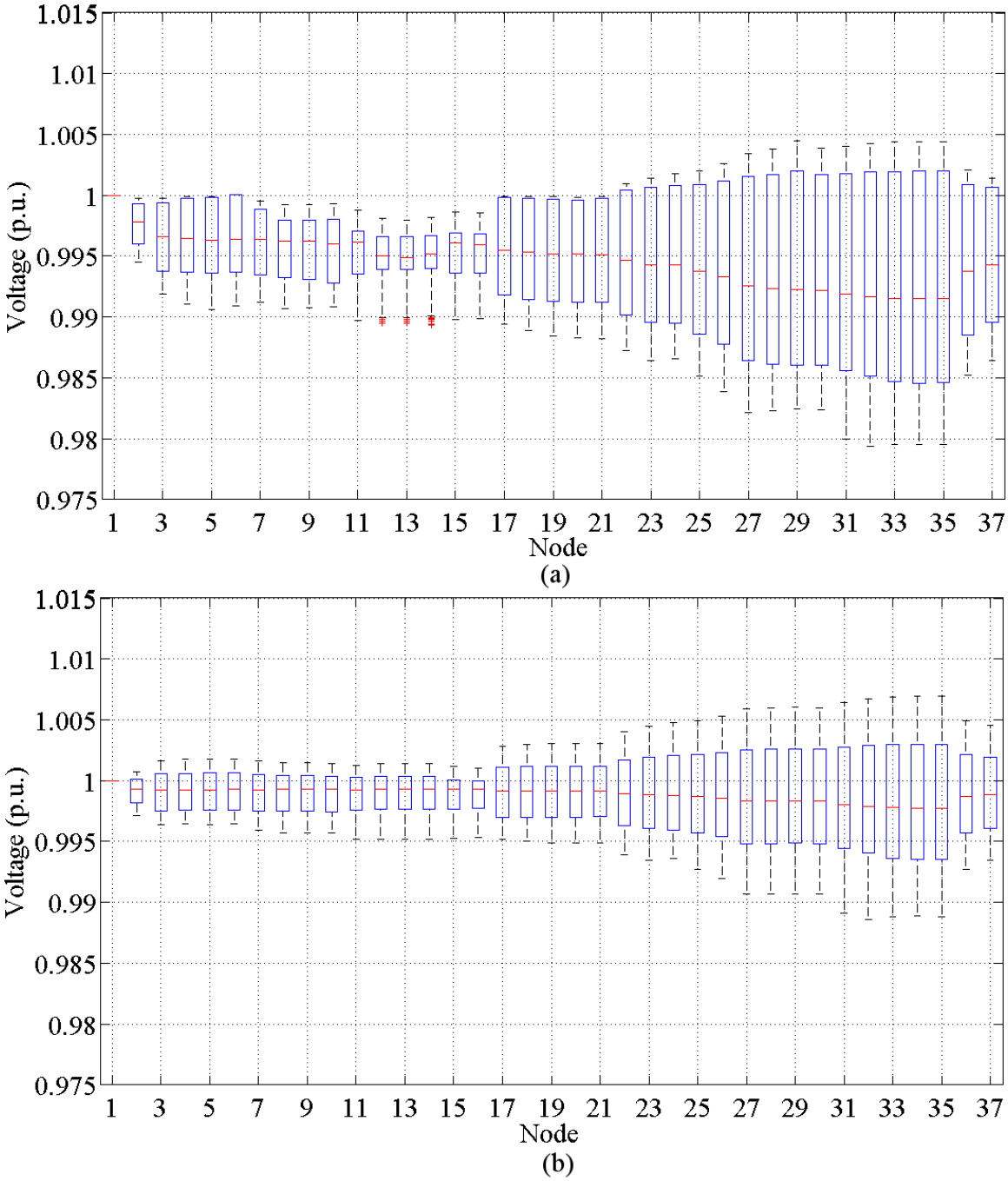

Figure 3.19 Voltage variation of IEEE 37-node three-phase system over 24-hour period in low-wind profile. Sub figures (a) and (b) represent voltage without DWG/NaS and voltage with DWG/NaS/Reactive power compensation, respectively.

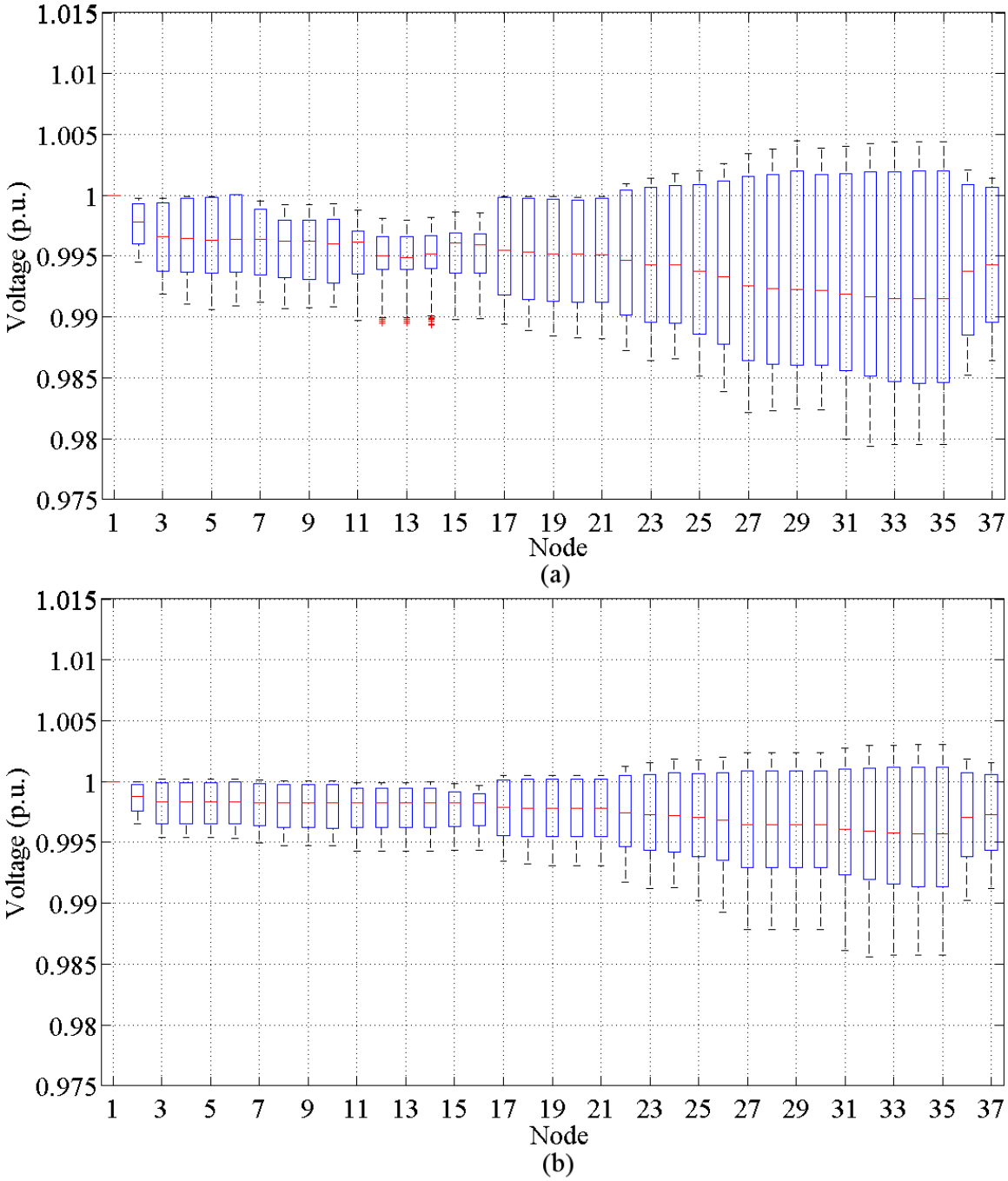

Figure 3.20 illustrates availability of DWG and NaS to supply base power demand of the system for a 24-hour period as a percentage of total system power demand. Availability of DWG and NaS for base power demands was 40% - 82% in low-wind profile and 46% - 93% in high-

wind profile. DWG and NaS high availability was achieved during low demand periods. Therefore, optimum sizing and siting of DWG and NaS fulfilled base power demand of the system for 24 hours.

Figure 3.20 Availability of DWG/ NaS to supply base power demand of the system over a 24-hour period

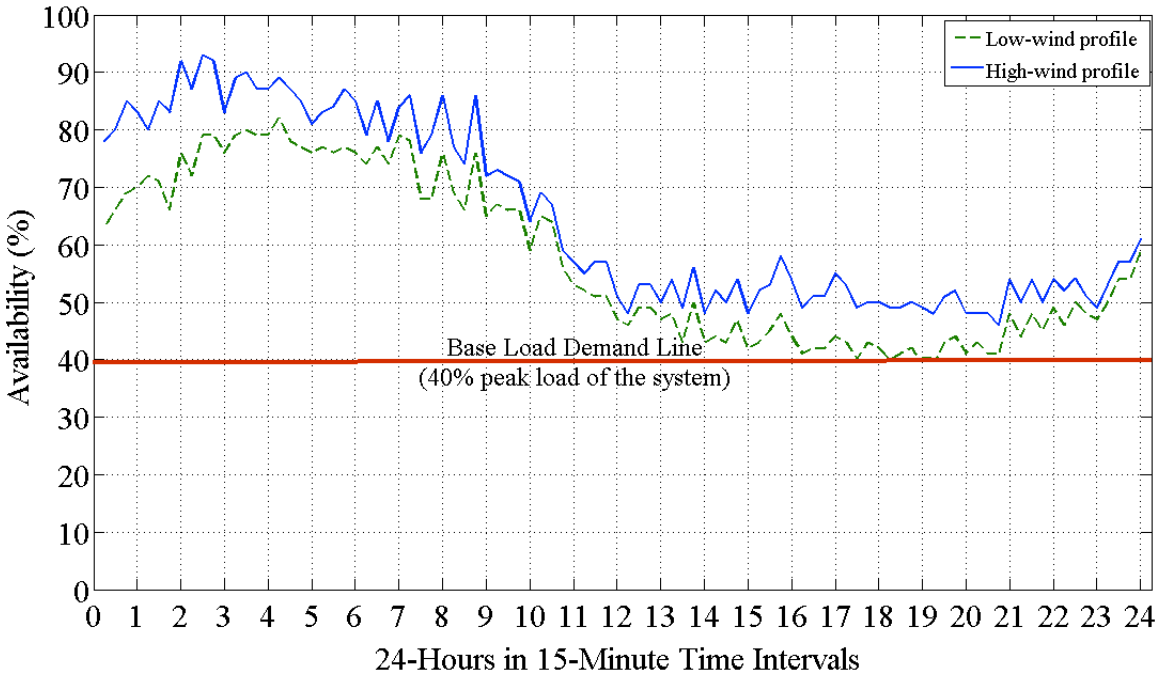

NES and SPP for the Pareto set are presented in Table 3.11.

Table 3.11 NES and SPP calculations for the selected solution

NES only with DWG	NES only with NaS	NES with DWG/NaS	SPP	SPP (Including NaS salvage benefits)
$243329.48/yr	$339349.68/yr	$582679.16/yr	10.85-yrs [a] 14.98-yrs [b]	9.92-yrs [a] 14.06-yrs [b]

NES was calculated by

$$NES_w = (8760)P_T C_p C_{en} - W_{om} P_T \quad (3.55)$$

where P_T is total capacity of wind generation (kW) , C_p is wind turbine capacity factor, C_{en} is energy price (S/kWh), and W_{om} is wind turbine annual maintenance cost ($/kW-yr).

SPP was calculated by

$$SPP = \frac{C_{in} P_T i_f}{NES_w} \tag{3.56}$$

where C_{in} is installed cost of wind ($/kW), P_T is total capacity of wind generation (kW), i_f is incentive factor, and NES_w is net present savings of wind turbines ($).

NES and SPP calculations utilized following parameters: wind turbine capacity factor was assumed to be 29%, installed cost of wind power was a=$2220/kW (capacity >1 MW), b=$6389/kW (10kW < capacity <100kW), annual O&M for wind was $38/kW-yr, average energy price for wind power was $0.13106/kWh, installed cost of NaS was $3000/kW, annual O&M cost was $5.007/kW-yr, average energy price for NaS was $0.13324/kWh (difference between peak load energy price and off-peak energy price), and tax incentive for DWG and NaS was 30%.

Overall power variations (charging and discharging) of NaS systems are illustrated in Figure 3.21. NaS capacities were optimized to adjust discharge rate based on the next 1.5 hours was calculated using hourly load forecast and previous load variation pattern.

Figure 3.21 Charging/discharging cycle of 50kW/25kW NaS modules

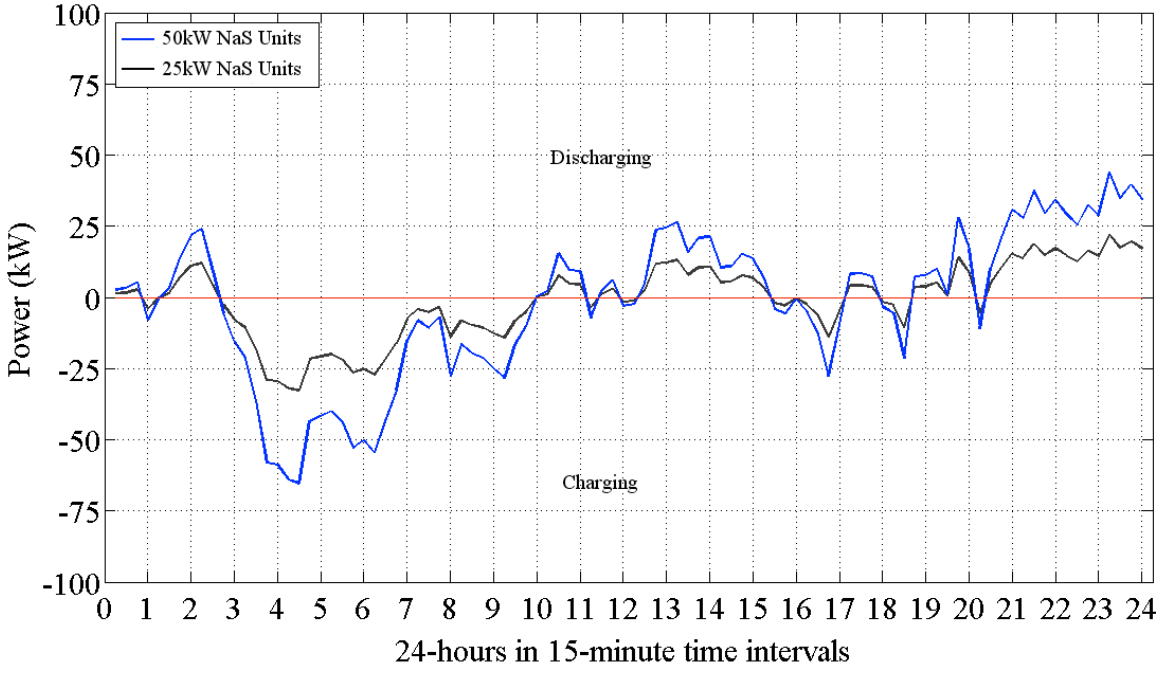

NaS modules oversee the total load demand of the distribution system. Therefore, all 50kW NaS module share a charging/discharging scenario, while all the 25kW NaS modules share another charging/discharging scenario. Figure 3.22 illustrates energy variation of 50kW and 25kW NaS battery modules.

Figure 3.22 50kW and 25kW NaS units energy variation

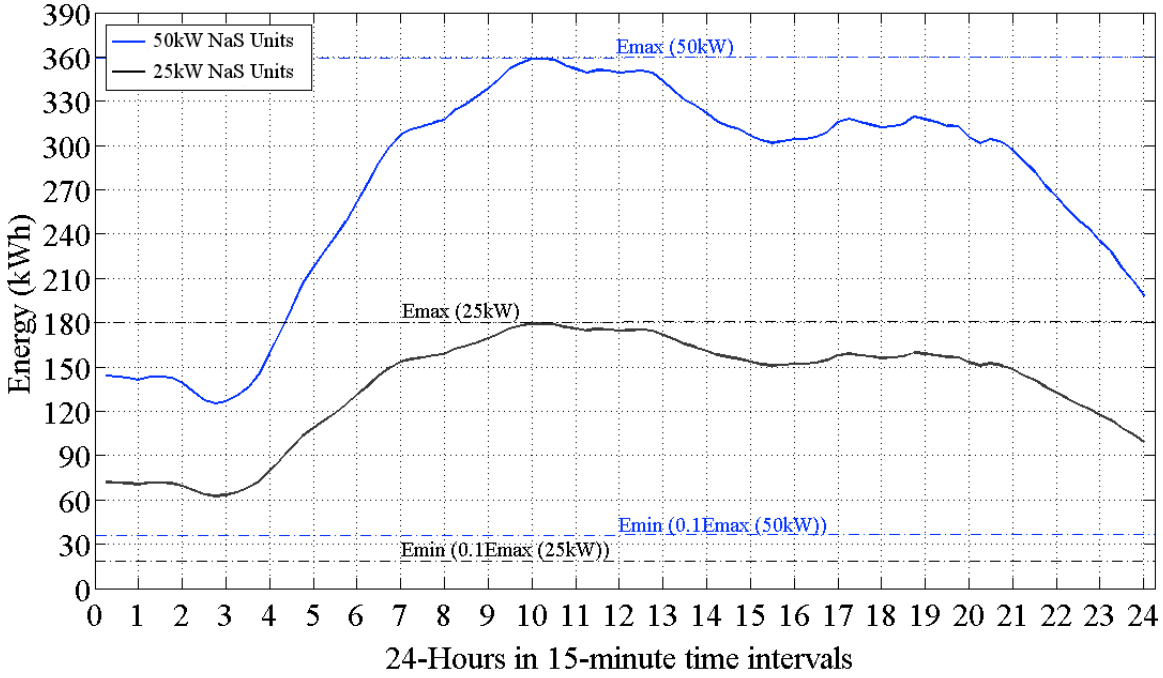

In base power supply mode, 50kW and 25kW NaS modules DOD were less than 50%, respectively.

Islanding the IEEE-37 system with DWG and NaS to sustain the system in grid power failure

A power grid failure, lasting a maximum of 1.5 hours, was introduced to the IEEE 37-node test feeder. System PF was corrected using capacitor bank available in a NW100 (±45 kVar) turbine. When smaller capacity (rated capacity < 100 kW) wind turbines were used, reactive power capability was assumed to be 45% of the rated capacity of the turbine. In DWG's active power generating state, local reactive power compensation was equal to the difference between 45% of rated capacity of the wind turbine and reactive power needed to improve power quality of wind generation (PF≥0.99).

System power losses in low- and high-wind profiles are presented in Figures 3.23 and 3.24. Power losses of the system in an islanded state were lower than power losses in grid-connected state. Low power loss is a result of onsite power generation and micro-management of reactive power supply.

In islanded operation state, network power losses demonstrated a sudden increase as a result of pulse power supply and altered system power flow. At 230% discharge rate, a 50kW NaS module experiences 100% discharge within 1.5 hours, thereby, perform as NaS module with 115kW power rating. NaS module discharge efficiency was assumed to decrease from 90% to 77% in pulse power mode, causing sudden increase in total system loss. Figure 3.25 presents the pulse power capability of NaS module.

Figure 3.23 Power loss of IEEE 37-node test feeder in islanded operation during power grid failure from 6:30 PM – 8:00 PM in low-wind profile.

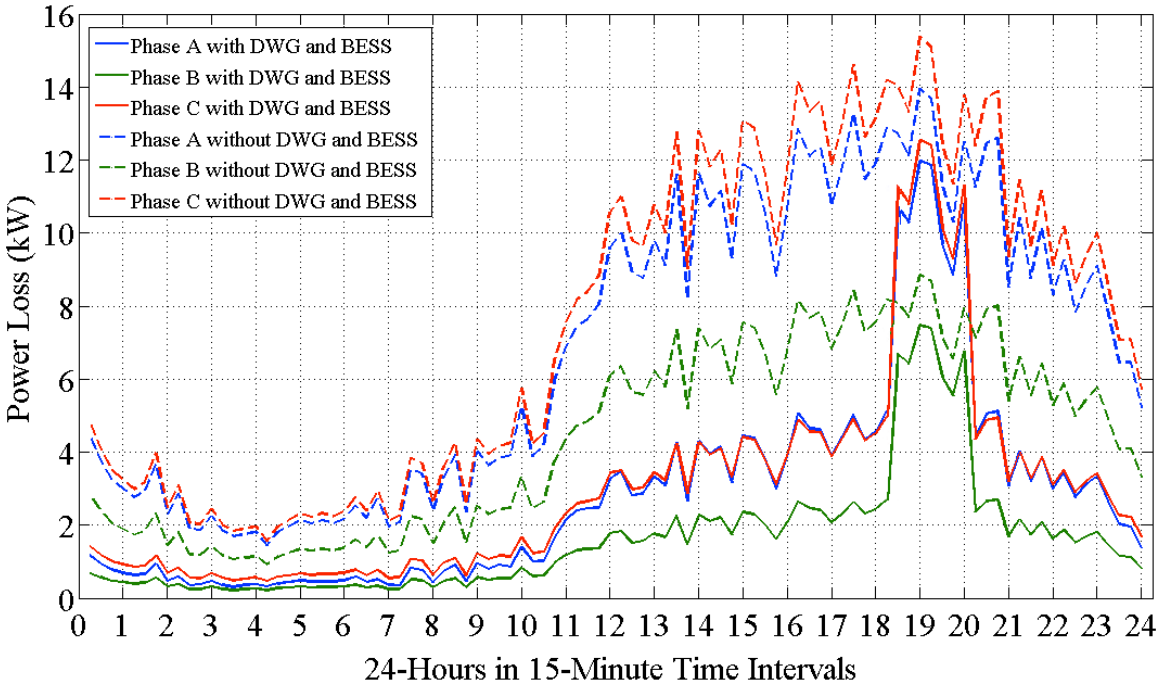

Figure 3.24 Power loss of IEEE 37-node test feeder in islanded operation during power grid failure from 6:30 PM – 8:00 PM in high-wind profile.

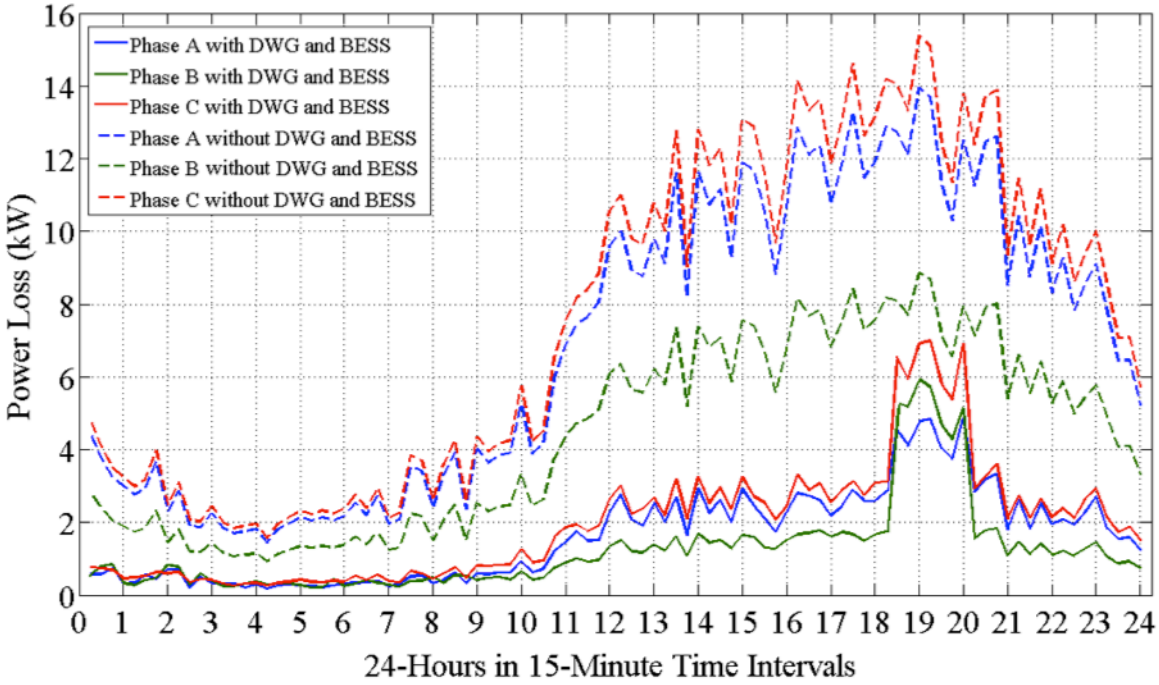

Figure 3.25 Pulse power capability of NaS unit

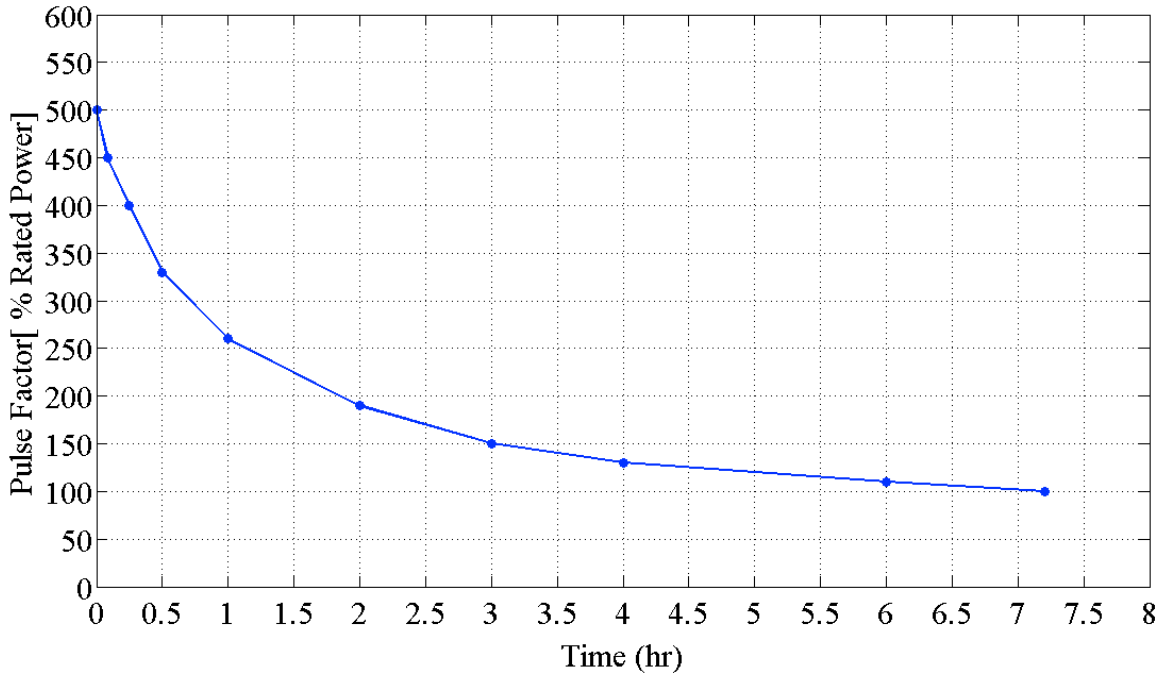

Figures 3.26 and 3.27, (a) and (b), represent the voltage profile of the system in grid-connected state and islanded state (6:30 PM to 8:00 PM) in high-wind and low-wind profiles, respectively.

Figure 3.26 Voltage variation of IEEE 37-node three-phase system over 24-hour period in high-wind profile. Sub figures (a) and (b) represent voltage with DWG/NaS and voltage with DWG/NaS with power failure, respectively.

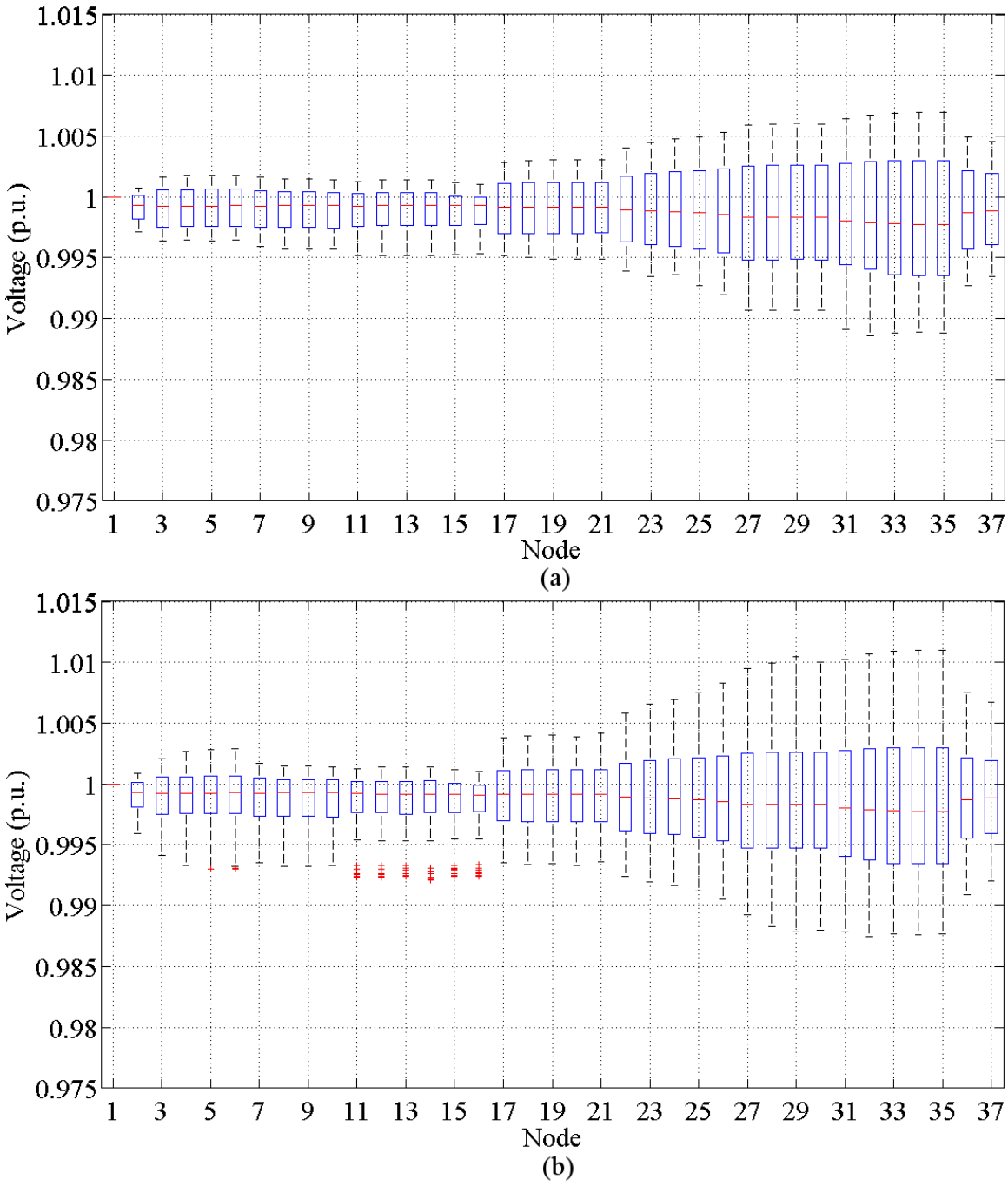

Figure 3.27 Voltage variation of IEEE 37-node three-phase system over 24-hour period in low-wind profile. Sub figures (a) and (b) represent voltage with DWG/NaS and voltage with DWG/NaS with power failure, respectively.

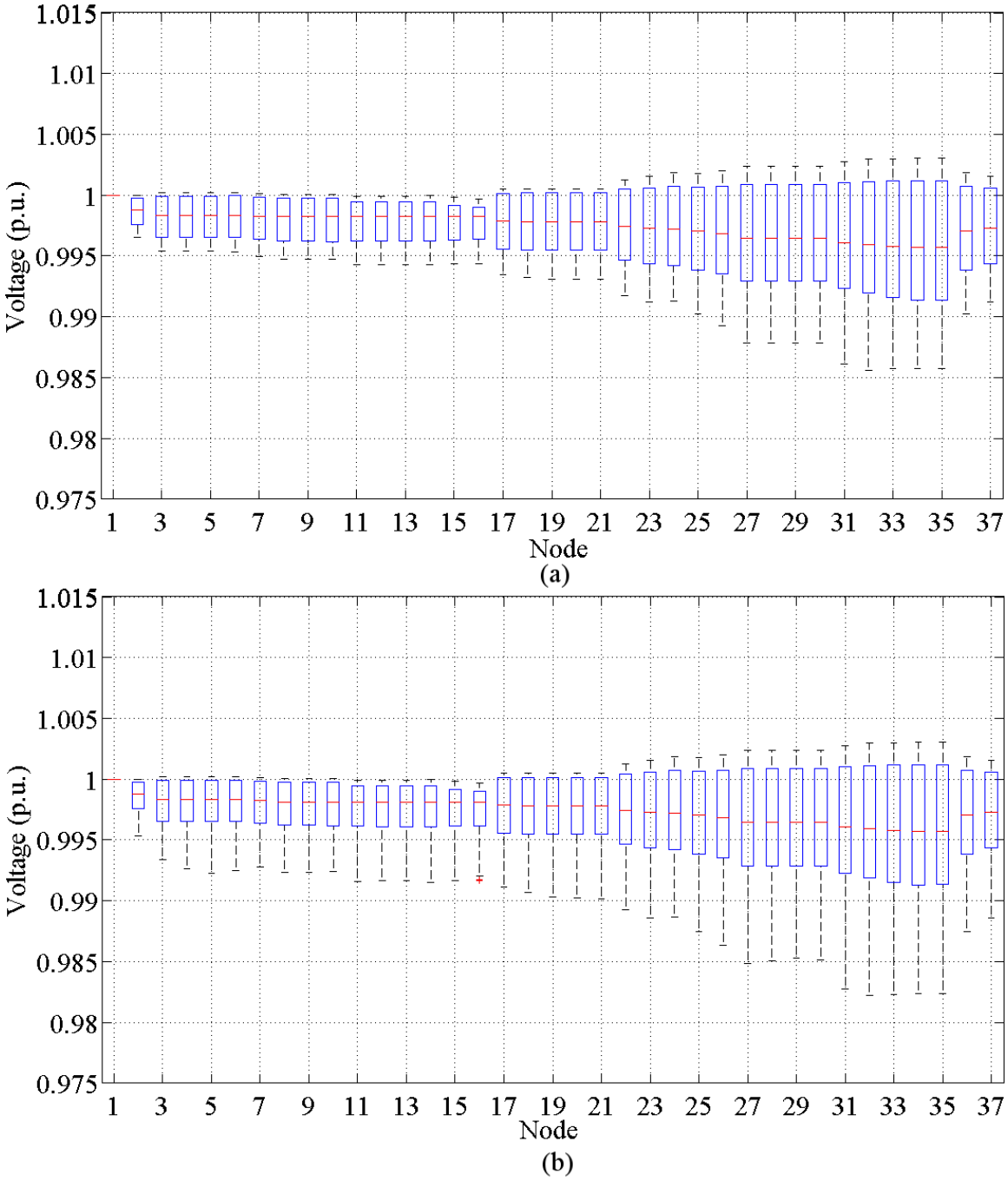

Figure 3.28 illustrates the availability of DWG and NaS to achieve islanded state of the system during grid power failure lasting a maximum of 1.5 hours, as a percentage of the systems'

total power demand. Availability of DWG and NaS ranged from 40% to 100% considering low- and high-wind profiles, consequently, fulfilling total power demand of the system for 1.5 hours.

Figure 3.28 Availability of DWG/NaS to sustain IEEE 37-node test system in a power grid failure lasting 1.5 hours.

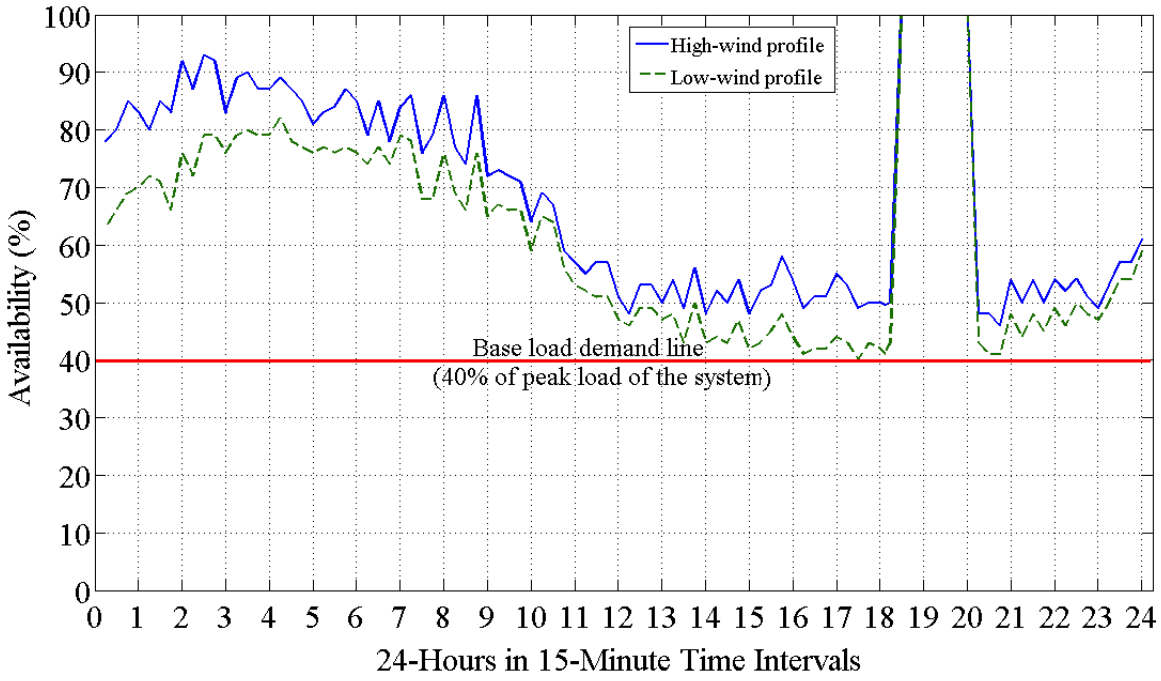

Figure 3.29 illustrates NaS charging/discharging pattern during main grid failure. Figure 3.30 demonstrates pulse power capability used by the NaS units, to supply the system's energy demand, over a period of 1.5 hours.

Figure 3.29 Charging/discharging cycle of 50kW/25kW NaS modules including power usage

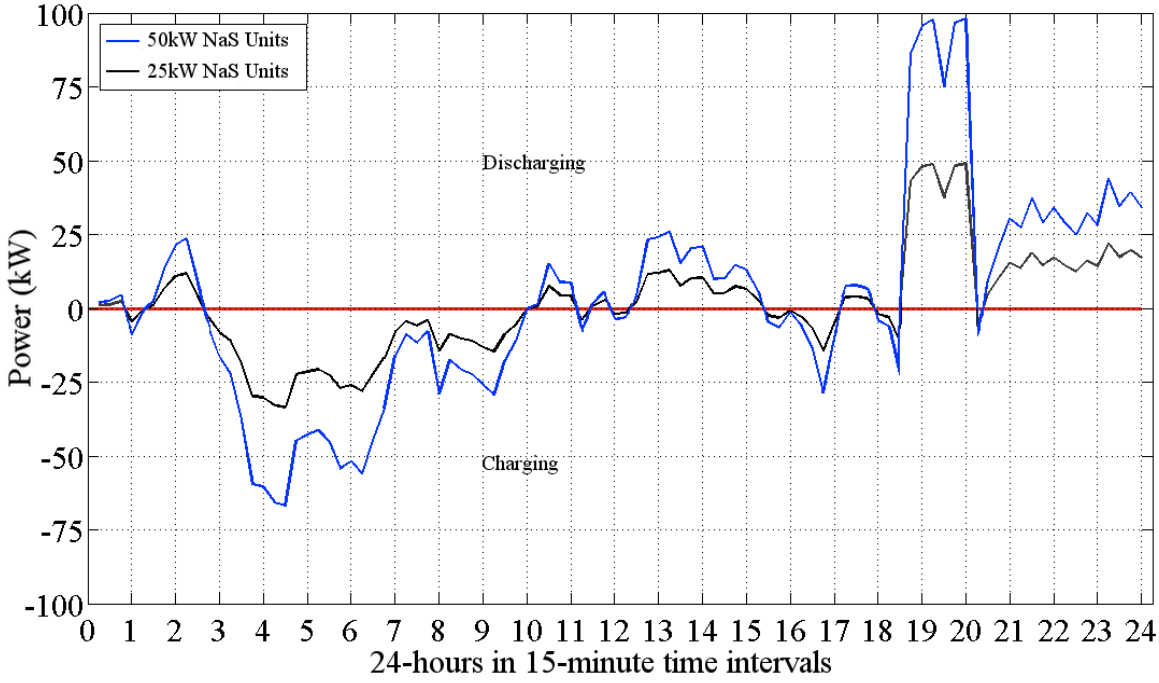

Figure 3.30 50kW and 25kW NaS units' energy variation and pulse power discharge

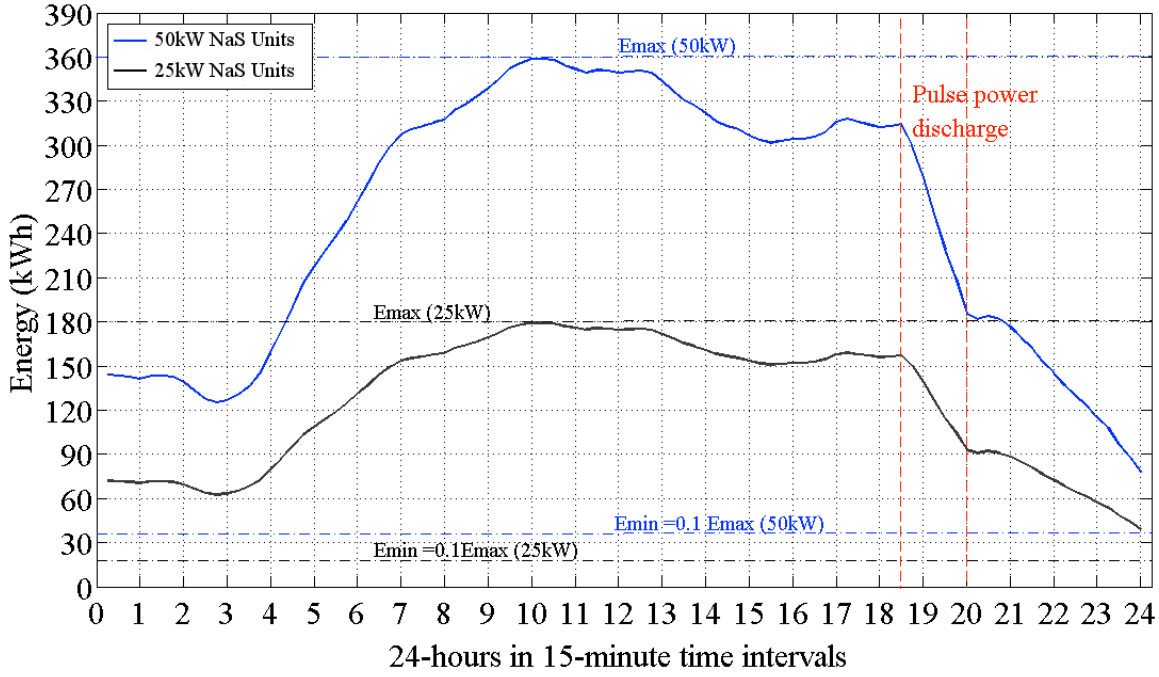

Summary

The IEEE 37-node test feeder was used to optimized DWG and NaS with reference to real power loss, voltage profile, availability of DWG/NaS and PV of savings in order to supply base power demand of the system and sustain the system for a maximum of 1.5 hours during a power grid failure. Selected results distinctly demonstrated, with 48.76% of peak load demand as DWG and 33.52% peak load demand as NaS, can supply the base load demand of the system. In addition, DWG and NaS can fully sustain IEEE 37-node test system in the event of power grid failure lasting up 1.5 hours.

Pulse power capability of NaS battery systems helped supply remaining power demand of the system unable to sustain from DWG generation. The ability to self-adjust the NaS discharge rate was a primary factor that affected the islanded operation of the IEEE 37-node test feeder. Additional decreases in installed costs, increased efficiency, and extra tax incentives will decrease the cost of future renewable energy projects. Geographical locations with average wind class higher than 3, may permit wind generation capacity less than 48.76% of peak load demand and/or decrease NaS capacities.

Benefits associated with DWG, such as decreased power system losses, improved power quality, improved voltage profile, local reactive power supply, and low carbon footprint emphasizes the use of RDG over CDG. PV of savings can further improved by considering DWG benefits, such as carbon footprint, heat generation, and air pollutant particle generation,

Key lessons learned from this research proved that capacity and placement of DWG and NaS can successfully optimized to sustain a three-phase distribution system's base power demand. DWG's ability to supply reactive power irrelevant to working condition of the wind turbine decreased system power loss and allowed islanded operation of the distribution system in the event of power grid failure. Minimum capacity of NaS balanced intermittent wind generation

and provided pulse power if grid failure was less than the total installed capacity of DWG. Candidate nodes of NaS placement were not necessarily nodes with DWG.

The ultimate goal underlines the research is grid independency through DWG and BESS. As anticipated, the study identified ways in which DWG and BESS can contribute to grid independency. While this is an enormous undertaking, the study proved to be a small step in this direction.

References

[1] J. Bennett, "The agency of assemblages and the North American blackout," *Public Culture,* vol. 17, pp. 445, 2005.

[2] P. Hines, J. Apt and S. Talukdar, "Large blackouts in North America: Historical trends and policy implications," *Energy Policy,* vol. 37, pp. 5249-5259, 2009.

[3] Dobson, B. A. Carreras, V. E. Lynch and D. E. Newman, "Complex systems analysis of series of blackouts: Cascading failure, critical points, and self-organization," *Chaos: An Interdisciplinary Journal of Nonlinear Science,* vol. 17, pp. 026103, 2007.

[4] Wang and M. H. Nehrir, "Analytical approaches for optimal placement of distributed generation sources in power systems," *Power Systems, IEEE Transactions on,* vol. 19, pp. 2068-2076, 2004.

[5] G. Celli, E. Ghiani, S. Mocci and F. Pilo, "A multiobjective evolutionary algorithm for the sizing and siting of distributed generation," *Power Systems, IEEE Transactions on,* vol. 20, pp. 750-757, 2005.

[6] R. Singh and S. Goswami, "Optimum siting and sizing of distributed generations in radial and networked systems," *Electric Power Components and Systems,* vol. 37, pp. 127-145, 2009.

[7] M. E. H. Golshan and S. Ali Arefifar, "Optimal allocation of distributed generation and reactive sources considering tap positions of voltage regulators as control variables," *European Transactions on Electrical Power,* vol. 17, pp. 219-239, 2007.

[8] P. Siano, P. Chen, Z. Chen and A. Piccolo, "Evaluating maximum wind energy exploitation in active distribution networks," *Generation, Transmission & Distribution, IET,* vol. 4, pp. 598-608, 2010.

[9] P. Siano, C. Cecati, H. Yu and J. Kolbusz, "Real time operation of smart grids via FCN networks and optimal power flow," *Industrial Informatics, IEEE Transactions on,* vol. 8, pp. 944-952, 2012.

[10] H. Hedayati, S. A. Nabaviniaki and A. Akbarimajd, "A method for placement of DG units in distribution networks," *Power Delivery, IEEE Transactions on,* vol. 23, pp. 1620-1628, 2008.

[11] K. Nara, Y. Hayashi, K. Ikeda and T. Ashizawa, "Application of tabu search to optimal placement of distributed generators," in *Power Engineering Society Winter Meeting, 2001. IEEE,* 2001, pp. 918-923.

[12] P. S. Georgilakis and N. D. Hatziargyriou, "Optimal distributed generation placement in power distribution networks: Models, methods, and future research," *IEEE Trans. Power Syst.,* vol. 28, pp. 3420-3428, 2013.
[13] C. L. Borges and D. M. Falcao, "Optimal distributed generation allocation for reliability, losses, and voltage improvement," *International Journal of Electrical Power & Energy Systems,* vol. 28, pp. 413-420, 2006.
[14] T. Shukla, S. Singh, V. Srinivasarao and K. Naik, "Optimal sizing of distributed generation placed on radial distribution systems," *Electric Power Components and Systems,* vol. 38, pp. 260-274, 2010.
[15] G. Carpinelli, G. Celli, F. Pilo and A. Russo, "Embedded generation planning under uncertainty including power quality issues," *European Transactions on Electrical Power,* vol. 13, pp. 381-389, 2003.
[16] G. P. Harrison, A. Piccolo, P. Siano and A. R. Wallace, "Hybrid GA and OPF evaluation of network capacity for distributed generation connections," *Electr. Power Syst. Res.,* vol. 78, pp. 392-398, 2008.
[17] K. Vinothkumar and M. Selvan, "Fuzzy embedded genetic algorithm method for distributed generation planning," *Electric Power Components and Systems,* vol. 39, pp. 346-366, 2011.
[18] K. Deb, A. Pratap, S. Agarwal and T. Meyarivan, "A fast and elitist multiobjective genetic algorithm: NSGA-II," *Evolutionary Computation, IEEE Transactions on,* vol. 6, pp. 182-197, 2002.
[19] I. Zamani and M. Irving, "A novel approach to distributed energy resource planning using NSGA-II," in *Universities Power Engineering Conference (UPEC), 2012 47th International,* 2012, pp. 1-5.
[20] M. Ahmadi, A. Yousefi, A. Soroudi and M. Ehsan, "Multi objective distributed generation planning using NSGA-II," in *Power Electronics and Motion Control Conference, 2008. EPE-PEMC 2008. 13th,* 2008, pp. 1847-1851.
[21] F. Banihashemi, H. Lesani and A. S. Makhzani, "Locating and capacity determination of distributed generations using none-dominated sorting genetic algorithm," in *PowerTech (POWERTECH), 2013 IEEE Grenoble,* 2013, pp. 1-8.
[22] W. Sheng, K. Liu, Y. Liu, X. Meng and Y. Li, "Optimal Placement and Sizing of Distributed Generation via an Improved Nondominated Sorting Genetic Algorithm II," 2014.
[23] Z. Shi, Y. Peng and W. Wei, "Optimal sizing of DGs and storage for microgrid with interruptible load using improved NSGA-II," in *Evolutionary Computation (CEC), 2014 IEEE Congress on,*2014, pp. 2108-2115.
[24] R. Kwartin, "The Cost and Performance of Distributed Wind Turbines, 2010-35 Final Report," 2010.
[25] R. Wiser, "2013 Wind technologies market report," 2014.
[26] A. N. Celik, "A statistical analysis of wind power density based on the Weibull and Rayleigh models at the southern region of Turkey," *Renewable Energy,* vol. 29, pp. 593-604, 2004.
[27] M. C. Kintner-Meyer, P. J. Balducci, C. Jin, T. B. Nguyen, M. A. Elizondo, V. Viswanathan, X. Guo and F. Tuffner, *Energy Storage for Power Systems Applications: A*

Regional Assessment for the Northwest Power Pool (NWPP). Pacific Northwest National Laboratory, 2010.
[28] E. Sarasua, M. G. Molina and P. E. Mercado, *Dynamic Modelling of Advanced Battery Energy Storage System for Grid-Tied AC Microgrid Applications.* INTECH Open Access Publisher, 2013.
[29] B. L. Norris, J. Newmiller and G. Peek, "NAS® battery demonstration at American Electric Power," *Sandia Report (SAND20066740),* 2007.
[30] S. Schoenung, "Energy Storage Systems Cost Update (SAND2011-2730)," *Sandia National Laboratories, Albuquerque,* 2011.
[31] S. M. Schoenung and W. V. Hassenzahl, "Long-vs. Short-Term Energy Storage Technologies Analysis. A Life-Cycle Cost Study. A Study for the DOE Energy Storage Systems Program," *Sandia National Laboratories,* 2003.
[32] R. Carnegie, D. Gotham, D. Nderitu and P. V. Preckel, "Utility scale energy storage systems," 2013.
[33] J. McGinness, *Electrical Energy Storage,* 1982.
[34] J. Eyer and G. Corey, "Energy storage for the electricity grid: Benefits and market potential assessment guide," *Sandia National Laboratories,* pp. 69-73, 2010.
[35] S. Favuzza, M. G. Ippolito and E. R. Sanseverino, "Crowded comparison operators for constraints handling in NSGA-II for optimal design of the compensation system in electrical distribution networks," *Advanced Engineering Informatics,* vol. 20, pp. 201-211, 2006.
[36] B. Kroposki, C. Pink, R. DeBlasio, H. Thomas, M. Simoes and P. K. Sen, "Benefits of power electronic interfaces for distributed energy systems," *Energy Conversion, IEEE Transactions on,* vol. 25, pp. 901-908, 2010.
[37] D. Popović, J. Greatbanks, M. Begović and A. Pregelj, "Placement of distributed generators and reclosers for distribution network security and reliability," *International Journal of Electrical Power & Energy Systems,* vol. 27, pp. 398-408, 2005.
[38] R. Willis and B. A. Finney, *Environmental Systems Engineering and Economics.* Springer Science & Business Media, 2004.
[39] G. L. W. Collaborative, "Best PracticesforSustainable Wind Energy Development in the Great Lakes Region,".
[40] S. L. Ferrell and E. A. DeVuyst, "Decommissioning wind energy projects: An economic and political analysis," *Energy Policy,* vol. 53, pp. 105-113, 2013.
[41] S. N. Heritage, "Research and guidance on restoration and decommissioning of onshore wind farms," 2013.
[42] N. Lu, M. Weimar, Y. Makarov, J. Ma and V. Viswanathan, *The Wide-Area Energy Storage and Management system–battery Storage Evaluation; 2009,* .
[43] M. Kintner-Meyer, P. Balducci, W. Colella, M. Elizondo, C. Jin, T. Nguyen, V. Viswanathan and Y. Zhang, "National assessment of energy storage for grid balancing and arbitrage: Phase 1, WECC," *Pacific Northwest National Lab Oratory: Richland, WA,* 2012.
[44] S. J. Kazempour, M. P. Moghaddam, M. Haghifam and G. Yousefi, "Electric energy storage systems in a market-based economy: Comparison of emerging and traditional technologies,"*Renewable Energy,* vol. 34, pp. 2630-2639, 2009.
[45] J. K. Yura, 'Electric Schedule E-7: Residential Time-of-Use Service', 2011. [Online]. Available: http://www.pge.com/tariffs/tm2/pdf/ELEC_SCHEDS_E-7.pdf. [Accessed: 08-Sep- 2014].

[46] *Feed-in Tariff*, 1st ed. Pacific Gas and Electric, 2011, p. 2. K. Iba, R. Ideta and K. Suzuki, "Analysis and operational records of NAS battery," in *Universities Power Engineering Conference, 2006. UPEC'06. Proceedings of the 41st International,* 2006, pp. 491-495.
[47] S. Tegen, M. Hand, B. Maples, E. Lantz, P. Schwabe and A. Smith, "2011 Cost of Wind Energy," *Contract,* vol. 303, pp. 275-300, 2013.
[48] B. S. Dhillon, *Life Cycle Costing for Engineers.* CRC Press, 2009.

Chapter 4 - Discussion, Conclusion, Recommendation, Implications

Introduction

Since 1995, optimum renewable distributed generation planning (ORDGP) has been an area of research for integrates RDG in distribution systems. Articles pertaining to ORDGP have primarily addressed aspects such as optimizing predetermined number of RDG in a distribution system [1], analyzing impacts of RDG in distribution systems operation [2,3], and regulating RDG power [4]. However, ORDGP complexities such as reliability of power supply, excessive land use in bulk energy generation, and availability of power have limited increased application of RDG in power distribution systems. However, RDG benefits such as minimal environmental impact, unlimited and free energy resource, promotion of cost-effective energy production, and energy price stability have caused increased RDG installation in power systems. In addition, recent federal power regulations and policies [5-7] have encouraged supply high percentage of energy demand with RDG. Therefore, ORDGP must address questions such as maximizing RDG in distribution systems and islanded operation of micro-grids with RDG.

Although ORDGP research articles have been published [8-11], no article have addressed optimizing DWG and NaS energy storage to supply base power demand of a three-phase unbalanced radial distribution system. This research primarily focused on DWG/NaS to supply base power demand (40% of peak power demand) and fully sustain a three-phase unbalanced radial distribution system during power grid failure. The literature emphasizes three optimization methods to achieve ORDGP: analytical, numerical, and heuristic. A meta-heuristic method, NSGA-II [12], optimizes DWG/NaS to supply base power demand of a system with reference to system power loss, voltage profile, DWG/NaS availability, and present value of savings.

Research Questions

Question One

Research question one addresses optimum capacity and placement of DWG necessary to meet base power requirements of IEEE 37-node three-phase unbalanced radial distribution system when combined with required NaS capacity. NSGA-II optimization of DWG/NaS with respect to power losses, voltage profile, DWG/NaS availability and present value of savings calculated fifty solutions of DWG capacity and placement required to supply base power demand of the IEEE 37-node test feeder and sustain the grid for a maximum of 1.5 hours during a power grid failure.

In order to prevent unnecessary installation cost (ground clearance, excavation, etc.), DWG capacities were divided by 25 (to determine the required number of 25kW wind turbines) and rounded to the nearest integer. When more than two turbines needed to be installed at a given location, 75kW wind turbines assumed to satisfy the capacity as required. Therefore, DWG capacity required achieving primary objectives of the study ranged between 44.69% and 48.76% of the total peak load demand of the system.

Question Two

Research question two address optimum capacity and placement of NaS necessary to meet base power requirements of IEEE 37-node three-phase unbalanced radial distribution system when combined with required DWG capacity. Although the minimum capacity of commercially available NaS unit is 50kW, the assumption was made that 25kW NaS units were also available. Therefore, total NaS capacity required achieving primary objectives of the study ranged between 33.52% and 35.55% of the total peak load demand of the system.

Question Three

Cost effectiveness of the solution selected from first Pareto front was evaluated using the payback period of DWG/NaS results. Table 3.11 was used as a reference to calculate dollar value of energy savings presented in Table 4.1. Price of energy was assumed to be \$0.13106/kWh (renewable energy selling price) and average energy price (grid energy buying price) was assumed to be \$0.150865/kWh. Therefore, the difference between selling and buying energy was \$0.019805/kWh. Project lifetime was expected to be 20 years.

Table 4.1 Revenue of energy savings

Simple payback period (Years)	Revenue of energy savings (\$)	Simple payback period (Including BESS salvage benefits) (Years)	Revenue of energy savings (\$)
10.85 [(a)]	1349391.32	9.92 [(a)]	1486542.57
14.98 [(b)]	740321.80	14.06 [(b)]	875998.30

(a) Simple payback time with DWG installed cost \$2220/kWh

(b) Simple payback time with DWG installed cost \$6389/kWh

According to data in Table 4.1, base power demand of the system can be cost-effectively provided with DWG/NaS.

Question Four

Results from modeling and simulating optimum DWG/NaS planning in three-phase unbalanced radial distribution system with respect to power losses, voltage profile, DWG/NaS availability and present value of savings primarily altered current understanding of power system operation. The unexpected discovery was made that NaS can be allocated in a node irrelevant to the presence of DWG a result of constraints on NaS charging. NaS units can charged from grid energy in off-peak hours or wind energy, depending on forecasted wind resource availability for the next hour of operation.

DWG's ability to compensate reactive power locally is one of the primary factors that facilitated islanded operation of the distribution system during power grid failure. Power system

complications such as low system power factor (PF), low voltage profile, and deprived power quality due to lack of necessary reactive power source can ultimately blackout the system.

Total DWG/NaS capacities necessary to supply base power demand of the IEEE 37-node test feeder and sustain power in the event of a power system failure for 1.5 hours was 82.28% of the total peak load demand of the system. Although total DWG/NaS capacity required providing base power demand of the system is higher than conventional power generator capacities, revenue from energy savings, as presented in Table 4.1, support the economic viability of the project.

Discussion

This dissertation study challenged the norm of power distribution system operation by considering DWG/NaS as the supply of base power demand of a three-phase unbalanced radial distribution system and source to sustain the system for 1.5 hours in a power grid failure. Power distribution system is the most complex part of the power system, thereby creating analytical, engineering, and modeling challenges when attempting to determine optimum placement and capacities of DWG/NaS.

The IEEE 37-node test system was simulated in Matlab environment to assess the impact of increased DWG/NaS resulting from allocation of 44.69% to 48.76% of DWG and 33.52% to 35.55% of NaS as a percentage of peak load demand of the system. Reactive power demand of the system must be satisfied using DWG in order to attain islanded operation of the distribution system during power grid failure. NaS constraints on minimum percentage on DOD during normal operation of the distribution system must be changed from 90% to 100% during grid power failure to prevent oversizing NaS units in the system.

Limitation

This study contained several limitations. The distribution system must depend on a single renewable energy source, wind; therefore, decrease the ability of supplying system's base power demand during low-wind speeds periods, lower than the cutting-in wind speed of DWG. In addition, optimized capacity of NaS is 33.52% to 35.55% of peak load demand, which is lower than the base power demand of the system. Although DWG produced required amount of power to 100% charge all NaS units, NaS can store only 5940kWh of energy. Therefore, NaS is only capable of supplying base energy demand of the system for a maximum of 9.03 hours. Consequently, if power grid failure occurred between 6:30 PM and 8:00 PM (1.5 hours) at which time wind generation is zero and NaS units are fully charged, NaS could only sustain the system for a maximum of 29 minutes operating at 331% pulse power factor.

Multi-sourced RDG units or various BESS effects on total installed capacity or placement were not addressed. In addition, DWG and NaS units were assumed to work without failure, which is not factual and a single wind turbine power curve was used to model DWG generation of the system, which is not realistic. Therefore, various wind turbine production curves could cause total optimized capacity installed in the system to vary. Geographical constraints on DWG/NaS, such as wind resource and land availability, were also neglected. Limitations of the study are opportunities to extend related study.

Conclusion

This study successfully demonstrated that DWG/NaS capacity and placement can be optimized with respect to power loss, voltage profile, DWG/NaS availability, and present value of savings in order to supply base power demand (40% of peak-load demand) in a three-phase

unbalanced radial distribution system and sustain the system for a maximum of 1.5 hours in the event of grid power failure.

DWG's reactive power compensation ability and pulse power capability of NaS units are primary characteristics that assist islanded operation of the power distribution system in the event of grid failure. Use of second-by-second data rather than 15-minute data can decrease variability in power demand, power generation, and related curves. In addition, use of second-by-second data may reduce optimum capacity needed to supply the base power demand of the system [13].

Use of DWG/NaS to supply base power demand of the distribution system improved the voltage profile, network losses, and system savings and improve the overall power quality of the system. Reactive power compensation ability of DWG further reduced the power system losses and improved the system PF.

Future Direction and Implication

This research could extend to accommodate a diverse set of renewable energy generators, such as photovoltaic, geothermal units, and biogas turbines as DG. In addition, various grid energy storage systems, such as PHE, CAES and fuel cells, could install when geographical and other constraints permit. Geographical constraints could be implemented to analyze DWG/NaS optimization. Assumptions such as all allocated DWG follow a single generation curve could be lifted to introduce multiple power generation curves and wind speed patterns to smooth total renewable generation in the system.

Violations of power system security could be identified and novel power system security protocols could be implemented to comply with increased accommodation of renewable generation. Finally, the study could be extended to investigate the ultimate goal of this research:

continuous islanded operation of three-phase unbalanced distribution system through DWG and BESS.

References

[1] Y. M. Atwa and E. El-Saadany, "Optimal allocation of ESS in distribution systems with a high penetration of wind energy," *Power Systems, IEEE Transactions on,* vol. 25, pp. 1815-1822, 2010.

[2] M. Begovic, A. Pregelj, A. Rohatgi and D. Novosel, "Impact of renewable distributed generation on power systems," in *2013 46th Hawaii International Conference on System Sciences,* 2001, pp. 2008-2008.

[3] M. Thomson and D. Infield, "Impact of widespread photovoltaics generation on distribution systems," *Renewable Power Generation, IET,* vol. 1, pp. 33-40, 2007.

[4] N. C. Scott, D. J. Atkinson and J. E. Morrell, "Use of load control to regulate voltage on distribution networks with embedded generation," *Power Systems, IEEE Transactions on,* vol. 17, pp. 510-515, 2002.

[5] L. Bird, M. Bolinger, T. Gagliano, R. Wiser, M. Brown and B. Parsons, "Policies and market factors driving wind power development in the United States," *Energy Policy,* vol. 33, pp. 1397-1407, 2005.

[6] G. R. Timilsina, L. Kurdgelashvili and P. A. Narbel, "Solar energy: markets, economics and policies," *Renewable and Sustainable Energy Reviews,* vol. 16, pp. 449-465, 2012.

[7] H. B. Puttgen, P. R. Macgregor and F. C. Lambert, "Distributed generation: Semantic hype or the dawn of a new era?" *Power and Energy Magazine, IEEE,* vol. 1, pp. 22-29, 2003.

[8] L. F. Ochoa and G. P. Harrison, "Minimizing energy losses: Optimal accommodation and smart operation of renewable distributed generation," *Power Systems, IEEE Transactions on,* vol. 26, pp. 198-205, 2011.

[9] Y. Atwa and E. El-Saadany, "Probabilistic approach for optimal allocation of wind-based distributed generation in distribution systems," *IET Renewable Power Generation,* vol. 5, pp. 79-88, 2011.

[10] L. Wang and C. Singh, "PSO-based multi-criteria optimum design of a grid-connected hybrid power system with multiple renewable sources of energy," in *Swarm Intelligence Symposium, 2007. SIS 2007. IEEE,* 2007, pp. 250-257.

[11] W. Tan, M. Y. Hassan, M. S. Majid and H. A. Rahman, "Optimal distributed renewable generation planning: A review of different approaches," *Renewable and Sustainable Energy Reviews,* vol. 18, pp. 626-645, 2013.

[12] K. Deb, S. Agrawal, A. Pratap and T. Meyarivan, "A fast elitist non-dominated sorting genetic algorithm for multi-objective optimization: NSGA-II," *Lecture Notes in Computer Science,* vol. 1917, pp. 849-858, 2000.

[13] M. S. Vijayarengan, *Coordinated Operations of Distributed Wind Generation in a Distribution System using PMUs,* 2012.

Appendix A - NSGA-II Optimization Results

Table A.1 NES and SPP calculations for NSGA-II optimization.

Solution	NES with DWG/NaS ($)	SPP[a] (years)	SPP[a] (years) with NaS Salvage Benefits	SPP[b] (years)	SPP[b] (years) with NaS Salvage Benefits
1	618635.76	14.98	14.05	10.85	9.93
2	589748.94	14.98	14.05	10.90	9.96
3	554400.02	14.99	14.10	10.65	9.75
4	582679.16	14.98	14.06	10.85	9.92
5	575913.21	14.99	14.09	10.68	9.78
6	582375.32	14.98	14.03	10.97	10.02
7	575913.21	14.99	14.09	10.68	9.78
8	568539.59	14.99	14.07	10.75	9.84
9	575913.21	14.99	14.09	10.68	9.78
10	575609.37	14.98	14.06	10.80	9.88
11	582679.16	14.98	14.06	10.85	9.92
12	568539.59	14.99	14.07	10.75	9.84
13	575609.37	14.98	14.06	10.80	9.88
14	568539.59	14.99	14.07	10.75	9.84
15	590052.78	14.98	14.07	10.78	9.87
16	589748.94	14.98	14.05	10.90	9.96
17	582983.00	14.99	14.08	10.73	9.82
18	568539.59	14.99	14.07	10.75	9.84
19	590052.78	14.98	14.07	10.78	9.87
20	590052.78	14.98	14.07	10.78	9.87
21	618635.76	14.98	14.05	10.85	9.93
22	582679.16	14.98	14.06	10.85	9.92
23	582679.16	14.98	14.06	10.85	9.92
24	604192.35	14.98	14.05	10.88	9.94
25	575609.37	14.98	14.06	10.80	9.88
26	590052.78	14.98	14.07	10.78	9.87
27	590052.78	14.98	14.07	10.78	9.87
28	590052.78	14.98	14.07	10.78	9.87
29	568539.59	14.99	14.07	10.75	9.84
30	575609.37	14.98	14.06	10.80	9.88
31	582679.16	14.98	14.06	10.85	9.92
32	582679.16	14.98	14.06	10.85	9.92
33	590356.62	14.99	14.09	10.66	9.77
34	575609.37	14.98	14.06	10.80	9.88
35	604496.19	14.98	14.07	10.76	9.85
36	582983.00	14.99	14.08	10.73	9.82
37	582679.16	14.98	14.06	10.85	9.92
38	582679.16	14.98	14.06	10.85	9.92
39	611262.14	14.98	14.04	10.92	9.98
40	597122.57	14.98	14.06	10.83	9.91
41	575609.37	14.98	14.06	10.80	9.88
42	611565.97	14.98	14.06	10.81	9.89
43	604192.35	14.98	14.05	10.88	9.94
44	575609.37	14.98	14.06	10.80	9.88
45	582983.00	14.99	14.08	10.73	9.82
46	590356.62	14.99	14.09	10.66	9.77
47	590052.78	14.98	14.07	10.78	9.87
48	590052.78	14.98	14.07	10.78	9.87
49	590052.78	14.98	14.07	10.78	9.87
50	582679.16	14.98	14.06	10.85	9.92

a - SPP without NaS salvage benefits. b - SPP with NaS salvage benefits.

Table A.2 NSGA-II Optimization results for objective functions values.

Solution	Real Power Loss (kW)	Voltage Deviation (p.u.)	Availability	PV ($)
1	412	0.012	0.440	273000000
2	402	0.015	0.402	240000000
3	440	0.011	0.405	233000000
4	400	0.013	0.415	252000000
5	472	0.009	0.400	220000000
6	400	0.013	0.443	269000000
7	418	0.009	0.401	219000000
8	420	0.009	0.401	220000000
9	392	0.009	0.401	222000000
10	439	0.012	0.418	265000000
11	508	0.012	0.413	254000000
12	509	0.012	0.422	251000000
13	402	0.012	0.407	247000000
14	486	0.011	0.425	253000000
15	494	0.010	0.403	227000000
16	464	0.015	0.400	236000000
17	443	0.012	0.433	262000000
18	470	0.012	0.425	254000000
19	404	0.013	0.414	252000000
20	439	0.012	0.418	265000000
21	440	0.012	0.427	259000000
22	492	0.011	0.413	250000000
23	467	0.012	0.420	257000000
24	460	0.012	0.433	263000000
25	418	0.012	0.403	245000000

Solution	Real Power Loss (kW)	Voltage Deviation (p.u.)	Availability	PV ($)
26	414	0.011	0.409	238000000
27	436	0.012	0.416	266000000
28	428	0.010	0.408	233000000
29	438	0.010	0.406	232000000
30	437	0.012	0.405	249000000
31	409	0.013	0.415	252000000
32	410	0.013	0.414	252000000
33	459	0.013	0.405	248000000
34	420	0.012	0.403	246000000
35	405	0.013	0.404	250000000
36	440	0.012	0.405	249000000
37	482	0.012	0.409	248000000
38	498	0.011	0.416	249000000
39	425	0.012	0.438	271000000
40	428	0.012	0.433	268000000
41	459	0.012	0.407	249000000
42	478	0.012	0.432	263000000
43	447	0.011	0.401	232000000
44	429	0.012	0.402	249000000
45	455	0.012	0.404	243000000
46	418	0.012	0.414	255000000
47	498	0.011	0.414	243000000
48	494	0.010	0.403	227000000
49	477	0.012	0.409	248000000
50	428	0.010	0.409	233000000

Table A.3 NSGA-II optimization results for DWG capacity and location, solutions 1-17.

Node	DWG Capacity (kW)																	
1	75	75	75	75	75	75	75	75	75	75	75	75	75	75	75	75	75	75
2	75	75	75	75	75	75	75	75	75	75	75	75	75	75	75	75	75	75
3	25	25	0	25	25	25	25	25	25	25	25	25	25	25	25	25	25	25
4	75	75	25	75	75	75	75	75	75	75	75	75	75	75	75	75	75	75
5	75	75	25	75	75	75	75	75	75	75	75	75	75	75	75	75	75	75
6	75	75	100	75	75	75	75	75	75	75	75	75	75	75	75	75	75	75
7	75	75	75	75	75	75	75	75	75	75	75	75	75	75	75	75	75	75
8	25	25	25	25	25	25	25	25	25	25	25	25	25	25	25	25	25	25
9	75	75	75	75	75	75	75	75	75	75	75	75	75	75	75	75	75	75
10	100	100	100	100	100	100	100	100	100	100	100	100	100	100	100	100	100	100
11	0	0	0	0	0	0	0	0	0	0	0	0	0	0	0	0	0	0
12	25	25	25	25	25	25	25	25	25	25	25	25	25	25	25	25	25	25
13	75	75	75	25	25	25	25	25	25	25	25	25	25	25	25	75	75	25
14	0	0	0	0	0	0	0	0	0	0	0	0	0	0	0	0	0	0
15	75	75	75	75	75	75	75	75	75	75	75	75	75	75	75	75	75	75
16	0	0	0	0	0	0	0	0	0	0	0	0	0	0	0	0	0	0
17	25	0	0	0	25	25	25	25	25	25	25	25	25	25	25	25	25	25
18	0	0	0	0	0	0	0	0	0	0	0	0	0	0	0	0	0	0
19	25	0	0	25	25	25	25	25	25	25	25	25	25	25	25	25	25	25
20	0	0	0	0	0	0	0	0	0	0	0	0	0	0	0	0	0	0
21	25	25	25	25	25	25	25	25	25	25	25	25	25	25	25	25	25	25
22	75	75	75	75	75	75	75	75	75	75	75	75	75	75	75	75	75	75
23	100	100	100	100	75	75	75	75	75	75	100	75	100	100	75	100	100	100
24	0	0	0	0	0	0	0	0	0	0	0	0	0	0	0	0	0	0
25	0	0	0	0	0	0	0	0	0	0	0	0	0	0	0	0	0	0
26	25	25	25	25	25	25	25	25	25	25	25	25	25	25	25	25	25	25
27	0	0	0	0	0	0	0	0	0	0	0	0	0	0	0	0	0	0
28	75	75	75	75	75	75	75	75	75	75	75	75	75	75	75	75	75	75
29	25	25	25	25	25	25	25	25	25	25	25	25	25	25	25	25	25	25
30	0	0	0	0	0	0	0	0	0	0	0	0	0	0	0	0	0	0
31	0	0	0	0	0	0	0	0	0	0	0	0	0	0	0	0	0	0
32	25	25	25	25	25	25	25	25	25	25	25	25	25	25	25	25	25	25
33	0	0	0	0	0	0	0	0	0	0	0	0	0	0	0	0	0	0
34	0	0	0	0	0	0	0	0	0	0	0	0	0	0	0	0	0	0
35	0	0	0	0	0	0	0	0	0	0	0	0	0	0	0	0	0	0
36	0	0	0	0	0	0	0	0	0	0	0	0	0	0	0	0	0	0
37	25	25	25	25	0	25	0	0	25	25	25	25	25	25	25	25	25	25
Total (kW)	1275	1225	1100	1200	1150	1225	1150	1150	1175	1200	1150	1175	1150	1200	1225	1175		

Table A.4 NSGA-II optimization results for DWG capacity and location, solutions 18-34.

Node	DWG Capacity (kW)																		
1	75	75	75	75	75	75	75	75	75	75	75	75	75	75	75	75	75	75	75
2	75	75	75	75	75	75	75	75	75	75	75	75	75	75	75	75	75	75	75
3	25	25	25	25	25	25	25	25	25	25	25	25	25	25	25	25	25	25	25
4	75	75	75	75	75	75	75	75	75	75	75	75	75	75	75	75	75	75	75
5	25	75	75	75	75	75	75	75	75	75	75	75	75	75	75	75	75	75	25
6	75	75	75	75	100	75	75	75	75	75	75	75	75	75	75	75	75	75	75
7	75	75	75	75	75	75	75	75	75	75	75	75	75	75	75	75	75	75	75
8	25	25	25	25	25	25	25	25	25	25	25	25	25	25	25	25	25	25	25
9	75	75	75	75	75	75	75	75	75	75	75	75	75	75	75	75	75	75	75
10	100	100	100	100	100	100	100	100	100	100	100	100	100	100	100	100	100	100	100
11	0	0	0	0	0	0	0	0	0	0	0	0	0	0	0	0	0	0	0
12	25	25	0	25	25	25	25	25	0	25	25	25	25	25	25	25	25	25	25
13	25	25	25	75	25	25	75	25	25	25	25	25	75	25	25	25	75	75	75
14	0	0	0	0	0	0	0	0	0	0	0	0	0	0	0	0	0	0	0
15	75	75	75	75	75	75	75	75	75	75	75	75	75	75	75	75	75	75	75
16	0	0	0	0	0	0	0	0	0	0	0	0	0	0	0	0	0	0	0
17	25	0	25	25	25	25	25	25	25	25	25	25	25	25	25	25	25	25	0
18	0	0	0	0	0	0	0	0	0	0	0	0	0	0	0	0	0	0	0
19	25	25	25	25	25	25	25	25	25	25	25	25	25	25	25	25	25	25	25
20	0	0	0	0	0	0	0	0	0	0	0	0	0	0	0	0	0	0	0
21	25	25	25	25	25	25	25	25	25	25	25	25	25	25	25	25	25	25	25
22	75	75	75	75	75	75	75	75	75	75	75	75	75	75	75	75	75	75	75
23	100	100	100	100	100	75	75	100	100	75	75	100	75	75	100	100	100	100	100
24	0	0	0	0	0	0	0	0	0	0	0	0	0	0	0	0	0	0	0
25	0	0	0	0	0	0	0	0	0	0	0	0	0	0	0	0	0	0	0
26	25	25	25	25	25	25	25	25	25	25	25	25	25	25	25	25	25	25	25
27	0	0	0	0	0	0	0	0	0	0	0	0	0	0	0	0	0	0	0
28	75	75	75	75	75	75	75	75	75	75	75	75	75	75	75	75	75	75	75
29	25	25	25	25	25	25	25	25	25	25	25	25	25	25	25	25	25	25	25
30	0	0	0	0	0	0	0	0	0	0	0	0	0	0	0	0	0	0	0
31	0	0	0	0	0	0	0	0	0	0	0	0	0	0	0	0	0	0	0
32	25	25	25	25	25	25	25	25	25	25	25	25	25	25	25	25	25	25	25
33	0	0	0	0	0	0	0	0	0	0	0	0	0	0	0	0	0	0	0
34	0	0	0	0	0	0	0	0	0	0	0	0	0	0	0	0	0	0	0
35	0	0	0	0	0	0	0	0	0	0	0	0	0	0	0	0	0	0	0
36	0	0	0	0	0	0	0	0	0	0	0	0	0	0	0	0	0	0	0
37	0	25	25	25	25	25	25	25	25	25	25	25	25	25	25	25	25	25	25
Total (kW)	1150	1200	1200	1275	1200	1200	1250	1175	1200	1200	1200	1150	1175	1200	1200	1175	1200	1175	1175

Table A.5 NSGA-II optimization results for DWG capacity and location, solutions 35-50.

Node	DWG Capacity (kW)															
1	75	75	75	75	75	75	75	75	75	75	75	75	75	75	75	75
2	75	75	75	75	75	75	75	75	75	75	75	75	75	75	75	75
3	25	25	25	25	25	25	25	0	25	0	25	25	25	25	25	25
4	75	75	75	75	75	75	75	75	75	75	75	75	75	75	75	75
5	75	25	75	75	75	25	75	75	25	75	75	75	75	75	75	75
6	75	75	75	75	75	75	100	100	75	75	75	75	75	75	75	75
7	75	75	75	75	75	75	75	25	75	75	75	75	75	75	75	75
8	25	25	25	25	25	25	25	25	25	25	25	25	25	25	25	25
9	75	75	75	75	75	75	75	25	75	75	75	75	75	75	75	75
10	100	100	100	100	100	100	100	100	100	75	75	100	100	100	100	100
11	0	0	0	0	0	0	0	0	0	0	0	0	0	0	0	0
12	25	25	25	25	25	25	25	25	25	25	25	25	25	25	25	25
13	25	75	25	75	75	25	25	25	75	25	25	25	25	25	25	25
14	0	0	0	0	0	0	0	0	0	0	0	0	0	0	0	0
15	75	75	75	75	25	75	75	75	75	75	75	75	75	75	75	75
16	0	0	0	0	0	0	0	0	0	0	0	0	0	0	0	0
17	0	0	25	25	25	0	25	0	0	25	0	25	25	0	0	25
18	0	0	0	0	0	0	0	0	0	0	0	0	0	0	0	0
19	25	0	25	25	25	0	25	25	0	25	25	25	25	25	25	25
20	0	0	0	0	0	0	0	0	0	0	0	0	0	0	0	0
21	25	25	25	25	25	25	25	25	25	25	25	25	25	25	25	25
22	75	75	75	75	75	75	75	75	75	75	75	75	75	75	75	75
23	100	100	100	75	100	100	100	100	100	100	100	100	75	75	100	75
24	0	0	0	0	0	0	0	0	0	0	0	0	0	0	0	0
25	0	0	0	0	0	0	0	0	0	0	0	0	0	0	0	0
26	25	25	25	25	25	25	25	25	25	25	25	25	25	25	25	25
27	25	0	0	0	0	0	0	0	0	0	0	0	0	0	0	0
28	75	75	75	75	75	75	75	75	75	75	75	75	75	75	75	75
29	25	25	25	25	25	25	25	25	25	25	25	25	25	25	25	25
30	0	0	0	0	0	0	0	0	0	0	0	0	0	0	0	0
31	0	0	0	0	0	0	0	0	0	0	0	0	0	0	0	0
32	25	25	25	25	25	25	25	25	25	25	25	25	25	25	25	25
33	0	0	0	0	0	0	0	0	0	0	0	0	0	0	0	0
34	0	0	0	0	0	0	0	0	0	0	0	0	0	0	0	0
35	0	0	0	0	0	0	0	0	0	0	0	0	0	0	0	0
36	0	0	0	0	0	0	0	0	0	0	0	0	0	0	0	0
37	25	25	25	25	25	25	25	25	25	25	25	25	25	25	25	25
Total (kW)	1225	1175	1200	1200	1275	1225	1175	1250	1100	1175	1175	1175	1200	1200	1200	1200

Table A.6 NSGA-II optimization results for NaS capacity and location, solutions 1-17.

Node	NaS Capacity (kW)																
1	0	0	0	0	0	0	0	0	0	0	0	0	0	0	0	0	0
2	25	25	25	25	25	25	25	25	25	25	25	25	25	25	25	25	25
3	0	0	0	0	0	0	0	0	0	0	0	0	0	0	0	0	0
4	25	0	25	0	25	0	25	0	25	0	25	0	25	0	25	0	25
5	25	25	25	25	25	25	25	25	25	25	25	25	25	25	25	25	25
6	0	0	0	0	0	0	0	0	0	0	0	0	0	0	0	0	0
7	25	0	25	0	25	0	25	0	25	0	25	0	25	0	25	0	25
8	25	0	25	0	25	0	25	0	25	0	25	0	25	0	25	0	25
9	0	0	0	0	0	0	0	0	0	0	0	0	0	0	0	0	0
10	0	25	0	25	0	25	0	25	0	25	0	25	0	25	0	25	0
11	25	25	25	25	25	25	25	25	25	25	25	25	25	25	25	25	25
12	25	25	25	25	25	25	25	25	25	25	25	25	25	25	25	25	25
13	25	25	25	25	25	25	25	25	25	25	25	25	25	25	25	25	25
14	25	25	25	25	25	25	25	25	25	25	25	25	25	25	25	25	25
15	50	50	50	50	50	50	50	50	50	50	50	50	50	50	50	50	50
16	25	25	25	25	25	25	25	25	25	25	25	25	25	25	25	25	25
17	50	25	50	25	50	25	50	25	50	25	50	25	50	25	50	25	25
18	0	0	0	0	0	0	0	0	0	0	0	0	0	0	0	0	0
19	0	0	0	0	0	0	0	0	0	0	0	0	0	0	0	0	0
20	0	0	0	0	0	0	0	0	0	0	0	0	0	0	0	0	0
21	25	25	25	25	25	25	25	25	25	25	25	25	25	25	25	25	25
22	50	50	50	50	50	50	50	50	50	50	50	50	50	50	50	50	50
23	0	25	25	25	0	25	25	25	25	25	25	25	25	25	0	0	0
24	25	25	25	25	25	25	25	25	25	25	25	25	25	25	25	25	25
25	25	25	25	25	25	25	25	25	25	25	25	25	25	25	25	25	25
26	50	50	50	50	50	50	50	50	50	50	50	50	50	50	50	50	50
27	50	50	50	50	50	50	50	50	50	50	50	50	50	50	50	50	50
28	25	50	50	50	50	25	50	50	50	50	50	50	50	50	50	50	25
29	25	25	25	25	25	0	25	25	25	25	25	25	25	25	25	25	25
30	25	25	25	25	25	25	25	25	25	25	25	25	25	25	25	25	25
31	25	25	25	25	25	25	25	25	25	25	25	25	25	25	25	25	25
32	25	25	25	25	25	0	25	0	25	25	25	25	25	25	25	25	25
33	50	25	50	50	50	50	50	50	50	50	50	50	50	50	50	50	50
34	25	25	25	25	25	25	25	25	25	25	25	25	25	25	25	25	25
35	25	25	25	25	25	25	25	25	25	25	25	25	25	25	25	25	25
36	50	50	50	50	50	50	50	50	50	50	50	50	50	50	50	50	50
37	25	25	25	25	25	25	25	25	25	25	25	25	25	25	25	25	25
Total (kW)	875	825	825	825	850	800	850	825	850	825	825	825	825	825	850	825	850

Table A.7 NSGA-II optimization results for NaS capacity and location, solutions 18-34.

Node	NaS Capacity (kW)																	
1	0	0	0	0	0	0	0	0	0	0	0	0	0	0	0	0	0	0
2	25	25	25	25	25	25	25	25	25	25	25	25	25	25	25	25	25	25
3	0	25	0	0	0	0	0	0	0	0	0	0	0	0	0	0	0	0
4	0	0	0	25	0	25	25	25	25	25	25	25	25	25	25	25	25	0
5	25	25	25	25	25	25	25	25	25	25	25	25	25	25	25	25	25	25
6	25	0	0	0	0	0	0	0	0	0	0	0	0	0	0	0	0	25
7	25	0	25	25	25	25	25	25	25	25	25	25	25	25	25	25	25	25
8	0	0	25	25	25	25	25	25	25	25	25	25	25	25	25	25	25	0
9	0	0	0	0	0	0	0	0	0	0	0	0	0	0	0	0	0	0
10	25	25	0	0	0	0	0	0	0	0	0	0	0	0	0	0	0	0
11	25	25	25	25	25	25	25	25	25	25	25	25	25	25	25	25	25	25
12	25	25	25	25	25	25	25	25	25	25	25	25	25	25	25	25	25	25
13	25	25	25	25	25	25	25	25	25	25	25	25	25	25	25	25	25	25
14	25	25	25	25	25	25	25	25	25	25	25	25	25	25	25	25	25	25
15	50	50	50	50	50	50	50	50	50	50	50	50	50	50	50	50	50	50
16	25	25	25	25	25	25	25	25	25	25	25	25	25	25	25	25	25	25
17	50	50	50	50	50	50	50	50	50	50	50	50	50	50	50	50	50	50
18	25	0	25	0	0	0	0	0	0	0	0	0	0	0	0	0	0	0
19	0	0	0	0	0	0	0	0	0	0	0	0	0	0	0	0	0	0
20	0	0	0	0	0	0	0	0	0	0	0	0	0	0	0	0	0	0
21	25	25	25	25	25	25	25	25	25	25	25	25	25	25	25	25	25	25
22	50	50	50	50	50	50	50	50	50	50	50	50	50	50	50	50	50	50
23	0	0	0	0	0	0	0	0	0	0	0	0	0	0	0	0	0	0
24	25	25	25	25	25	25	25	25	25	25	25	25	25	25	25	25	25	25
25	25	25	25	25	25	25	25	25	25	25	25	25	25	25	25	25	25	25
26	25	50	50	50	50	50	50	50	50	50	50	50	50	50	50	50	50	50
27	50	50	50	50	50	50	50	50	50	50	50	50	50	50	50	50	50	50
28	50	50	50	50	50	50	50	50	50	50	50	50	50	50	50	50	50	50
29	25	25	25	25	25	25	25	25	25	25	25	25	25	25	25	25	25	25
30	25	25	25	25	25	25	25	25	25	25	25	25	25	25	25	25	25	25
31	25	25	25	25	25	25	25	25	25	25	25	25	25	25	25	25	25	25
32	25	25	25	25	25	25	25	25	25	25	25	25	25	25	25	25	25	25
33	25	25	50	50	50	50	50	50	50	50	50	50	50	50	50	50	50	50
34	25	25	25	25	25	25	25	25	25	25	25	25	25	25	25	25	25	25
35	25	25	25	25	25	25	25	25	25	25	25	25	25	25	25	25	25	25
36	50	50	50	50	50	50	50	50	50	50	50	50	50	50	50	50	50	50
37	25	25	25	25	25	25	25	25	25	25	25	25	25	25	25	25	25	0
Total (kW)	875	850	825	850	825	850	875	825	850	875	825	850	875	850	875	850	850	825

Table A.8 NSGA-II optimization results for NaS capacity and location, solutions 35-50.

Node	NaS Capacity (kW)																
1	0	0	0	0	0	0	0	0	0	0	0	0	0	0	0	0	0
2	25	25	25	25	25	25	25	25	25	25	25	25	25	25	25	25	25
3	0	0	0	0	0	0	0	0	0	0	0	0	0	0	0	0	0
4	0	0	0	0	0	0	0	0	0	0	0	0	0	0	0	0	0
5	25	25	25	25	25	25	25	25	25	25	25	25	25	25	25	25	25
6	0	0	0	0	0	0	0	0	0	0	0	0	0	0	0	0	0
7	25	25	25	25	25	25	25	25	25	25	25	25	25	25	25	25	25
8	0	0	0	0	0	0	0	0	0	0	0	0	0	0	0	0	0
9	0	0	0	0	0	0	0	0	0	0	0	0	0	0	0	0	0
10	0	0	0	0	0	0	0	0	0	0	0	0	0	0	0	0	0
11	25	25	25	25	25	25	25	25	25	25	25	25	25	25	25	25	25
12	25	25	25	25	25	25	25	25	25	25	25	25	25	25	25	25	25
13	25	25	25	25	25	25	25	25	25	25	25	25	25	25	25	25	25
14	25	25	25	25	25	25	25	25	25	25	25	25	25	25	25	25	25
15	50	50	50	50	50	50	50	50	50	50	50	50	50	50	50	50	50
16	25	25	25	25	25	25	25	25	25	25	25	25	25	25	25	25	25
17	50	50	50	50	50	50	50	50	50	50	50	50	50	50	50	50	50
18	0	0	0	0	0	0	0	0	0	0	0	0	0	0	0	0	0
19	0	0	0	0	0	0	0	0	0	0	0	0	0	0	0	0	0
20	0	0	0	0	0	0	0	0	0	0	0	0	0	0	0	0	0
21	25	25	25	25	25	25	25	25	25	25	25	25	25	25	25	25	25
22	50	50	50	50	50	50	50	50	50	50	50	50	50	50	50	50	50
23	0	0	0	0	0	0	0	0	0	0	0	0	0	0	0	0	0
24	25	25	25	25	25	25	25	25	25	25	25	25	25	25	25	25	25
25	25	25	25	25	25	25	25	25	25	25	25	25	25	25	25	25	25
26	25	25	25	25	25	25	25	25	25	25	25	25	25	25	25	25	25
27	50	50	50	50	50	50	50	50	50	50	50	50	50	50	50	50	50
28	50	50	50	50	50	50	50	50	50	50	50	50	50	50	50	50	50
29	25	25	25	25	25	25	25	25	25	25	25	25	25	25	25	25	0
30	25	25	25	25	25	25	25	25	25	25	25	25	25	25	25	25	25
31	25	25	25	25	25	25	25	25	25	25	25	25	25	25	25	25	25
32	25	25	25	25	25	25	25	25	25	25	25	25	25	25	25	25	25
33	50	50	50	50	50	50	50	50	50	50	50	50	50	50	50	50	50
34	25	25	25	25	25	25	25	25	25	25	25	25	25	25	25	25	25
35	25	25	25	25	25	25	25	25	25	25	25	25	25	25	25	25	25
36	50	50	50	50	50	50	50	50	50	50	50	50	50	50	50	50	50
37	25	25	25	25	25	25	25	25	25	25	25	25	25	25	25	25	25
Total (kW)	825	850	850	875	825	825	850	825	850	850	825	850	825	825	825	875	825

Appendix B - IEEE 37-Node Test Feeder Data

Table B.1 Line configuration data.

Node A	Node B	Length (ft.)	Config.
701	702	960	722
702	705	400	724
702	713	360	723
702	703	1320	722
703	727	240	724
703	730	600	723
704	714	80	724
704	720	800	723
705	742	320	724
705	712	240	724
706	725	280	724
707	724	760	724
707	722	120	724
708	733	320	723
708	732	320	724
709	731	600	723
709	708	320	723
710	735	200	724
710	736	1280	724
711	741	400	723
711	740	200	724
713	704	520	723
714	718	520	724
720	707	920	724
720	706	600	723
727	744	280	723
730	709	200	723
733	734	560	723
734	737	640	723
734	710	520	724
737	738	400	723
738	711	400	723
744	728	200	724
744	729	280	724
775	709	0	XFM-1
799	701	1850	721

Table B.2 Cable configuration.

Config.	Phasing	Cable	Spacing ID
721	A B C	1,000,000 AA, CN	515
722	A B C	500,000 AA, CN	515
723	A B C	2/0 AA, CN	515
724	A B C	#2 AA, CN	515

Table B.3 Load data.

Node	Load Model	Ph-1 (kW)	Ph-1 (kVAr)	Ph-2 (kW)	Ph-2 (kVAr)	Ph-3 (kW)	Ph-3 (kVAr)
701	D-PQ	140	70	140	70	350	175
712	D-PQ	0	0	0	0	85	40
713	D-PQ	0	0	0	0	85	40
714	D-I	17	8	21	10	0	0
718	D-Z	85	40	0	0	0	0
720	D-PQ	0	0	0	0	85	40
722	D-I	0	0	140	70	21	10
724	D-Z	0	0	42	21	0	0
725	D-PQ	0	0	42	21	0	0
727	D-PQ	0	0	0	0	42	21
728	D-PQ	42	21	42	21	42	21
729	D-I	42	21	0	0	0	0
730	D-Z	0	0	0	0	85	40
731	D-Z	0	0	85	40	0	0
732	D-PQ	0	0	0	0	42	21
733	D-I	85	40	0	0	0	0
734	D-PQ	0	0	0	0	42	21
735	D-PQ	0	0	0	0	85	40
736	D-Z	0	0	42	21	0	0
737	D-I	140	70	0	0	0	0
738	D-PQ	126	62	0	0	0	0
740	D-PQ	0	0	0	0	85	40
741	D-I	0	0	0	0	42	21
742	D-Z	8	4	85	40	0	0
744	D-PQ	42	21	0	0	0	0
Total		727	357	639	314	1091	530

Table B.4 Transformer data.

	kVA	kV-high	kV-low	R - %	X - %
Substation:	2,500	230 D	4.8 D	2	8
XFM -1	500	4.8 D	.480 D	0.09	1.81

Configuration 721: Z (R +jX) in ohms per mile

$$\begin{bmatrix} 0.2926 + 0.1973i & 0.0673 - 0.0368i & 0.0337 - 0.0417i \\ 0.0673 - 0.0368i & 0.2646 + 0.1900i & 0.0673 - 0.0368i \\ 0.0337 - 0.0417i & 0.0673 - 0.0368i & 0.2926 + 0.1973i \end{bmatrix}$$

Configuration 722: Z (R +jX) in ohms per mile

$$\begin{bmatrix} 0.4751 + 0.2973i & 0.1620 - 0.0326i & 0.1234 - 0.0607i \\ 0.1620 - 0.0326i & 0.4488 + 0.2678i & 0.1629 - 0.0326i \\ 0.1234 - 0.0607i & 0.1629 - 0.0326i & 0.4751 + 0.2973i \end{bmatrix}$$

Configuration 723: Z (R +jX) in ohms per mile

$$\begin{bmatrix} 1.2936 + 0.6713i & 0.4871 + 0.2111i & 0.4585 + 0.1521i \\ 0.4871 + 0.2111i & 1.3022 + 0.6326i & 0.4871 + 0.2111i \\ 0.4585 + 0.1521i & 0.4871 + 0.2111i & 1.2936 + 0.6713i \end{bmatrix}$$

Configuration 724: Z (R +jX) in ohms per mile

$$\begin{bmatrix} 2.0952 + 0.7758i & 0.5204 + 0.2738i & 0.4926 + 0.2123i \\ 0.5204 + 0.2738i & 2.1068 + 0.7398i & 0.5204 + 0.2738i \\ 0.4926 + 0.2123i & 0.5204 + 0.2738i & 2.0952 + 0.7758i \end{bmatrix}$$